Study on Fabrication and Characterization of Chalcogenide-based Thin Film Photovoltaic Devices of Environmental Harmony Type

(環境調和型カルコゲナイド系薄膜太陽電池の作製と特性評価に関する研究)

July, 2018

Doctor of Engineering

Mitsuki Nakashima

中嶋　崇喜

Toyohashi University of Technology

別紙５－２（論文博士（和文））

平成　30　年　7　月　9　日

機械工学専攻			
氏名	中嶋　崇喜	紹介教員	伊﨑　昌伸

論文内容の要旨（博士）

博士学位論文名	環境調和型カルコゲナイド系薄膜太陽電池の作製と特性評価に関する研究

(要旨　1,200 字程度)

近年、化石燃料の枯渇や、地球温暖化などの環境問題を受け、再生可能エネルギーに関する研究がすすめられている。その中でも太陽光を使用したエネルギー変換技術の普及が進んでいる。太陽光を直接電気エネルギーに変換する装置として太陽電池がある。現在、希少元素を使用せず、資源豊富な元素のみで構成される Cu_2ZnSnS_4 系太陽電池が、低コストかつ無毒な環境調和型カルコゲナイド系薄膜太陽電池として注目され、多くの研究機関で研究されている。しかし、実用化レベルの高い変換効率が得られる安全な作製方法は確立していない。それ故、いくつかの安全な作製方法でこれらの太陽電池を作製し、その特性を調査することは非常に重要である。このような観点から本研究は遂行された。

本研究では、我々が考案した真空蒸着法、硫化法、熱処理法により、$Cu_2ZnSnSe_4$ と Cu_2SnS_3 薄膜及び太陽電池を作製し、それらの特性を調査することを目的とする。

まず、$Cu_2ZnSnSe_4$ 化合物を蒸着材料に使用し、真空蒸着法のみで $Cu_2ZnSnSe_4$ 薄膜及び太陽電池を作製し、その特性を調査した。また、作製した薄膜への熱処理の効果も調査した。$Cu_2ZnSnSe_4$ 化合物を蒸着材料に使用した薄膜太陽電池の作製は、今までに報告例がなく、初めての試みである。作製した太陽電池は、350nm から 1400nm の非常に広い波長範囲で量子効率を持っていたことから、考案した作製方法は広い量子効率範囲を持つ太陽電池の作製に効果的であると考えられる。

次に、真空蒸着法により形成した Sn/Cu プリカーサを硫化することにより Cu_2SnS_3 薄膜及び太陽電池を作製した。この時、プリカーサ形成時の Cu/Sn 比を変化させ、それぞれの特性から Cu/Sn 比の最適値を調査した。Cu/Sn 比が 1.67 の時、開放電圧が最大となる 247.5 mV が得られた。したがって、本作製方法における Cu_2SnS_3 薄膜太陽電池の Cu/Sn 比の最適値はおよそ 1.67 であると考えられる。

さらに、Cu_2SnS_3 への NaF や KF のアルカリ金属添加の効果を調査した。NaF 添加では、NaF/Sn/Cu プリカーサを硫化して Cu_2SnS_3 薄膜を成膜するプロセスにおいて、NaF/Cu 比の増加と共に太陽電池特性が向上し、NaF/Cu=0.075 の時、Cu_2SnS_3 薄膜太陽電池において、当時の世界最高となる 4.63%の変換効率が得られた。また、KF 添加では、NaF/Sn/Cu プリカーサを硫化後、KF を添加し再度熱処理を行う 2 段階熱処理法において、4.63%の変換効率を記録した太陽電池の 283 mV を超える、293 mV の開放電圧が得られた。

最後に、Cu_2SnS_3 への Ag 添加の効果を調査した。Ag/(Ag+Cu)比を変化させ、真空蒸着法により形成した NaF/Sn/(Ag+Cu)プリカーサを硫化することにより$(Cu,Ag)_2SnS_3$ 薄膜及び太陽電池を作製した。Ag/(Ag+Cu)比を増加させると、格子定数がベガード則に従って変化しており、$(Cu,Ag)_2SnS_3$ が作製できたと考えられる。最も特性が良かった太陽電池で、4.07%の変換効率を示し、$(Cu,Ag)_2SnS_3$ において世界初となる発電特性が得られた。さらに、Ag/(Ag+Cu)比の増加によるバンドギャップの拡張が確認できた。

別紙５－１（論文博士（英文））

Date of Submission (month day, year): July 9, 2018

Department: Mechanical Engineering			
Applicant's name	Mitsuki Nakashima	Contact faculty	Masanobu Izaki

Abstract（Doctor）

Title of Thesis	Study on Fabrication and Characterization of Chalcogenide-based Thin Film Photovoltaic Devices of Environmental Harmony Type

Approx. 800 words

Recently, the many researches on renewable energy are carrying out to solve the environmental problems such as the depletion of fossil fuels and the global warming. Especially, the technologies of energy conversion using solar energy are spreading widely. Solar cells are electronic devices which converts solar energy directly into electrical energy through the photovoltaic effect. Now, many research organizations are researching the Cu_2ZnSnS_4-based solar cells as the chalcogenide-based thin film solar cells of the environmental harmony type which are composed of earth-abundant materials with no rare elements, low-cost and nontoxic. However, the safe fabrication methods which obtain the high conversion efficiency of the practical use level have not been established. Therefore, it is very important to investigate the characteristics of these solar cells fabricated by several methods with a safe process. This study has been performed from the above standpoint.

This thesis presents the investigation of the characteristics of the $Cu_2ZnSnSe_4$ and Cu_2SnS_3 thin films and solar cells fabricated by our proposed method such as vacuum evaporation, sulfurization and annealing methods.

First, the $Cu_2ZnSnSe_4$ thin films and solar cells were fabricated by the new vacuum evaporation method which used only the deposition stage using the $Cu_2ZnSnSe_4$ compound as the starting evaporation materials, and its characteristics were investigated. Furthermore, influences by annealing of the characteristics of these thin films and solar cells were investigated. The fabrication method of thin film solar cell using $Cu_2ZnSnSe_4$ compound is unprecedented, and our proposed method in this chapter is the first time. The film compositions, the film structures, the film morphologies, cell performances of these thin films and solar cells were characterized by electron probe microanalysis, X-ray diffraction, Raman spectroscopy, scanning electron microscopy, quantum efficiencies, and Current-voltage characteristics measurements, and these properties were discussed. The solar cells fabricated by this process had quantum efficiency in the wavelength range between 350 nm and 1400 nm. Therefore, the proposed method can be effectively used to produce thin films characterized by wide quantum efficiency ranges.

Next, the Cu_2SnS_3 thin films and solar cells were fabricated by sulfurization process from the stacked Cu/Sn precursors deposited by sequential evaporation of Sn and Cu elements. The

Cu/Sn molar ratio of the evaporation materials was changed, and the optimum value of the Cu/Sn molar ratio was investigated. The film composition, the film structure, the film morphology, and cell performances of these thin films and solar cells were discussed. The largest open-circuit voltage of 247.5 mV was obtained with Cu/Sn molar ratio of 1.67, therefore it is considered that the optimum value of Cu/Sn molar ratio of the evaporation materials in this fabrication method is vicinity of 1.67.

In addition, the effects to the characteristics of the Cu_2SnS_3 thin films and solar cells by the alkaline metals doping such as sodium and potassium were investigated. The film composition, the film structure, the film morphology, cell performances and quantum efficiencies of the Cu_2SnS_3 thin films and solar cells fabricated with alkaline metals doping were discussed. By sodium addition, the Cu_2SnS_3 thin films and solar cells were fabricated by sulfurization from the NaF/Cu/Sn stacked precursor deposited by the sequential evaporation of Sn, Cu and NaF. The cell performances of these Cu_2SnS_3 solar cells had an upward trend with increasing NaF/Cu molar ratio, and the Cu_2SnS_3 solar cell which was fabricated with NaF/Cu = 0.075 molar ratio demonstrated the record conversion efficiency of the Cu_2SnS_3 solar cells of 4.63%. By potassium addition, Cu_2SnS_3 solar cells fabricated by annealing KF/film-bilayer samples (film-bilayer means the thin film fabricated by sulfurization from the NaF/Cu/Sn stacked precursor) demonstrated the open-circuit voltage of 293 mV.

Finally, the effects of Ag doping on the characteristics of Cu_2SnS_3 thin films and solar cells were investigated. The $(Cu,Ag)_2SnS_3$ thin films and solar cells which were Ag doping of CTS were fabricated by sulfurization from the NaF/Sn/(Ag+Cu) stacked precursors deposited by sequential evaporation of Ag, Cu and Sn elements and NaF, and the Ag/(Ag+Cu) molar ratio of the evaporation materials and the sulfurization temperatures were varied. The film composition, the film structure, the film morphology, cell performances and quantum efficiencies of the $(Cu,Ag)_2SnS_3$ thin films and solar cells were discussed. The lattice spacing increased along Vegard's law with increasing the Ag/(Ag+Cu) molar ratio in films, and it is considered that the $(Cu,Ag)_2SnS_3$ was fabricated. The best solar cell fabricated with Ag/(Ag+Cu) = 0.05 at sulfurization temperature of 570 °C showed the conversion efficiency of 4.07%, and it was the first reports of $(Cu,Ag)_2SnS_3$ thin film solar cells. Furthermore, the expansion of the band-gap energy was seen with increasing the Ag/(Ag+Cu) molar ratio.

CONTENTS

CHAPTER 2: $Cu_2ZnSnSe_4$ thin film solar cells fabricated by thermal evaporation

CHAPTER 3: Cu_2SnS_3 thin film solar cells fabricated by sulfurization from Cu/Sn stacked precursors

CHAPTER 4: Cu_2SnS_3 thin film solar cells fabricated by sulfurization from NaF/Cu/Sn stacked precursor

CHAPTER 5: Cu_2SnS_3 thin film solar cells with KF addition fabricated by sulfurization

CHAPTER 6: $(Cu,Ag)_2SnS_3$ thin film solar cells fabricated by sulfurization

CHAPTER 7: Summary

CHAPTER 1

Introduction

1.1 Global energy situation

1.1.1 Energy consumption of the world and energy sources

The world primary energy consumptions continue increasing with economic growth and continued increasing by an average of 2.6% a year from 3,700 million tonne of oil equivalent (TOE) of 1965 and reached 13,200 million TOE in 2016. Figure 1.1 shows the change of the world energy consumption. The fossil fuels such as oil, coal and natural gas accounts for 80% or more of the energy sources of the whole energy consumption. The energy source accounting

for the biggest share in the whole energy consumption in particular is oil, and its ratio is over 30%. However, it is estimated that the oil which has been used as a main energy source for economic development so far dries up approximately 50 years later. The consumption of the coal spread as inexpensive fuel for power generation around an Asian region where economic growth was remarkable, and its ratio is approximately 30%. The consumption of the natural gas increased by the developed countries which strongly needs the correspondence to climate change, and its ratio is over 20%. On the other hand, the nuclear energy and the renewable energy which does not depend on the fossil fuels increased for global warming countermeasures and for relaxation of the international competition of the acquisition of fossil fuels resource. The growth rate of the energy consumption of renewable energy has become biggest in recent years, especially. In addition, it is expected that the ratio of the renewable energy will spread because the generation cost with renewable energy is decreasing.

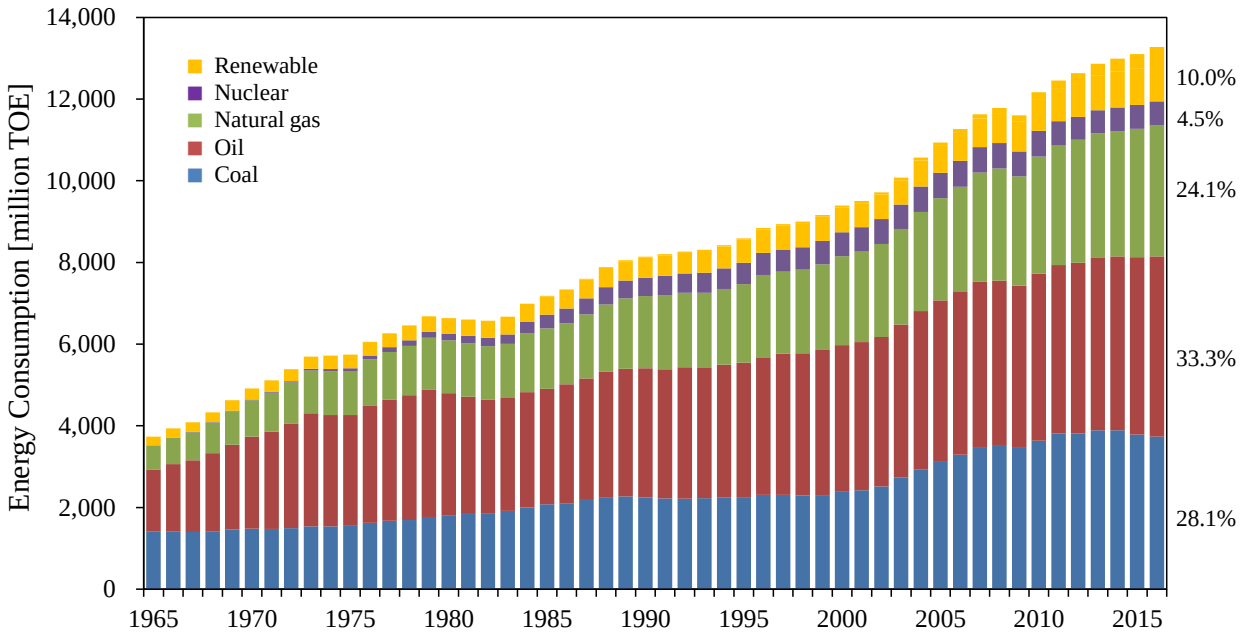

Figure 1.1 Change of the world energy consumption. **[1]**

1.1.2 Renewable energy

Now, an argument about the influence on global environment with the greenhouse gases are continuing throughout the world. The greenhouse gases which were generated artificially are carbon dioxide (CO_2), methane (CH_4), nitrous oxide (N_2O) and chlorofluorocarbons (CFCs), and CO_2 occupies the share of more than 70% of whole greenhouse gases. Figure 1.2 shows the ratio of the kinds of the greenhouse gases. The CO_2 is one cause of global warming and the most influential, and the quantity of the atmospheric CO_2 increases with the consumption of fossil fuels increasing year by year. Thus, the renewable energy such as hydro energy, biomass energy, wind energy and solar photovoltaic energy is attracting attention as the clean energy in consideration of the global environment. Figure 1.3 shows the change of the world renewable energy consumption. The hydro energy is the most spread renewable energy and has the share of approximately 70% of whole renewable energy. A lot of the biomass energy using plants to the raw materials is used in the developing countries mainly. In China, United States and Germany, the many wind energy are used, and in recent years, a market of the marine wind-generated electricity is spreading. The solar photovoltaic energy spread rapidly after 2005, and this growth rate is largest in whole renewable energy. The one of this factor was introduction of the Feed-in Tariff (FIT) system. In our country, the solar photovoltaic energy spread significantly after 2012 with introduction of the FIT system.

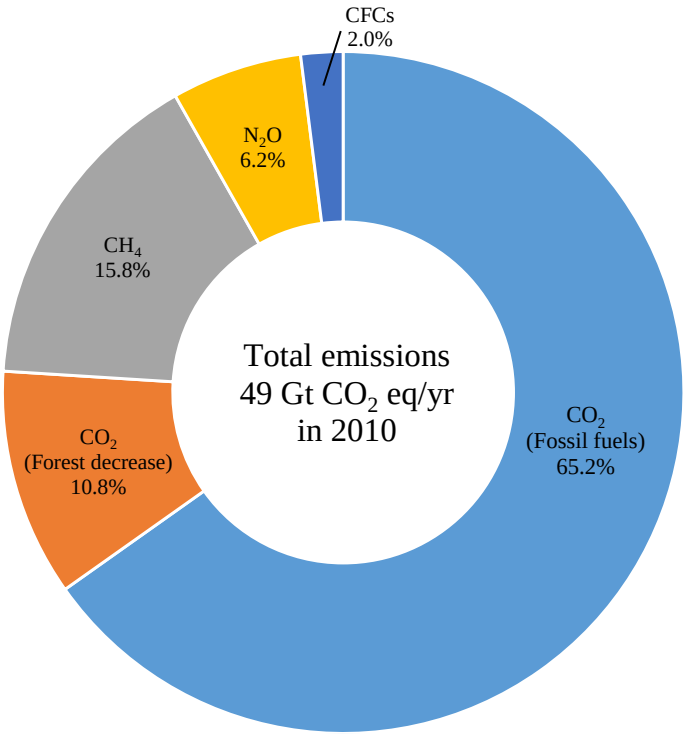

Figure 1.2 Ratio according to the kind of the greenhouse gases. **[2]**

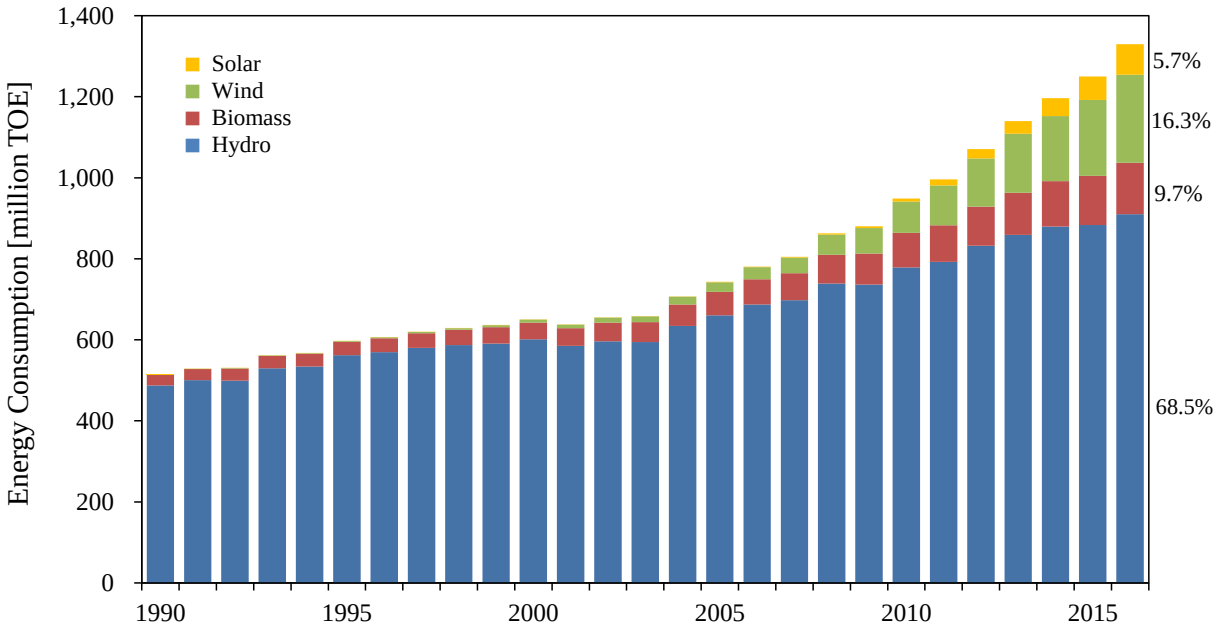

Figure 1.3 Change of the world renewable energy consumption. **[1]**

1.2 Photovoltaic devices

1.2.1 Introduction of photovoltaic devices

Photovoltaic devices are electronic devices which converts solar energy directly into electrical energy through the photovoltaic effect, and those are typical semiconductor p-n junction devices. Figure 1.4 shows structure of the p-n junction and state of the energy band. The p-n junction are formed by joining n-type and p-type semiconductor material. Since the n-type region has excess electrons as majority carriers and the p-type has excess holes, electrons diffuse from the n-type side to the p-type side. Similarly, holes diffuse from the p-type side to the n-type side. In vicinity of junction, electrons and holes are recombined, and the depletion layer is formed. When the light which has energy more than band-gap energy (Eg) enters on the p-n junction devices, electrons are excited from the valence band to the conduction band and electrical charge carriers, electrons and holes, are generated. And connecting the p-n junction devices to outside circuit, this generated carriers can take out as electric current.

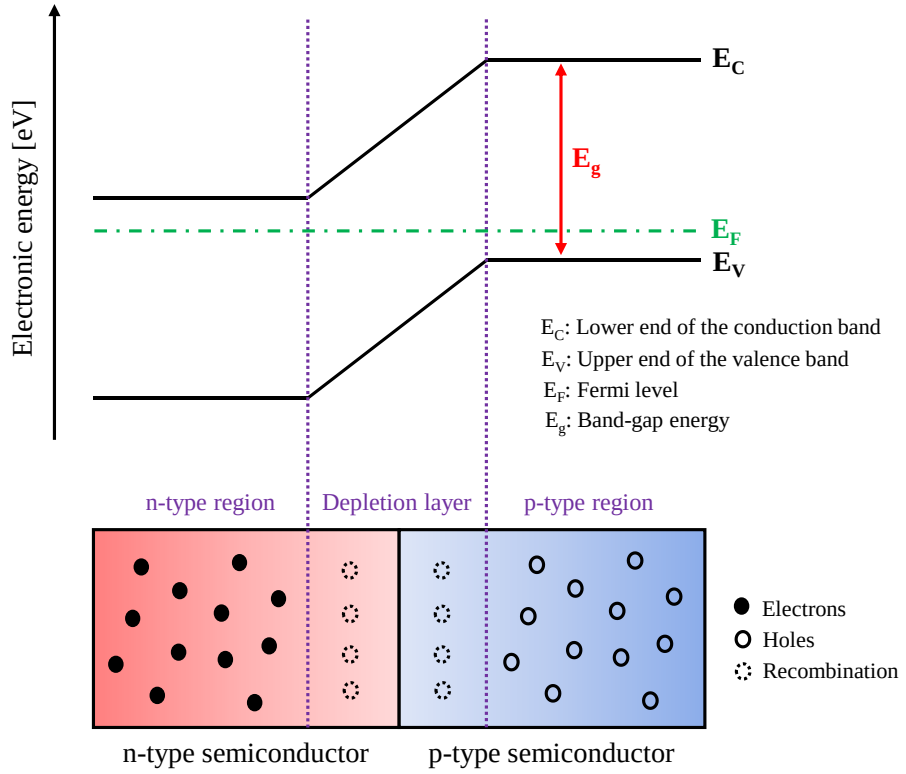

Figure 1.4 Structure of the p-n junction and state of the energy band.

1.2.2 The present conditions of the conversion efficiency of solar cells

Existing photovoltaic technologies include silicon-based solar cells and compound solar cells. In particular, compound solar cells include gallium-arsenide (GaAs), cadmium-telluride (CdTe) and chalcogenide-based such as copper-indium-selenide (Cu(In, Ga)Se_2, CIGS) and copper-zinc-tin-sulfied-based (Cu_2ZnSnS_4-based, CZTS-based). In 1961, the conversion efficiency limit of solar cells that takes all these factors into account was first derived by Shockley and Queisser. **[3]** Figure 1.5 shows the limiting conversion efficiency of a single junction solar cell under standard 1-sun (AM 1.5 100mW/cm^2) illumination as a function of band-gap energy. **[3, 4]** This is called S-Q limit. According to this data, the maximum conversion efficiency is obtained for a band-gap energy of a semiconductor of 1.34 eV and is 33.7%. Figure 1.6 shows the type of solar cells and the conversion efficiency revolution from 1975 to 2015 **[5]**. Silicon has a band-gap energy of 1.12 eV which is near an ideal value. A crystalline silicon heterojunction solar cell had achieved the conversion efficiency of 25.6%. **[6, 7]** In addition, the global photovoltaic market is dominated by silicon solar modules, and its market share is more than 90%. **[8]** GaAs solar cells which has a band-gap energy of 1.42 eV close to the optimum had achieved the record efficiency for a single junction solar cell of 28.8%. **[6, 9]** Furthermore, these solar cells are used for space-use because thermoresistance and radiation tolerance are superior, but they have high production cost in comparison with other solar cells. CdTe is a near-ideal band-gap energy of 1.43 eV, and the conversion efficiencies of this solar cells had achieved more than 20%. **[10, 11]** However, it is using cadmium which has strong toxicity, and tellurium which is a rare metal. In recent years, the researches of chalcogenide-based solar cells are increasing. Those solar cell materials have high absorption coefficient, therefore they can fabricate very thin, and the fabrication cost is lower than silicon solar cells, in addition, the toxicity of chalcogenide-based solar cells is smaller than CdTe solar cells. Furthermore, it is expected that the conversion efficiency is improved more from S-Q limit.

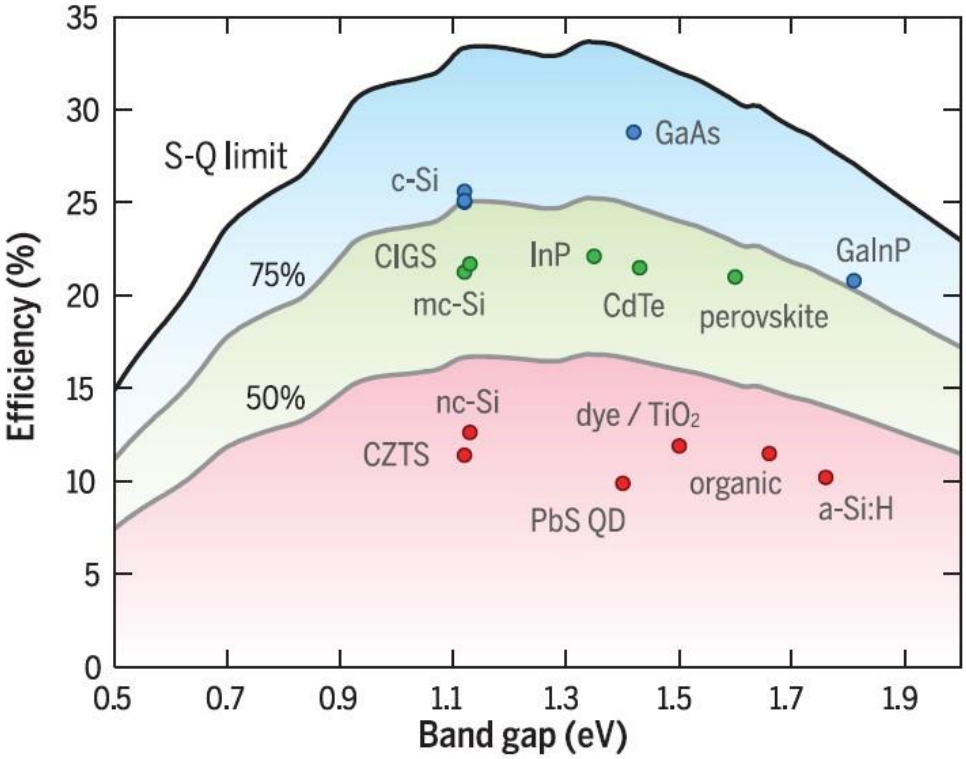

Figure 1.5 S-Q limit and the conversion efficiencies of solar cells. **[3, 4]**

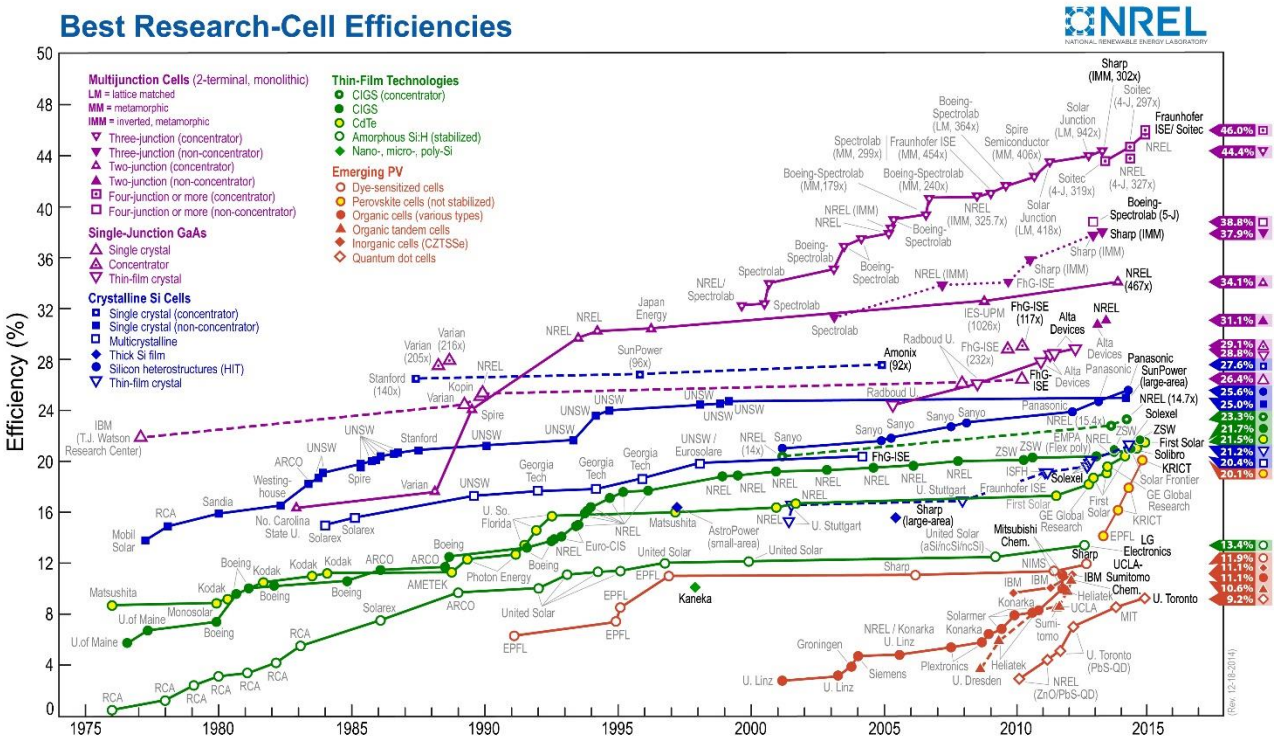

Figure 1.6 Conversion efficiency revolution from 1975 to 2015. **[5]**

1.3 Chalcogenide-based solar cells

1.3.1 $Cu(In,Ga)Se_2$

In the chalcogenide-based solar cells, a $Cu(In,Ga)Se_2$ (CIGS) solar cell is recording the highest conversion efficiency of 22.6% in 2016 **[12]**. CIGS has a chalcopyrite crystal structure and its band-gap energy can be continuously tuned from 1.0 eV in $CuInSe_2$ to 1.7 eV in $CuGaSe_2$ by gradual substitution of Ga for In. **[13]** Average band-gap energy values of 1.1 to 1.2 eV, and the Ga / (Ga + In) molar ratio of around 0.3 are used in record efficiency solar cells. **[12]** In recent years, the technique of alkaline metals doping such as sodium and potassium has been reported, **[12, 14-18]** and it helped set high efficiencies of CIGS solar cells. **[12, 15]** In addition, other CIGS solar cells fabricated by various methods have been reported as shown in Table 1.1.

Table 1.1 Research trends of CIGS solar cells.

Fabrication method	V_{oc} [mV]	J_{sc} [mA/cm^2]	Fill factor	Conversion efficiency [%]	Absorber type	Ref.
Co-evaporation	741	37.8	0.806	22.6	CIGS	**[12]**
	736	35.1	0.789	20.4	CIGS	**[14]**
	757	34.8	0.791	20.8	CIGS	**[15]**
	757	35.7	0.776	21.0	CIGS	**[17]**
Evaporation and selenization	709	33.5	0.783	18.6	CIGS	**[18]**
Electrodeposition and selenization	475.1	37.5	0.658	11.7	CIGS	**[19]**

1.3.2 Cu_2ZnSnS_4-based

The I_2-II-IV-VI_4 quaternary semiconductors are expected as the indium-free photovoltaic materials for the absorbing layer of thin film solar cells. In particular, Cu_2ZnSnS_4-based (CZTS-based) thin film are considered to be promising materials for low cost absorber layers with earth-abundant elements which does not include rare elements such as In. CZTS-based thin films include Cu_2ZnSnS_4 (CZTS), $Cu_2ZnSnSe_4$ (CZTSe) and $Cu_2ZnSn(S,Se)_4$ (CZTSSe). CZTS-based thin films have an absorption coefficient of more than 10^4 cm^{-1}, and the band-gap energy can control from 1.0 eV in CZTSe to 1.5 eV in CZTS by changing the ratio of Se and S **[20-24]**. Firstly, Ito et al. reported the photovoltaic effect in the heterojunction diode consisting of the CZTS thin film fabricated by atom beam sputtering of quaternary compound target and the cadmium tin oxide transparent conductive film. **[25]** After then, Katagiri et al. reported many researches for the fabrication and characterization of CZTS thin films **[26-28]**, and their solar cell showed the conversion efficiency over 6.7% in 2008. **[28]** Recently, Tajima et al. reported CZTS thin film solar cells fabricated by sputtering and sulfurization have achieved the record conversion efficiency of 9.1%. **[29, 30]** Lee et al. reported the record conversion efficiency of 11.6% for CZTSe thin film solar cells produced by four-source (Cu, Zn, Sn and Se) thermal co-evaporation and selenization process. **[31]** As of today, the CZTSSe thin film solar cells manufactured by a hydrazine-based solution deposition process have achieved the highest conversion efficiency of whole CZTS-based solar cells equal to 12.6%. **[32]** In addition, a number of researches of CZTS-based thin film solar cells have been reported as shown in Table 1.2. Furthermore, several research groups have described the improvement of thin film solar cell characteristics by alkaline metals addition similar to CIGS solar cell. **[21, 31, 33]** However, the conversion efficiencies of CZTS-based thin film solar cells are still lower than that of CIGS solar cells, and the innovative fabrication methods in consideration of safety and high conversion efficiency of CZTS-based thin film solar cells are not established yet.

Table 1.2 Research trends of CZTS-based thin film solar cells.

Fabrication method	V_{oc} [mV]	J_{sc} [mA/cm^2]	Fill factor	Conversion efficiency [%]	Absorber type	Ref.
Evaporation	400	6.0	0.277	0.66	CZTS	**[26]**
	377	37.4	0.649	9.15	CZTSe	**[21]**
	423	40.6	0.673	11.6	CZTSe	**[31]**
	422	29.5	0.60	7.51	CZTSSe	**[35]**
Sputtering	610	17.9	0.62	6.77	CZTS	**[28]**
	700	21.3	0.63	9.1	CZTS	**[30]**
	359	20.7	0.43	3.2	CZTSe	**[34]**
	462	22.8	0.621	6.6	CZTSSe	**[36]**
Solution processing	516.9	18.9	0.528	5.14	CZTS	**[37]**
	422.8	38.7	0.619	10.1	CZTSSe	**[22]**
	459.8	34.5	0.698	11.1	CZTSSe	**[38]**
	513.4	35.2	0.698	12.6	CZTSSe	**[32]**
Electrodeposition	540	12.6	0.464	3.16	CZTS	**[39]**
	567	22.0	0.581	7.3	CZTS	**[40]**

1.3.3 Cu_2SnS_3

Cu_2SnS_3 (CTS) is ternary semiconductor which zeroed the zinc ratio of CZTS having similar crystal structure to CZTS-based. CTS has high absorption coefficient of over 10^4 cm^{-1} and band-gap energy of 0.93 to1.77 eV, therefore it is a promising candidate for environmentally compatible, low-cost, nontoxic solar cell materials. **[41-45]** Firstly, Kuku and Fakolujo reported on a solar cell with a conversion efficiency of 0.11% from a CTS absorber layer fabricated by direct evaporation. **[41]** To date, many research organizations have reported the fabrication and characterization of CTS thin film solar cells **[41-58]**. Berg et al. reported on a CTS thin-film solar cell with a 0.54% efficiency using electroplated precursors. **[45]** Koike et al. and Chino et al. reported substrate-type CTS thin film solar cells prepared by the sulfurization of electroplated Cu–Sn precursors and evaporated Cu/Sn stacked precursors with conversion efficiencies of 2.84 and 2.54%, respectively. **[46, 47]** The process of sulfurization by electron beam evaporation in an atmosphere of N_2 and sulfur vapor using Cu–Sn precursors was reported by Aihara and co-workers, and they achieved 2.92% conversion efficiency. **[48, 49]** Recently, Kanai et al. have reported a CTS thin film solar cell with 4.29% conversion efficiency, which was fabricated by co-evaporation and short annealing. **[50]** In addition, as other fabrication processes, sputtering **[51-53]**, solid state reaction **[54-56]**, and pulsed laser deposition **[57, 58]** had been reported. Currently, the conversion efficiencies of CTS thin film solar cells lower than that of CZTS-based solar cells, and it is considered that the one of this factor is low V_{oc}. The high cell performances in CTS thin film solar cell were V_{oc} of 258 mV, J_{sc} of 35.6 mA/cm^2, fill factor of 0.467 and conversion efficiency of 4.29 %. **[50]** On the other hand, that in CZTSSe were V_{oc} of 513.4 mV, J_{sc} of 35.2 mA/cm^2, fill factor of 0.698 and conversion efficiency of 12.6 %, **[32]** and this V_{oc} was approximately double in comparison with the value of CTS. Therefore, it is considered that the improvement of V_{oc} of CTS thin film solar cells greatly contributes to improvement of its conversion efficiencies.

The characteristics of CTS thin film solar cells which have been reported in recent years are shown in Table 1.3.

Table 1.3 Research trends of CTS thin film solar cells.

Fabrication method	V_{oc} [mV]	J_{sc} [mA/cm^2]	Fill factor	Conversion efficiency [%]	Absorber type	Ref.
Electrodeposition and sulfurization	104	17.1	0.304	0.54	CTS	**[45]**
Electron beam evaporation and sulfurization	211	28.0	0.43	2.54	CTS	**[47]**
	242	28.9	0.417	2.92	CTS	**[48]**
	244	29.0	0.385	2.7	CTS	**[49]**
Co-evaporation and short annealing	258	35.6	0.467	4.29	CTS	**[50]**
Sputtering	197	3.60	0.261	0.20	CTS	**[52]**
Pulse laser deposition	260	11.90	0.24	0.82	CTS	**[58]**

1.4 Research objective

The scientific aim of our research is the investigation on the properties of CZTSe and CTS thin film solar cells in the chalcogenide-based photovoltaic devices fabricated using a new preparation process. In order to reduce the CO_2 emission in the worldwide, a low-cost and efficient solar cell have to be developed for the earth. In the CZTS-based thin film solar cells, the highest conversion efficiency was obtained by a hydrazine-based solution deposition process having toxicity **[32]**. On the other hand, as nontoxic processes, the CZTSe thin films are usually fabricated by a two-step process, which consists of precursor preparation followed by annealing. The single-step thermal evaporation process is the technique of only deposition with no annealing, and the simplification of fabrication process is expected. In this process, there are no reports of the fabrication methods using the CZTSe compound for starting materials. Therefore, the first objective of this study is investigation of the characteristics of the CZTSe thin films and solar cells fabricated by the single-step thermal evaporation process using the CZTSe ingots for starting materials. In addition, the effect of annealing of the CZTSe thin films fabricated by thermal evaporation process were investigated. In the CTS thin film solar cells, good cell performances were obtained with Cu/Sn molar ratio of approximately 1.9. **[50]** In addition, there are no reports of the techniques of alkaline metals doping which helped to improve the cell performances of CIGS and CZTS thin film solar cells. Therefore, the second objection of this study is the optimization of the Cu/Sn molar ratio of the CTS thin film solar cells, and investigation of the effect to the cell performances by the alkaline metals doping. Moreover, the values of V_{oc} of CTS thin film solar cells were lower than CIGS and CZTS-based. The band-gap energy of CTS (around 0.93 eV **[48-50]**) is lower than ideal value (around 1.4 eV **[3]**), and it is considered that it is one of the reason of low V_{oc}. The techniques of expansion of the band-gap energy by Ge and Ag doping have been reported in CZTS-based thin film solar cells **[59, 60]**. Therefore, the final objection of this study is investigation of the effect to the cell

performances of the CTS thin film solar cells by Ag doping.

1.5 Outline of this study

The content of the present thesis is described as follows.

In **Chapter 1**, the background including the energy consumption of the world and the energy sources, the introduction of renewable energies which considered the issue of global environment, the spread situation of renewable energy in the world, the introduction of the photovoltaic device as an energy source and the present conditions of the conversion efficiency of solar cells, the research trends of chalcogenide-based solar cells, and the objective of this study are presented.

In **Chapter 2**, the CZTSe thin films and solar cells which varied the Zn molar ratio of evaporation materials are fabricated by the single-step thermal evaporation process, and the CZTSe ingots are used as starting evaporation materials. The compositional, the structural, morphological, optical, and electrical characterization are investigated. In addition, the effects of annealing are investigated.

In **Chapter 3**, the CTS thin films and solar cells are fabricated by sulfurization from the stacked Cu/Sn precursors deposited by sequential evaporation of Sn and Cu elements. The Cu/Sn molar ratio of the evaporation materials is changed, and the optimum value of that is discussed. The compositional, the structural, morphological, and electrical characterization of the fabricated CTS thin films and solar cells are investigated.

In **Chapter 4**, the CTS thin films and solar cells are fabricated by sulfurization from NaF/Cu/Sn stacked precursor deposited by the sequential evaporation of Sn, Cu elements, and NaF. The NaF molar ratio of the evaporation materials is changed, and the effects of NaF

addition on the cell performances of CTS thin film solar cells are discussed, and their properties are investigated.

In **Chapter 5**, the CTS thin films and solar cells with KF addition are fabricated by sulfurization. Two kinds of KF addition methods, two-stage annealing and the use of four-layer precursors, are employed. The quantity of NaF and KF, and the annealing temperature are changed. The effective method of KF addition to improve the cell performances of CTS thin film solar cells are discussed, and their properties are investigated.

In **Chapter 6**, the $(Cu, Ag)_2SnS_3$ (CATS) thin films and solar cells which are Ag doping of CTS are fabricated by sulfurization. The Ag/(Ag+Cu) molar ratio of the evaporation materials is varied, and the effects of Ag doping on the characteristics of CTS thin films and solar cells are investigated, and their properties are discussed.

Finally, the summary of all results obtained was made in **Chapter 7**.

REFERENCES

[1] BP Statistical Review of World Energy 2017.

[2] Intergovernmental Panel on Clime Change (IPCC), Fifth Assessment Report: Climate Change 2013.

[3] W. Shockley, H. J. Queisser, Detailed Balance Limit of Efficiency of p-n Junction Solar Cells, J. Appl. Phys. **32**, 510 (1961).

[4] A. Polman, M. Knight, E. C. Garnett, B. Ehrler, W. C. Sinke, Photovoltaic materials: Present efficiencies and future challenges, Science **352**, aad4424 (2016).

[5] National Renewable Energy Laboratory, NREL.

[6] M. A. Green, K. Emery, Y. Hishikawa, W. Warta, E. D. Dunlop, Solar cell efficiency tables (version 45), Prog. Photovolt. Res. Appl. **23**, 1 (2015).

[7] K. Masuko, M. Shigematsu, T. Hashiguchi, D. Fujishima, M. Kai, N. Yoshimura, T. Yamaguchi, Y. Ichihashi, T. Mishima, N. Matsubara, T. Yamanishi, T. Takahama, M. Taguchi, E. Maruyama, S.Okamoto, Achievement of More Than 25% Conversion Efficiency With Crystalline Silicon Heterojunction Solar Cell, IEEE Journal of Photovoltaics **4**, 1433 (2014).

[8] D. D. Smith, P. J. Cousins, A. Masad, A. Waldhauer, S. Westerberg, M. Johnson, X. Tu, T. Dennis, G. Harley, G. Solomon, S. Rim, M. Shepherd, S. Harrington, M. Defensor, A. Leygo, P. Tomada, J. Wu, T. Pass, L. Ann, L. Smith, N. Bergstrom, C. Nicdao, P. Tipones, D. Vicente, Generation III high efficiency lower cost technology: Transition to full scale manufacturing, Proceedings of the 38th IEEE Photovoltaic Specialists Conference (PVSC), 1594 (2012).

[9] B. M. Kayes, H. Nie, R. Twist, S. G. Spruytte, F. Reinhardt, I. C. Kizilyalli, G. S. Higashi, 27.6% Conversion efficiency, a new record for single-junction solar cell under 1 sun illumination, Proceedings of the 37th IEEE Photovoltaic Specialists Conference (PVSC), 4 (2011).

[10] M. A. Green, K. Emery, Y. Hishikawa, W. Warta, E. D. Dunlop, Solar cell efficiency tables (version 46), Prog. Photovolt. Res. Appl. **23**, 805 (2015).

[11] J. J. Becker, M. Boccard, C. M. Campbell, Y. Zhao, M. Lassise, Z. C. Holman, Y.-H. Zhang, Loss Analysis of Monocrystalline CdTe Solar Cells With 20% Active-Area Efficiency, IEEE Journal of Photovoltaics **7**, 900 (2017).

[12] P. Jackson, R. Wuerz, D. Hariskos, E. Lotter, W. Witte, M. Powalla, Effect of heavy alkali elements in Cu(In,Ga)Se_2 solar cells with efficiencies up to 22.6%, Phys. Status Solidi: Rapid Res. Lett. **10**, 583 (2016).

[13] S.-H. Wei, S. B. Zhang, A. Zunger, Effects of Na on the electrical and structural properties of $CuInSe_2$, J. Appl. Phys. **85**, 7214 (1999).

[14] A. Chirilă, P. Reinhard, F. Pianezzi, P. Bloesch, A. R. Uhl, C. Fella, L. Kranz, D. Keller, C. Gretener, H. Hagendorfer, D. Jaeger, R. Erni, S. Nishiwaki, S. Buecheler, A. N. Tiwari, Potassium-induced surface modification of $Cu(In,Ga)Se_2$ thin films for high-efficiency solar cells, Nat. Mater. **12**, 1107 (2013).

[15] P. Jackson, D. Hariskos, R. Wuerz, W. Wischmann, M. Powalla, Compositional investigation of potassium doped $Cu(In,Ga)Se_2$ solar cells with efficiencies up to 20.8%, Phys. Status Solidi: Rapid Res. Lett. **8**, 219 (2014).

[16] P. Reinhard, B. Bissig, F. Pianezzi, E. Avancini, H. Hagendorfer, D. Keller, P. Fuchs, M. Döbeli, C. Vigo, P. Crivelli, S. Nishiwaki, S. Buecheler, A. N. Tiwari, Features of KF and NaF Postdeposition Treatments of $Cu(In,Ga)Se_2$ Absorbers for High Efficiency Thin Film Solar Cells, Chem. Mater. **27**, 5755 (2015).

[17] D. Herrmann, P. Kratzert, S. Weeke, M. Zimmer, J. D.-Reiss, R. Hunger, P. Lindberg, E. Wallin, O. Lundberg, L. Stolt, CIGS module manufacturing with high deposition rates and efficiencies, Proceedings of the 40th IEEE Photovoltaic Specialists Conference (PVSC), 2775 (2014).

[18] L. M. Mansfield, R. Noufi, C. P. Muzzillo, C. DeHart, K. Bowers, B. To, J. W. Pankow, R. C. Reedy, K. Ramanathan, Enhanced Performance in $Cu(In,Ga)Se_2$ Solar cells Fabricated by the Two-Step Selenization Process With a Potassium Fluoride Postdeposition Treatment, IEEE Journal of Photovoltaics **4**, 1650 (2014).

[19] R. N. Bhattacharya, CIGS-based solar cells prepared from electrodeposited stacked Cu/In/Ga layers, Sol. Energy Mater. Sol. Cells **113**, 96 (2013).

[20] C. Persson, Electronic and optical properties of Cu_2ZnSnS_4 and $Cu_2ZnSnSe_4$, J. Appl. Phys. **107**, 053710 (2010).

[21] I. Repins, C. Beall, N. Vora, C. DeHart, D. Kuciauskas, P. Dippo, B. To, J. Mann, W. C. Hsu, A. Goodrich, R. Noufi, Co-evaporated $Cu_2ZnSnSe_4$ films and devices, Sol. Energy Mater. Sol. Cells **101**, 154 (2012).

[22] S. Bag, O. Gunawan, T. Gokmen, Y. Zhu, T. K. Todorov, D. B. Mitzi, Low band gap liquid-processed CZTSe solar cell with 10.1% efficiency, Energy Environ. Sci. **5**, 7060 (2012).

[23] K. Wang, O. Gunawan, T. Todorov, B. Shin, S. J. Chey, N. A. Bojarczuk, D. Mitzi, S. Guha, Thermally evaporated Cu_2ZnSnS_4 solar cells, Appl. Phys. Lett. **97**, 143508 (2010).

[24] Q. Guo, G. M. Ford, W.-C. Yang, B. C. Walker, E. A. Stach, H. W. Hillhouse, R. Agrawal, Fabrication of 7.2% Efficient CZTSSe Solar Cells Using CZTS Nanocrystals, J. Am. Chem. Soc. **132**, 17384 (2010).

[25] K. Ito, T. Nakazawa, Electrical and Optical Properties of Stannite-Type Quaternary Semiconductor Thin Films, Jpn. J. Appl. Phys. **27**, 2094 (1988).

[26] H. Katagiri, N. Sasaguchi, S. Hando, S. Hoshino, J. Ohashi, T. Yokota, Preparation and evaporation of Cu_2ZnSnS_4 thin films by sulfurization of E-B evaporated precursors, Sol. Energy Mater. Sol. Cells **49**, 407 (1997).

[27] H. Katagiri, Cu_2ZnSnS_4 thin film solar cells, Thin Solid Films **480-481**, 426 (2005).

[28] H. Katagiri, K. Jimbo, S. Yamada, T. Kamiura, W. S. Maw, T. Fukano, T. Motohiro, Enhanced Conversion Efficiencies of Cu_2ZnSnS_4-Based Thin Film Solar Cells by Using Preferential Etching Technique, Appl. Phys. Express **1**, 041201 (2008).

[29] M. A. Green, K. Emery, Y. Hishikawa, W. Warta, E. D. Dunlop, Solar cell efficiency tables (version 47), Prog. Photovolt. Res. Appl. **24**, 3 (2016).

[30] S. Tajima, M. Umehara, M. Hasegawa, T. Mise, T. Itoh, Cu_2ZnSnS_4 photovoltaic cell with improved efficiency fabricated by high-temperature annealing after CdS buffer-layer deposition, Prog. Photovolt. Res. Appl. **25**, 14 (2017).

[31] Y. S. Lee, T. Gershon, O. Gunawan, T. K. Todorov, T. Gokmen, Y. Virgus, S. Guha, $Cu_2ZnSnSe_4$ Thin-Film Solar Cells by Thermal Co-evaporation with 11.6% Efficiency and Improved Minority Carrier Diffusion Length, Adv. Energy Mater. **5**, 1401372 (2015).

[32] W. Wang, M. T. Winkler, O. Gunawan, T. Gokmen, T. K. Todorov, Y. Zhu, D. Mitzi, Device Characteristics of CZTSSe Thin-Film Solar Cells with 12.6% Efficiency, Ext. Abstr. Adv. Energy Mater. **4**, 1301465 (2014).

[33] A. Nagaoka, H. Miyake, T. Taniyama, K. Kakimoto, Y. Nose, M.A. Scarpulla, K. Yoshino, Effects of sodium on electrical properties in Cu_2ZnSnS_4 single crystal, Appl. Phys. Lett. **104**, 152101 (2014).

[34] G. Zoppi, I. Forbes, R. W. Miles, P. J. Dale, J. J. Scragg, L. M. Peter, $Cu_2ZnSnSe_4$ thin film solar cells produced by selenisation of magnetron sputtered precursors, Prog. Photovolt. Res. Appl. **17**, 315 (2009).

[35] B. Shin, K. Wang, O. Gunawan, K. B. Reuter, S. J. Chey, N. A. Bojarczuk, T. Todorov, D. B. Mitzi, S. Guha, High efficiency $Cu_2ZnSn(S_xSe_{1-x})_4$ thin film solar cells by thermal co-evaporation, Proceedings of the 37th IEEE Photovoltaic Specialists Conference (PVSC), 2510 (2011).

[36] R. Lechner, S. Jost, J. Palm, M. Gowtham, F. Sorin, B. Louis, H. Yoo, R. A. Wibowo, R. Hock, $Cu_2ZnSn(S,Se)_4$ solar cells processed by rapid thermal processing of stacked elemental layer precursors, Thin Solid Films **535**, 5 (2013).

[37] K. Woo, Y. Kim, J. Moon, A non-toxic, solution-processed, earth abundant absorbing layer for thin-film solar cells, Energy Environ. Sci. **5**, 5340 (2012).

[38] T. K. Todorov, J. Tang, S. Bag, O. Gunawan, T. Gokmen, Y. Zhu, D. B. Mitzi, Beyond 11% Efficiency: Characteristics of State-of-the-Art $Cu_2ZnSn(S,Se)_4$ Solar Cells, Adv. Energy Mater. **3**, 34 (2013).

[39] H. Araki, Y. Kubo, K. Jimbo, W. S. Maw, H. Katagiri, M. Yamazaki, K. Oishi, A. Takeuchi, Preparation of Cu_2ZnSnS_4 thin films by sulfurization of co-electroplated Cu-Zn-Sn precursors, Phys. Status Solidi C **6**, 1266 (2009).

[40] S. Ahmed, K. B. Reuter, O. Gunawan, L. Guo, L. T. Romankiw, H. Deligianni, A High Efficiency Electrodeposited Cu_2ZnSnS_4 Solar Cell, Adv. Energy Mater. **2**, 253 (2012).

[41] T. A. Kuku, O. A. Fakolujo, Photovoltaic characteristics of thin films of Cu_2SnS_3, Sol. Energy Mater. **16**, 199 (1987).

[42] M. Bouaziz, M. Amlouk, S. Belgacem, Structural and optical properties of Cu_2SnS_3 sprayed thin films, Thin Solid Films **517**, 2527 (2009).

[43] M. Bouaziz, J. Ouerfelli, S. K. Srivastava, J. C. Bernède, M. Amlouk, Growth of Cu_2SnS_3 thin films by solid reaction under sulphur atmosphere, Vacuum **85**, 783 (2011).

[44] D. M. Berg, R. Djemour, L. Gütay, S. Siebentritt, P. J. Dale, X. Fontane, V. Izquierdo-Roca, A. Pérez-Rodriguez, Raman analysis of monoclinic Cu_2SnS_3 thin films, Appl. Phys. Lett. **100**, 192103 (2012).

[45] D. M. Berg, R. Djemour, L. Gutay, G. Zoppi, S. Siebentritt, P. J. Dale, Thin film solar cells based on the ternary compound Cu_2SnS_3, Thin Solid Films **520**, 6291 (2012).

[46] J. Koike, K. Chino, N. Aihara, H. Araki, R. Nakamura, K. Jimbo, H. Katagiri, Cu_2SnS_3 Thin-Film Solar Cells from Electroplated Precursors, Jpn. J. Appl. Phys. **51**, 10NC34 (2012).

[47] K. Chino, J. Koike, S. Eguchi, H. Araki, R. Nakamura, K. Jimbo, H. Katagiri, Preparation of Cu_2SnS_3 Thin Films by Sulfurization of Cu/Sn Stacked Precursors, Jpn. J. Appl. Phys. **51**, 10NC35 (2012).

[48] N. Aihara, H. Araki, A. Takeuchi, K. Jimbo, H. Katagiri, Fabrication of Cu_2SnS_3 thin films by sulfurization of evaporated Cu-Sn precursors for solar cells, Phys. Status Solidi C **10**, 1086 (2013).

[49] N. Aihara, A. Kanai, K. Kimura, M. Yamada, K. Toyonaga, H. Araki, A. Takeuchi, H. Katagiri, Sulfurization temperature dependences of photovoltaic properties in Cu_2SnS_3-based thin-film solar cells, Jpn. J. Appl. Phys. **53**, 05FW13 (2014).

[50] A. Kanai, K. Toyonaga, K. Chino, H. Katagiri, H. Araki, Fabrication of Cu_2SnS_3 thin-film solar cells with power conversion efficiency of over 4%, Jpn. J. Appl. Phys. **54**, 08KC06 (2015).

[51] P. A. Fernandes, P. M. Salomé, A. F. da Chnha, A study of ternary Cu_2SnS_3 and Cu_3SnS_4 thin films prepared by sulfurizing stacked metal precursors, J. Phys. D: Appl. Phys. **43**, 215403 (2010).

[52] Y. Dong, J. He, X. Li, W. Zhou, Y. Chen, L. Sun, P. Yang, J. Chu, Synthesis and optimized sulfurization time of Cu_2SnS_3 thin films obtained from stacked metallic precursors for solar cell application, Mater. Lett. **160**, 468 (2015).

[53] R. Bodeux, J. Leguay, S. Delbos, Influence of composition and annealing on the characteristics of Cu_2SnS_3 thin films grown by cosputtering at room temperature, Thin Solid Films **582**, 229 (2015).

[54] M. Onoda, X. Chen, A. Sato, H. Wada, Crystal structure and twinning of monoclinic Cu_2SnS_3, Mater. Res. Bull. **35**, 1563 (2000).

[55] S. Fiechter, M. Martinez, G. Schmidt, W. Henrion, Y. Tomm, Phase relations and optical properties of semiconducting ternary sulfides in the system Cu-Sn-S, J. Phys. Chem. Solids **64**, 1859 (2003).

[56] D. Tiwari, T. K. Chaudhuri, T. Shripathi, U. Deshpande, Synthesis of earth-abundant Cu_2SnS_3 powder using solid state reaction, J. Phys. Chem. Solids **75**, 410 (2014).

[57] R. B. Ettlinger, A. Cazzaniga, S. Canulescu, N. Pryds, J. Schou, Pulsed laser deposition from ZnS and Cu_2SnS_3 multicomponent targets, Appl. Surf. Sci. **336**, 385 (2015).

[58] S. A. Vanalakar, G. L. Agawane, A. S. Kamble, C. W. Hong, P. S. Patil, J. H. Kim, Fabrication of Cu_2SnS_3 thin film solar cells using pulsed laser deposition technique, Sol. Energy Mater. Sol. Cells **138**, 1 (2015).

[59] M. Morihama, F. Gao, T. Maeda, T. Wada, Crystallographic and optical properties of $Cu_2Zn(Sn_{1-x}Ge_x)Se_4$ solid solution, Jpn. J. Appl. Phys. **53**, 04ER09 (2014).

[60] W. Gong, T. Tabata, K. Takei, M. Morihama, T. Maeda, T. Wada, Crystallographic and optical properties of (Cu, $Ag)_2ZnSnS_4$ and (Cu, $Ag)_2ZnSnSe_4$ solid solutions, Phys. Status Solidi C **12** 700, (2015).

CHAPTER 2

$Cu_2ZnSnSe_4$ thin film solar cells fabricated by thermal evaporation

2.1 Introduction

In recent years, $Cu(In,Ga)Se_2$ (CIGS) thin-film solar cells have achieved the conversion efficiency as high as 20 % **[1,2]**; however, their mass production is limited by the availability of In and Ga rare metals, which makes earth-abundant copper-zinc-tin-chalcogen-based kesterites (not containing any rare metals) such as Cu_2ZnSnS_4 (CZTS), $Cu_2ZnSnSe_4$ (CZTSe), and $Cu_2ZnSn(S,Se)_4$ (CZTSSe)) good substitute materials for solid cell manufacturing. CZTS-

based are p-type semiconductor with direct band-gap energy of 1.0‑1.5 eV and have high optical absorption coefficient of around 10^4 cm^{-1} **[3]**. Firstly, CZTS thin films fabricated by atom beam sputtering of quaternary target compounds were reported by Ito et al. **[4]**, while the high conversion efficiency was achieved for CZTS thin-film solar cells fabricated by a two-layered process **[5, 6]**. Grossberg et al. described the preparation of CZTSSe solid solutions from CuSe(S), ZnS(Se), and SnSe(S) precursors for manufacturing CZTSSe-based solar cells **[7]**, and Levcenco et al. reported CZTSSe thin films produced by a chemical vapour transport technique **[8]**. Furthermore, Todorov et al. fabricated CZTSSe thin film solar cells with an efficiency of 9.7 % using solution-based deposition techniques **[9]**. As of today, the CZTSSe thin film solar cells manufactured by a hydrazine-based solution deposition process have achieved the record efficiency (for CZTS-based solar cells) equal to 12.6 % **[10]**, while the CZTSe thin film solar cells fabricated in 1997 by thermal co-evaporation of Cu, ZnSe, Sn, and Se were characterized by the efficiency of only 0.6 % **[11]**. Wibowo et al. reported the preparation of CZTSe thin films by RF magnetron sputtering of binary chalcogenide targets **[12]**, and Zoppi et al. fabricated thin-film solar cells with a conversion efficiency as high as 3.3 % by selenization of magnetron-sputtered precursors **[13]**. The conversion efficiency of 7.14 % was obtained by Kim et al. for thin film solar cells manufactured from CTSe and ZnSe precursors, which were annealed in $SnSe_2$ and Se vapours under N_2 flow **[14]**. In addition, Brammertz et al. reported the conversion efficiency of 9.7 % for solar cells produced by vacuum sputtering of Cu, Zn, and Sn targets followed by selenization in H_2Se atmosphere **[15]**, while Oueslati et al. achieved the conversion efficiency of 10.4 % using the same method **[16]**. Moreover, Repins et al. fabricated CZTSe solar cells with a conversion efficiency of 9.15 % by thermal co-evaporation of Cu, Zn, Sn, and Se on NaF/Mocoated soda-lime glass (SLG) substrates **[17]**, while the record conversion efficiency of 11.6 % was reported by Lee et al. for thin films deposited on the NaF/Mo/SLG substrates by four-source thermal co-evaporation

combined with selenization **[18]**. Previously, we have synthesized CZTSe ingots and then used them as evaporation materials to prepare precursors for the selenization process and obtained thin films characterized by an open-circuit voltage (V_{oc}) of 275 mV and short-circuit current density (J_{sc}) of 9.53 mA/cm^2 **[19]**. The CZTSe thin films are usually fabricated by a two-step process, which consists of precursor preparation followed by annealing. Sabli et al. reported the preparation of CZTSe thin films by thermal vacuum deposition process using CZTSe compound, however, solar cell performances have not been yet reported **[20–22]**.

2.2 Objective of this study

In this study, the CZTSe thin films were prepared from CZTSe compound by an industrial single-step evaporation process (which contains only the deposition stage) and then utilized for manufacturing solar cells for the first time. In the process of single element evaporation, it is considered that the lack of Sn and Zn occurs by re-evaporation, because of these high vapor pressures. On the other hand, in the process using CZTSe compound for evaporation material, it is estimated that the control of the composition of thin film is easy by suppression of that phenomenon. Furthermore, a single-step evaporation process is one of the low-cost fabrication process of solar cell which does not need the facilities such as electric furnaces in comparison with a two-step process. We have investigated the compositional, structural, morphological, optical, and electrical characterizations of thin films and solar cells fabricated by a single-step evaporation process using CZTSe compound. In addition, the effect of annealing on the morphology and compositions of these thin films and solar cells were investigated. The fabrication method of CZTSe thin film solar cells using CZTSe ingots in this chapter is the first method without precedent.

2.3 Experimental procedure

CZTSe thin films were fabricated at substrate temperatures and evaporation times specified in Figure 2.1. First, substrates were pre-heated for 5 min at 600 °C with the subsequent evaporation of CZTSe compound at a substrate temperature of 300 °C. Next, Zn, Sn, and Se were co-evaporated at a substrate temperature of 575 °C followed by Na_2Se evaporation. As a result of preliminary experiment, the solar cell which was fabricated by evaporation of only CZTSe compound did not generate electricity with the defect of the absorber layer and lack of Zn. In addition, Redinger et al. have reported that the solar cell performances were improved by crystallization with Sn and Se **[23]**, and Repins et al. have achieved high conversion efficiency in CZTSe thin film solar cell by using the technique of alkaline metals doping. **[17]** From the above, the third stage (Zn + Sn + Se) and the fourth stage (Na_2Se) of the evaporation material profile in this study were added to improve the solar cell performances. In the first experiment, the Zn content was varied between 2.0 and 3.0 at a constant contents for the remaining evaporation materials equal to Zn : Sn : CZTSe : Na_2Se = x : 1.2 : 1.2 : 0.024 (x = 2.0 and 3.0). In the CZTS thin film solar cell, Katagiri and Jinbo reported the high conversion efficiencies are obtained by Zn-rich composition. **[24]** Therefore, in the CZTSe thin film solar cell, it is considered that the high conversion efficiency may be obtained by Zn-rich composition, and the Zn and Sn contents of evaporation materials in this study were decided to the Zn/Sn molar ratios of 1.67 and 2.5 to become Zn-rich composition. In addition, the amount of as-deposited Se was maintained constant at 2.0 g. In the second experiment, the as-deposited CZTSe thin films were first placed inside vacuum-sealed glass ampoules containing elemental Se and Sn shots and then annealed under mixed Se and Sn atmosphere with a Sn/Se molar ratio of 0.2 for 30 min at 500 °C.

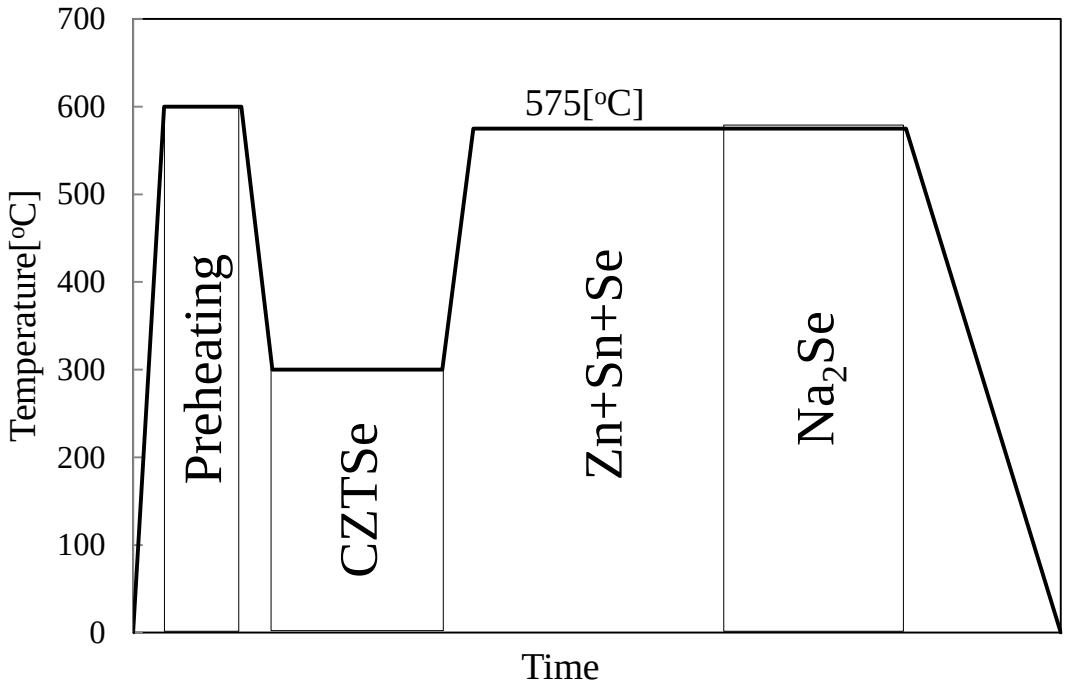

Figure 2.1 Substrate temperatures and the related evaporation material profile.

Figure 2.2 shows the structure of the CZTSe thin film solar cells in this study. Solar cells with a configuration of Al grid contact/Ga-doped ZnO transparent conducting layer/non-doped ZnO/CdS buffer layer/CZTSe absorber layer/Mo back contact/SLG substrate were fabricated using the following steps. CdS buffer layers of n-type semiconductor with thicknesses of 70 nm were deposited by a chemical bath deposition technique, while i-ZnO buffer layers with thicknesses of 50 nm were produced by radio frequency magnetron sputtering. Transparent conductive ZnO:Ga films with thicknesses of 0.4 μm were subsequently deposited by direct current magnetron sputtering of 3 wt. % Ga_2O_3-doped ZnO targets at a substrate temperature of 100 °C, and Al grids for the front electrode were produced from metal masks by vacuum evaporation. The sizes of the obtained solar cells without antireflection coatings were 5 × 5 mm^2. Compositions of the obtained thin films were determined from the results of the electron

probe microanalysis (EPMA) performed by energy dispersive spectrometry (EDS); their crystalline structure was examined by X-ray diffraction (XRD) and Raman spectroscopy (JASCO, NRS-1000) using incident laser light with wavelength of 532 nm and power density of 0.9 mW (with a 100× magnification lens), while their morphologies were studied by scanning electron microscopy (SEM). Current-voltage (J-V) characteristics and quantum efficiencies (QE) of the fabricated solar cells were measured using standard 1 sun (AM1.5, 100 mW/cm^2) illumination.

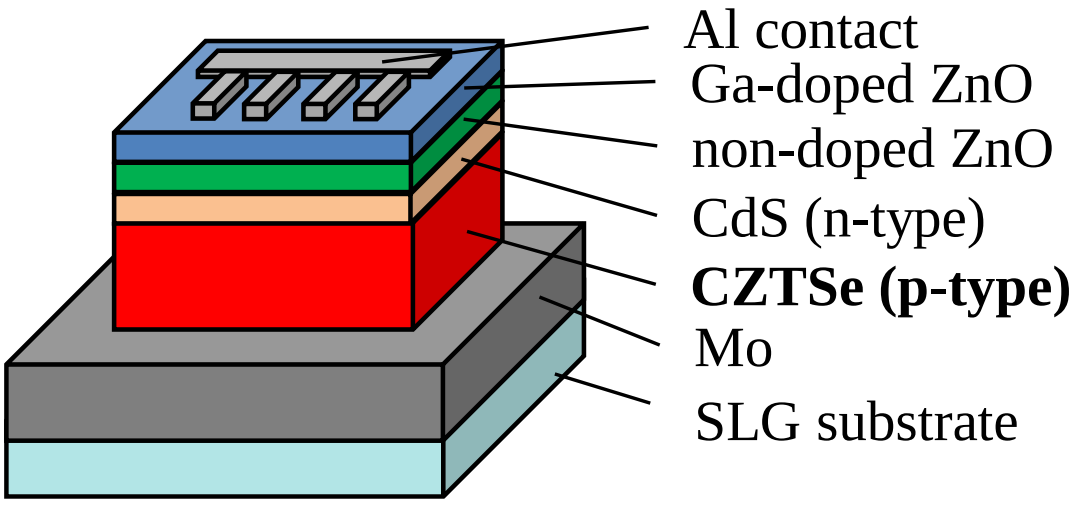

Figure 2.2 Structure of the CZTSe thin film solar cell.

2.4 Results and discussions

2.4.1 Film compositions

From EPMA analysis, the composition ratio of the as-deposited CZTSe thin film with a Zn content of 2.0 was Cu : Zn : Sn : Se = 22.7 : 13.5 : 13.8 : 50.0, and the composition ratio of the annealed CZTSe thin film with a Zn content of 2.0 was Cu : Zn : Sn : Se = 18.2 : 18.9 : 12.2 : 50.7. Figure 2.3 shows the dependence of the film composition determined by the EPMA analysis on the Zn content for the evaporation material utilized for manufacturing the as-deposited and annealed thin films. From these, the Sn content in the films decreased and the Zn content increased after annealing owing to Sn re-evaporation.

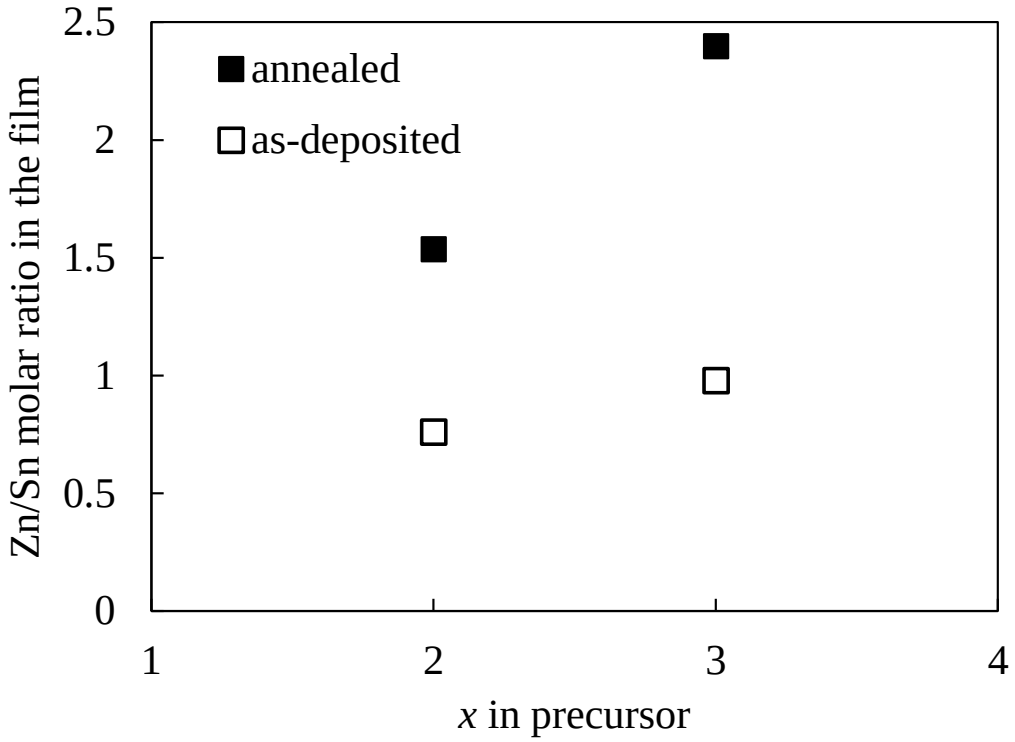

Figure 2.3 Dependence of the Zn/Sn molar ratio for the obtained films on the Zn content *x* in the evaporation materials.

2.4.2 Crystal structure

Figure 2.4 displays the XRD patterns for the as-deposited and annealed CZTSe thin films with a kesterite CZTSe structure indicating the presence of an additional SnSe phase in the as-deposited thin films. This extra SnSe phase disappeared after annealing, therefore it is considered that a single phase CZTSe was formed by promotion of the crystallization with annealing. In addition, it is considered that it affected increase of re-evaporation of Sn, consequently the Sn content in annealed films were decreased even though annealing under mixed Se and Sn atmosphere. Furthermore, an additional $MoSe_2$ peak observed for the annealed thin films.

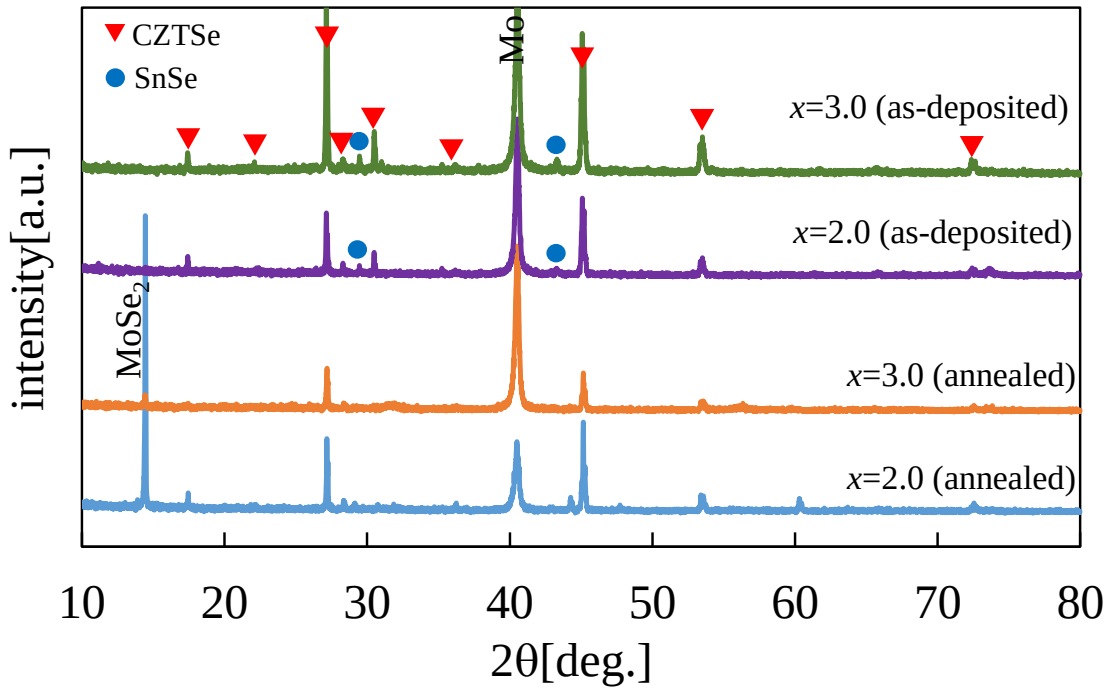

Figure 2.4 XRD patterns for the thin films produced by single-step evaporation with subsequent annealing at various Zn content.

Figure 2.5 shows the Raman spectra for the as-deposited and annealed CZTSe thin films, which are characterized by two dominant peaks at 172 cm^{-1} and 194 cm^{-1} corresponding to the CZTSe kesterite structure; the obtained data are in good agreement with the results reported earlier by Oueslati et al. **[16]** and by Juskenas et al. **[25]**. Furthermore, the Raman SnSe peaks at 108 cm^{-1}, 130 cm^{-1}, and 150 cm^{-1} detected by Fernandes et al. **[26]** were not observed for any of the samples indicating that the additional SnSe phase was formed in the vicinity of the Mo layer from XRD patterns.

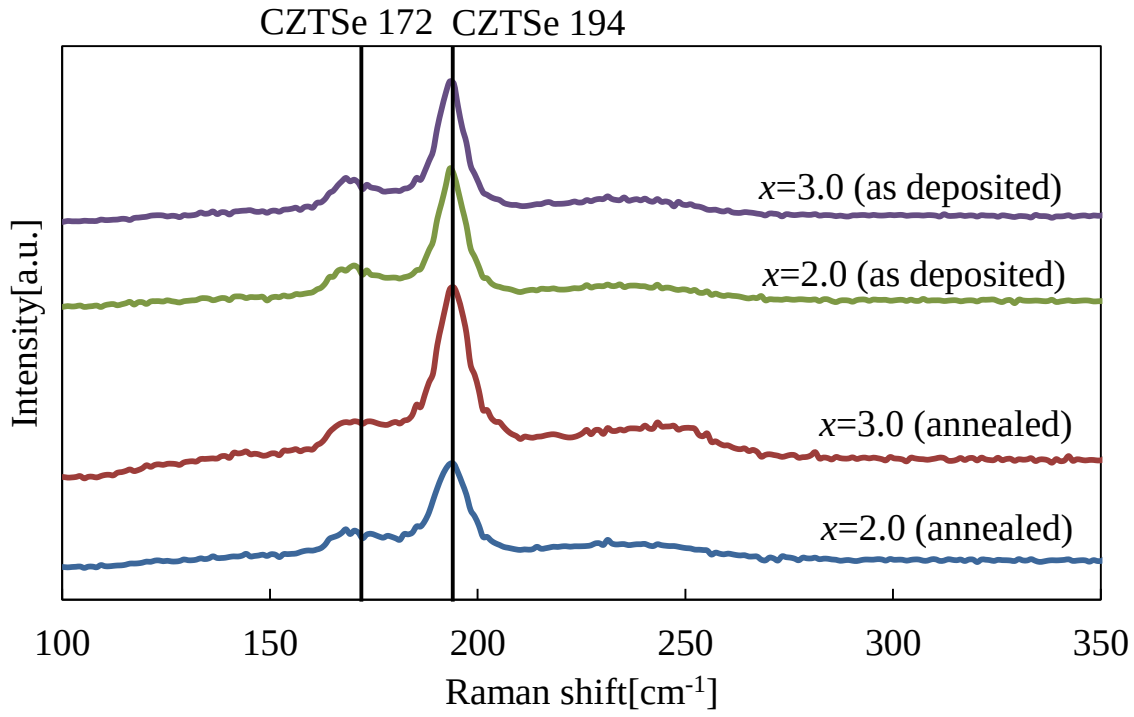

Figure 2.5 Raman spectra for the thin films prepared by single-step evaporation with subsequent annealing at various Zn content.

2.4.3 Film morphologies

The surface and cross-section morphologies for the as-deposited and annealed CZTSe thin films produced at various Zn content in the evaporation materials are depicted in Figure 2.6, which shows the increase in grain sizes for the fabricated CZTSe films after annealing; however, the formation of voids observed inside the annealed thin films could be also caused by the Sn re-evaporation during the annealing process. Furthermore, from cross-section morphologies, the change of thickness of $MoSe_2$ was not seen in the as-deposited thin films and the annealed thin films, so, it is considered that the remarkable changes of the back contact were nothing.

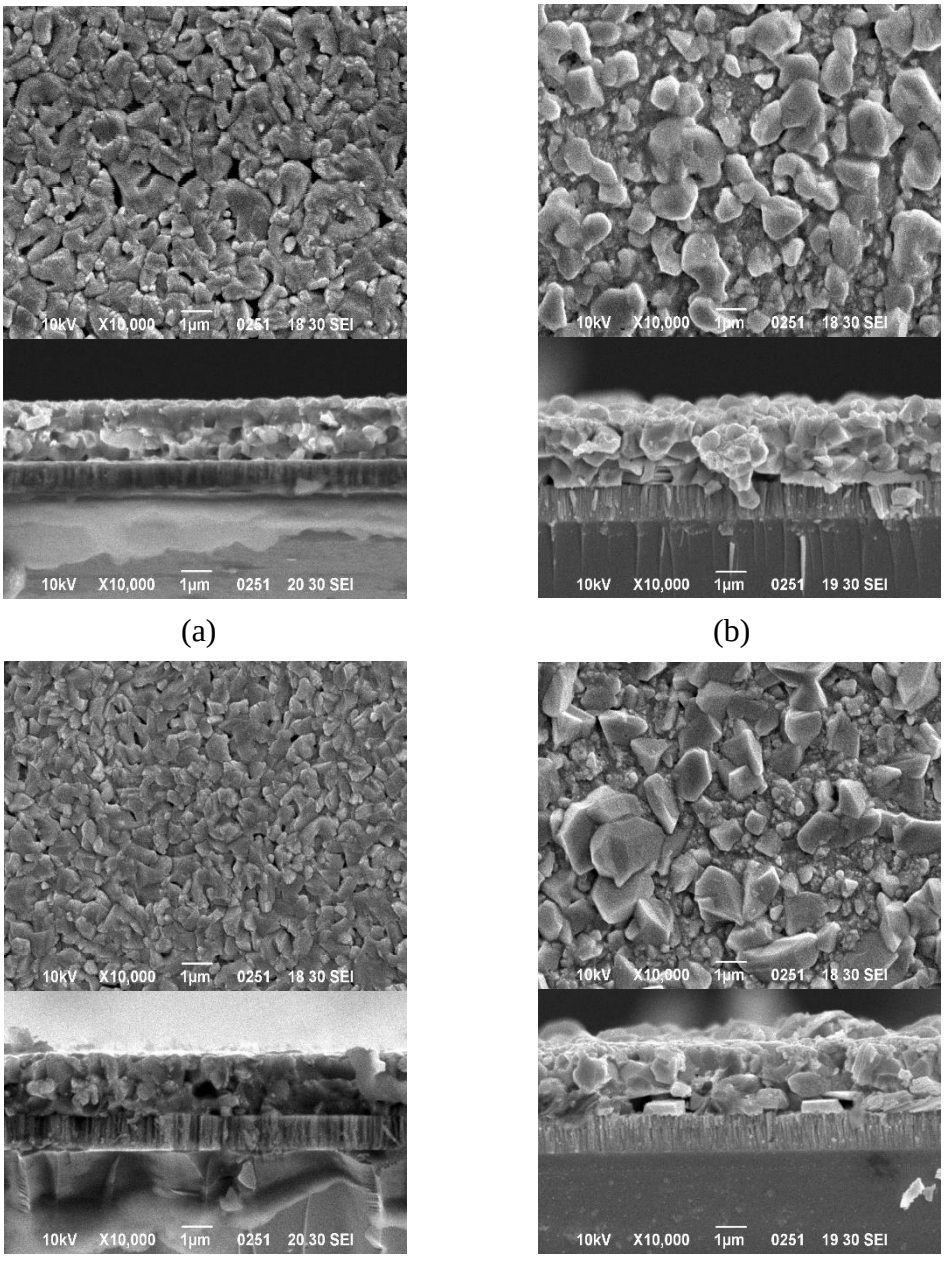

Figure 2.6 SEM micrographs of the surface and cross-sections of the CZTSe thin films prepared by single-step evaporation with or without subsequent annealing at Zn content of (a) 2.0 (as-deposited), (b) 2.0 (annealed), (c) 3.0 (as-deposited), and (d) 3.0 (annealed).

2.4.4 Cell performances

The J-V curves for the CZTSe thin film solar cells fabricated in this study are shown in Figure 2.7. The measured values of J_{sc} decreased, while the magnitudes of V_{oc} increased as compared with the corresponding values for the as-deposited samples. The best solar cell in this study fabricated from the as-deposited thin film with a Zn content of 2.0 was characterized by V_{oc} = 240 mV, J_{sc} = 27.6 mA/cm^2, Fill factor (FF) = 0.41, and conversion efficiency (η) = 2.76 %, while the cell performances of the solar cells fabricated by the single-step evaporation process were better than the annealing process added. However, V_{oc}, J_{sc} and FF are lower than the top data of the CZTSe thin film solar cell, and the best conversion efficiency in this study is around a quarter of the value of top data **[18]**. For improvement of cell performances, it is necessary to adjust our fabrication process about the control of thin film composition and the improvement of the quality of thin film.

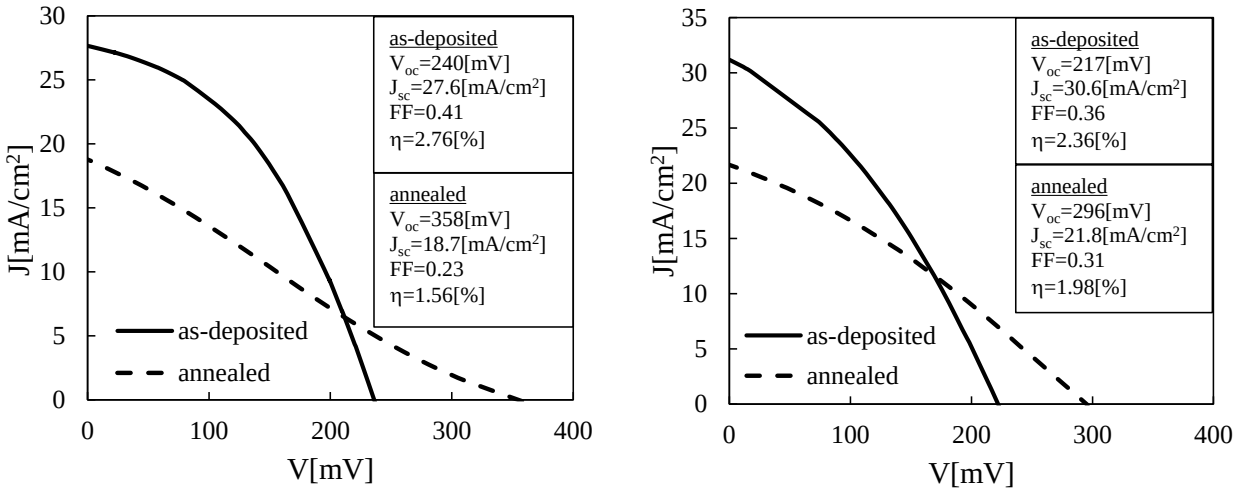

Figure 2.7 J–V characteristics of the CZTSe thin film solar cells fabricated by single-step evaporation with subsequent annealing at Zn content of (a) 2.0 and (b) 3.0.

2.4.5 Quantum efficiencies

Figure 2.8 shows the QE curves for the CZTSe thin film solar cells measured at a white light irradiation density of 1.57 mW/cm^2, indicating that the QE in the short-wavelength range below 500 nm was improved during annealing. However, the QE of the annealed samples deteriorated in comparison with that for the as-deposited samples across the long-wavelength range. Furthermore, the optical absorption for the as-deposited samples was observed at wavelengths above 1400 nm, while the absorption edge for the annealed samples was shifted to around 1250 nm. The value of QE of annealed samples between 500 and 1100 nm became lower than 50% of the data of the CZTS-based thin film solar cell which achieved the highest conversion efficiency **[10]**. It is considered that this cause is a small diffusion length of minority carrier by the defect of the CZTSe which is the absorber layer in annealed samples. In the as-deposited samples, it is considered that the absorption edge are over 1400 nm. From this, it is estimated that the band-gap energy is smaller than 0.88eV from $E_g = hc/q\lambda$ (wherein E_g is band-gap energy, h is Planck's constant, c is velocity of light, q is the electron charge and λ is wavelength of the absorption edge.). Assuming a very short minority carrier diffusion length, for a direct transition, a plot of $[h\nu \times \ln(1-QE)]^2$ against $h\nu$ (wherein ν is c/λ.) can be used to extrapolate the band-gap energy **[13]**. Sample transition energies were estimated by extrapolating the measured QE values, and the obtained band-gap energy for the annealed sample was equal to 1.06 eV, which was close to the early reported values for the CZTSe thin films **[3, 27]**. The absorption edge of CZTSe (with a band-gap energy equal to 1.0 eV) is 1240 nm, therefore, it is considered that the quantum efficiencies at wavelengths above 1240 nm in the as-deposited samples were caused by a material unlike CZTSe. The absorption edge of SnSe (with a band-gap energy equal to 0.86 eV **[28]**) is 1460 nm, and it is in good agreement with the obtained QE results in the as-deposited samples. Therefore, it is considered that the quantum efficiencies of high wavelengths in the as-deposited samples were caused by SnSe. From the above, it is considered that the SnSe

is coexisting with the CZTSe in the as-deposited samples. This assumption is in good agreement with the obtained XRD results for the additional SnSe phase in the as-deposited samples. The characteristics of the as-deposited solar cells depend on the CZTSe and SnSe, and it can be concluded that the proposed single-step evaporation process can be effectively used to fabricate thin films with wide QE ranges. Moreover, it is considered that these solar cells with narrow band-gap energies such as 1.06 eV and 0.86 eV fabricated by the proposed processes can be applied to the bottom device of the tandem solar cells.

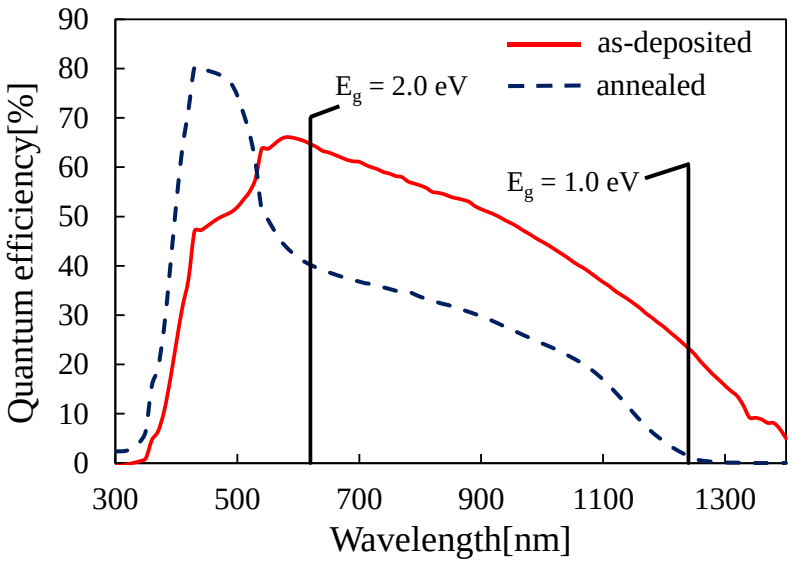

(a)

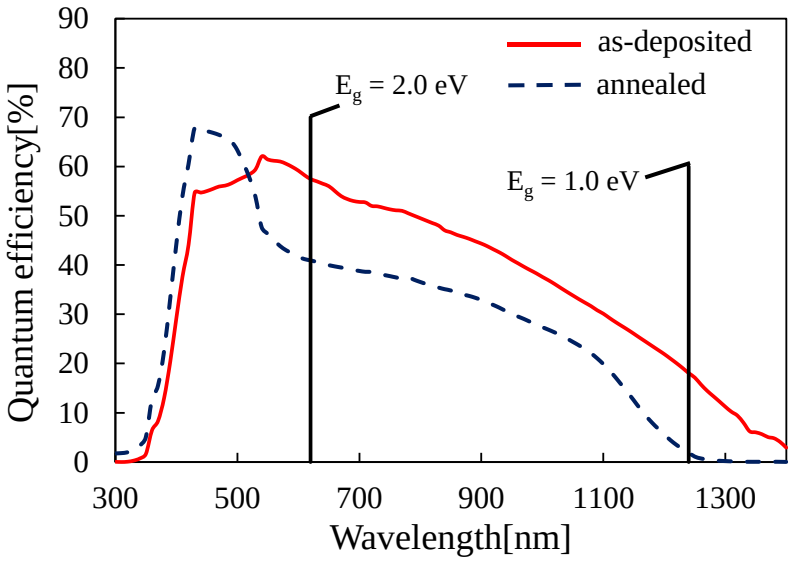

(b)

Figure 2.8 QE of the CZTSe thin film solar cells fabricated by single-step evaporation with subsequent annealing at Zn content of (a) 2.0 and (b) 3.0.

2.5 Conclusions

CZTSe thin films were successfully fabricated by using the new single-step evaporation process, and the effect of the additional annealing stage on the morphology and composition of the produced films was investigated. For all samples, both the obtained XRD patterns and Raman spectra exhibited features corresponding to the CZTSe kesterite structure. Furthermore, the additional SnSe phase formed in the vicinity of the Mo layer in the thin films fabricated by single-step evaporation completely disappeared after subsequent annealing. The grain sizes for the produced CZTSe thin films increased with annealing; however, their structure also contained some voids. The best solar cell in this study fabricated at a Zn content in the evaporation material equal to 2.0 without the annealing stage was characterized by V_{oc} = 240 mV, J_{sc} = 27.6 mA/cm^2, FF = 0.41, and η = 2.76 %. The obtained results of the QE measurements revealed that the solar cells fabricated by the single-step evaporation process exhibited QE variations in the wide wavelength range between 350 nm and 1400 nm. It means that the light with long wavelength of more than 1200nm is able to be used for generation effectively, and it may more increase the J_{sc}. Furthermore, it is considered that the solar cells which were fabricated by this proposed method having wide QE ranges are able to be applied for bottom cells of the tandem type solar cells and photosensor of the long wavelength range. In the solar cells, single-phase CZTSe without foreign phase of SnSe which has about 1.0 eV band-gap energy may improve the cell performances than the CZTSe coexisting with SnSe which has about 0.86 eV band-gap energy according to the Shocley and Queisser limits **[29]**. Therefore, it is important to investigate the fabrication of the single-phase CZTSe by the proposed method. Our group progressed this proposed method by adjustment of fabrication conditions and succeeded in fabricating single-phase CZTSe thin film solar cell without SnSe, which demonstrated 3.93% conversion efficiency **[30]**. I will continue investigation of the single-phase CZTSe solar cell by the proposed method.

REFERENCES

[1] P. Jackson, D. Hariskos, R.Wuerz, O. Kiowski, A. Bauer, T.M. Friedlmeier, M. Powalla, Properties of Cu(In,Ga)Se_2 solar cells with new record efficiencies up to 21.7%, Phys. Status Solidi Rapid Res. Lett. **9**, 28 (2015).

[2] A. Chirilă, P. Reinhard, F. Pianezzi, P. Bloesch, A. R. Uhl, C. Fella, L. Kranz, D. Keller, C. Gretener, H. Hagendorfer, D. Jaeger, R. Erni, S. Nishiwaki, S. Buecheler, A. N. Tiwari, Potassium-induced surface modification of Cu(In,Ga)Se_2 thin films for high-efficiency solar cells, Nat. Mater. **12**, 1107 (2013).

[3] C. Persson, Electronic and optical properties of Cu_2ZnSnS_4 and $Cu_2ZnSnSe_4$, J. Appl. Phys. **107**, 053710 (2010).

[4] K. Ito, T. Nakazawa, Electrical and Optical Properties of Stannite-Type Quaternary Semiconductor Thin Films, Jpn. J. Appl. Phys. **27**, 2094 (1988).

[5] S. Tajima, T. Itoh, H. Hazama, K. Ohishi, R. Asahi, Improvement of the open-circuit voltage of Cu_2ZnSnS_4 cells using a two-layered process, Proceedings of the 40th IEEE Photovoltaic Specialists Conference (PVSC), 0431 (2014).

[6] S. Tajima, M. Umehara, M. Hasegawa, T. Mise, T. Itoh, Cu_2ZnSnS_4 photovoltaic cell with improved efficiency fabricated by high-temperature annealing after CdS buffer-layer deposition, Prog. Photovolt. Res. Appl. **25**, 14 (2017).

[7] M. Grossberg, J. Krustok, J. Raudoja, K. Timmo, M. Altosaar, T. Raadik, Photoluminescence and Raman study of $Cu_2ZnSn(Se_xS_{1-x})_4$ monograins for photovoltaic applications, Thin Solid Films **519**, 7403 (2011).

[8] S. Levcenco, D. Dumcenco, Y. P.Wang, Y. S. Huang, C. H. Ho, E. Arushanov, V. Tezlevan, K. K. Tiong, Influence of anionic substitution on the electrolyte electroreflectance study of band edge transitions in single crystal $Cu_2ZnSn(S_xSe_{1-x})_4$ solid solutions, Opt. Mater. **34**, 1362 (2012).

[9] T. K. Todorov, K. B. Reuter, D. B. Mitzi, High-Efficiency Solar Cell with Earth-Abundant Liquid-Processed Absorber, Adv. Mater. **22**, E156 (2010).

[10] W. Wang, M. T. Winkler, O. Gunawan, T. Gokmen, T. K. Todorov, Y. Zhu, D. Mitzi, Device Characteristics of CZTSSe Thin-Film Solar Cells with 12.6% Efficiency, Ext. Abstr. Adv. Energy Mater. **4**, 1301465 (2014).

[11] T. M. Friedlmeier, N. Wieser, T. Walter, H. W. Schock, Heterojunctions Based on Cu_2ZnSnS_4 and $Cu_2ZnSnSe_4$ Thin Films, Proceedings of the 14th European Photovoltaic Solar Energy Conference (EUPVSEC), 1242 (1997).

[12] R. A. Wibowo,W. S. Kim, E. S. Lee, B. Munir, K. H. Kim, Single step preparation of quaternary $Cu_2ZnSnSe_4$ thin films by RF magnetron sputtering from binary chalcogenide targets, J. Phys. Chem. Solids **68**, 1908 (2007).

[13] G. Zoppi, I. Forbes, R. W. Miles, P. J. Dale, J. J. Scragg, L. M. Peter, $Cu_2ZnSnSe_4$ thin film solar cells produced by selenisation of magnetron sputtered precursors, Prog. Photovolt. Res. Appl. **17**, 315 (2009).

[14] K. M. Kim, K. H. Liao, H. Tampo, H. Shibata, S. Niki, $Cu_2ZnSnSe_4$ thin-film solar cells fabricated using Cu_2SnSe_3 and ZnSe bilayers, Appl. Phys. Express **8**, 042301 (2015).

[15] G. Brammertz, M. Buffiere, S. Oueslati, H. ElAnzeery, O. Touayar, C. Koble, J. Bekaert, M. Meuris, J. Poortmans, Characterization of defects in 9.7% efficient $Cu_2ZnSnSe_4$-CdS-ZnO solar cells, Appl. Phys. Lett. **103**, 163904 (2013).

[16] S. Oueslati, G. Brammertz, M. Buffiere, H. ElAnzeery, O. Touayar, C. Koble, J. Bekaert, M. Meuris, J. Poortmans, Physical and electrical characterization of high-performance $Cu_2ZnSnSe_4$ based thin film solar cells, Thin Solid Films **582**, 224 (2015).

[17] I. Repins, C. Beall, N. Vora, C. DeHart, D. Kuciauskas, P. Dippo, B. To, J. Mann, W. C. Hsu, A. Goodrich, R. Noufi, Co-evaporated $Cu_2ZnSnSe_4$ films and devices, Sol. Energy Mater. Sol. Cells **101**, 154 (2012).

[18] Y. S. Lee, T. Gershon, O. Gunawan, T. K. Todorov, T. Gokmen, Y. Virgus, S. Guha, $Cu_2ZnSnSe_4$ Thin-Film Solar Cells by Thermal Co-evaporation with 11.6% Efficiency and Improved Minority Carrier Diffusion Length, Adv. Energy Mater. **5**, 1401372 (2015).

[19] M. Nakashima, T. Yamaguchi, K. Kusumoto, S. Yukawa, J. Sasano, M. Izaki, Fabrication of $Cu_2ZnSnSe_4$ thin films by selenization of precursor using $Cu_2ZnSnSe_4$ compound for photovoltaic applications, Phys. Status Solidi C **12**, 729 (2015).

[20] N. Sabli, Z. A. Talib, W. M. M. Yunus, Z. Zainal, H. S. Hilal, M. Fujii, Effect of Argon Gas on Photoelectrochemical Characteristics of Film Electrodes Prepared by Thermal Vacuum Evaporation from Synthesized Copper Zinc Tin Selenide, Int. J. Electrochem. Sci. **8**, 10910 (2013).

[21] N. Sabli, Z. A. Talib, W. M. M. Yunus, Z. Zainal, H. S. Hilal, M. Fujii, New Technique for Efficiency Enhancement of Film Electrodes Deposited by Argon Gas Condensation from Metal Chalcogenide Sources, Int. J. Electrochem. Sci. **8**, 12038 (2013).

[22] N. Sabli, Z. A. Talib, W. M. M. Yunus, Z. Zainal, H. S. Hilal, M. Fujii, Film electrodes deposited from Cu_2SnSe_3 source in comparison with those deposited from SnSe and $Cu_2ZnSnSe_4$ sources by thermal vacuum evaporation: Effect of argon gas flow rate, Electrochim. Acta **139**, 238 (2014).

[23] A. Redinger, D. M. Berg, P. J. Dale, S. Siebentritt, The Consequences of Kesterite Equilibria for Efficient Solar Cells, J. Am. Chem. Soc. **133**, 3320 (2011).

[24] H. Katagiri, Development of Cu2ZnSnS4 (CZTS)-based Thin Film Solar Cells Using Abundant Materials, J. Vac. Soc. Jpn. **55**, 548 (2012).

[25] R. Juskenas, S. Kanapeckaite, V. Karpaviciene, Z. Mockus, V. Pakstas, A. Selskiene, R. Giraitis, G. Niaura, A two-step approach for electrochemical deposition of Cu-Zn-Sn and Se precursors for CZTSe solar cells, Sol. Energy Mater. Sol. Cells **101**, 277 (2012).

[26] P. A. Fernandes, M. G. Sousa, P. M. P. Salomé, J. P. Leitão, A. F. da Cunha, Thermodynamic pathway for the formation of SnSe and $SnSe_2$ polycrystalline thin films by selenization of metal precursors, CrystEngComm **15**, 10278 (2013).

[27] S. Ahn, S. Jung, J. Gwak, A. Cho, K. Shin, K. Yoon, D. Park, H. Cheong, J. H. Yun, Determination of band gap energy (E_g) of $Cu_2ZnSnSe_4$ thin films: On the discrepancies of reported band gap values, Appl. Phys. Lett. **97**, 021905 (2010).

[28] L. Zhao, S. Lo, Y. Zhang, H. Sun, G. Tan, C. Uher, C. Wolverton, V. P. Dravid, M. G. Kanatzidis, Ultralow thermal conductivity and high thermoelectric figure of merit in SnSe crystals, Nature **508**, 373 (2014).

[29] W. Shockley, H. J. Queisser, Detailed Balance Limit of Efficiency of p-n Junction Solar Cells, J. Appl. Phys. **32**, 510 (1961).

[30] T. Yamaguchi, T. Yamada, M. Nakashima, J. Sasano, M. Izaki, NaF Addition to $Cu_2ZnSnSe_4$ Thin Films Prepared by Sequential Evaporation from Compound, J. Nanoelectron. Optoelectron, **12**, 976 (2017).

CHAPTER 3

Cu_2SnS_3 thin film solar cells fabricated by sulfurization from Cu/Sn stacked precursors

3.1 Introduction

Ternary I_2-IV-VI_3 semiconductors, such as Cu_2SnS_3 (CTS), have been actively investigated as promising candidates for environmentally friendly, low-cost, nontoxic solar cell materials. CTS has band-gap energy of around 0.93–1.77 eV and a high absorption coefficient on the order of 10^4 cm^{-1} **[1–5]**. The first such report was by Kuku and Fakolujo, who reported CTS thin film solar cells fabricated by direct evaporation with conversion efficiency of 0.11 % **[1]**. Li et al.

used a solvothermal process to grow nanocrystalline CTS with a triclinic structure **[6]**. Onoda et al. characterized CTS with monoclinic structure prepared by conventional solid-state reaction **[7]**. CTS thin films were deposited using a spray-pyrolysis technique by Bouaziz et al. **[2]**. Berg et al. reported CTS thin film solar cell with 0.54 % conversion efficiency using electroplated precursors **[5]**. Furthermore, Chen et al. fabricated super straight-type CTS thin film solar cells for first time with 1.97 % conversion efficiency **[8]**. Subsequently, many other groups have reported CTS thin films and solar cells fabricated by several techniques, including sulfurization **[9–13]**, co-evaporation **[14]**, screen printing **[15]**, spin coating **[16]**, chemical deposition **[17]**, solvothermal process **[18]**, solid-state reaction **[19]**, spray-pyrolysis **[20]**. In particular, Kanai et al. reported good cell performances of CTS thin film solar cells with 4.29 % conversion efficiency using the method of coevaporation and short annealing. **[12]** In their report, the highest conversion efficiency was obtained with high annealing temperature of 570 ^{o}C and Cu/Sn molar ratio of 1.87.

3.2 Objective of this study

In this study, CTS thin films were prepared by crystallization in sulfur and tin mixing atmosphere from the stacked Cu/Sn precursors deposited by sequential evaporation of Sn and Cu elements. We have investigated the compositional, structural, morphological, and electrical characterizations of these thin films and solar cells. The aim of this chapter is investigation of the influence of the Cu/Sn molar ratio on the CTS thin film solar cell performances, and the optimum value of the Cu/Sn molar ratio of the CTS thin film solar cells have discussed. In addition, we have investigated the difference in composition of the depth direction of CTS thin films.

3.3 Experimental procedure

The stacked Sn/Cu precursor was deposited on Mo/soda lime glass substrate by sequential evaporation of Sn and Cu elements using ULVAC VPC-410 vacuum evaporation apparatus with two heating tungsten boats. The Cu/Sn molar ratio of the evaporation materials was changed from 1.33 to 2.0 under keeping constant at Cu molar ratio of 2.0 and a total Cu and Sn weight of 0.086 g. The stacked Sn/Cu precursor (10×50 mm^2 in size) was set in a vacuum-sealed glass ampoule with elemental sulfur and tin shots, where, an amount of sulfur and tin was constant at 0.936×10^{-3} mole and 0.187×10^{-3} mole, respectively. The precursor was crystallized by annealing in sulfur/tin mixing atmosphere for 30 min at 570 °C. We fabricated solar cells with a configuration of Al grid contact/ Ga-doped ZnO transparent conducting layer/ non-doped ZnO/ CdS buffer layer/ CTS absorber layer/ Mo back contact/SLG substrate. CdS buffer layer with a thickness of 70 nm was deposited by the chemical bath deposition technique. i-ZnO buffer layer with a thickness of 100 nm was deposited by RF magnetron sputtering from non-doped ZnO target in Ar and O_2 gases at room temperature. Transparent conductive ZnO : Ga film with a thickness of 0.4 μm was subsequently deposited by RF magnetron sputtering from a 3 wt. % Ga_2O_3-doped ZnO target in Ar gas at the substrate temperature of 100 °C. Al grids for the front electrode were produced from metal masks by vacuum evaporation. No antireflection coating was applied. The size of a solar cell is 5×5 mm^2. The composition of thin films was determined by electron probe microanalysis (EPMA) with energy dispersive spectrometry (EDS) detector. The crystalline structure of the thin films was examined by the Raman analysis. The surface morphology of the thin films were observed with scanning electron microscopy (SEM). Current-voltage (J-V) characteristics of solar cells were measured using standard 1 sun (AM1.5, 100 mW/cm^2) illumination.

3.4 Results and discussions

3.4.1 Film compositions

Figure 3.1 shows the dependence of the film composition determined by EPMA analysis on Cu/Sn molar ratio of the evaporating materials. In all samples, the Sn content was approximately constant with decreasing Sn molar ratio in the precursor. It is considered that the excessive Sn quantities were not absorbed into thin films by re-evaporation when the precursors were crystallized. The Cu/Sn molar ratios range in the thin films were from 1.43 to 1.87, and S/(Cu+Sn) molar ratios range were from 1.34 to 1.73.

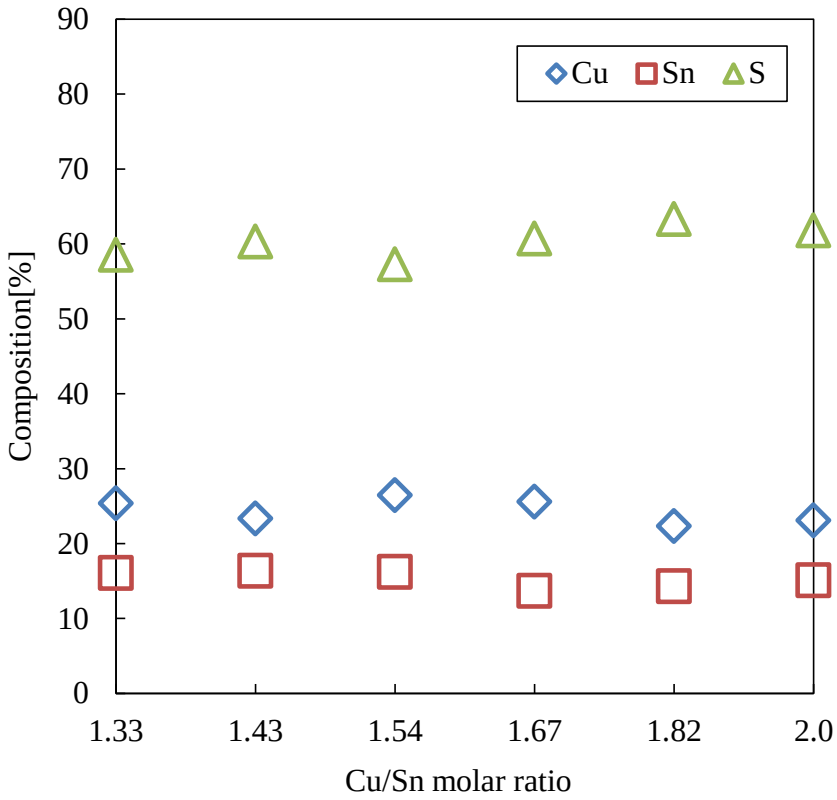

Figure 3.1 Dependence of the film composition on Cu/Sn molar ratio of the evaporating materials.

3.4.2 Crystal structure

Figure 3.2 shows the Raman spectra for CTS thin film prepared on Mo/SLG substrate at Cu/Sn molar ratio of 1.67. The spectra had two dominant peaks at 290 cm^{-1} and 352 cm^{-1} and the spectra also show weaker peaks at 314 cm^{-1} and 374 cm^{-1}. These peaks are in good agreement with those reported by Berg et al. **[4]**. Therefore, it is considered that the thin film is monoclinic CTS. The spectra in Figure 3.2 also show a weak peak at 475 cm^{-1}, and identification of it with the characteristic of CuS was reported by Suriakarthick et al. **[21]**.

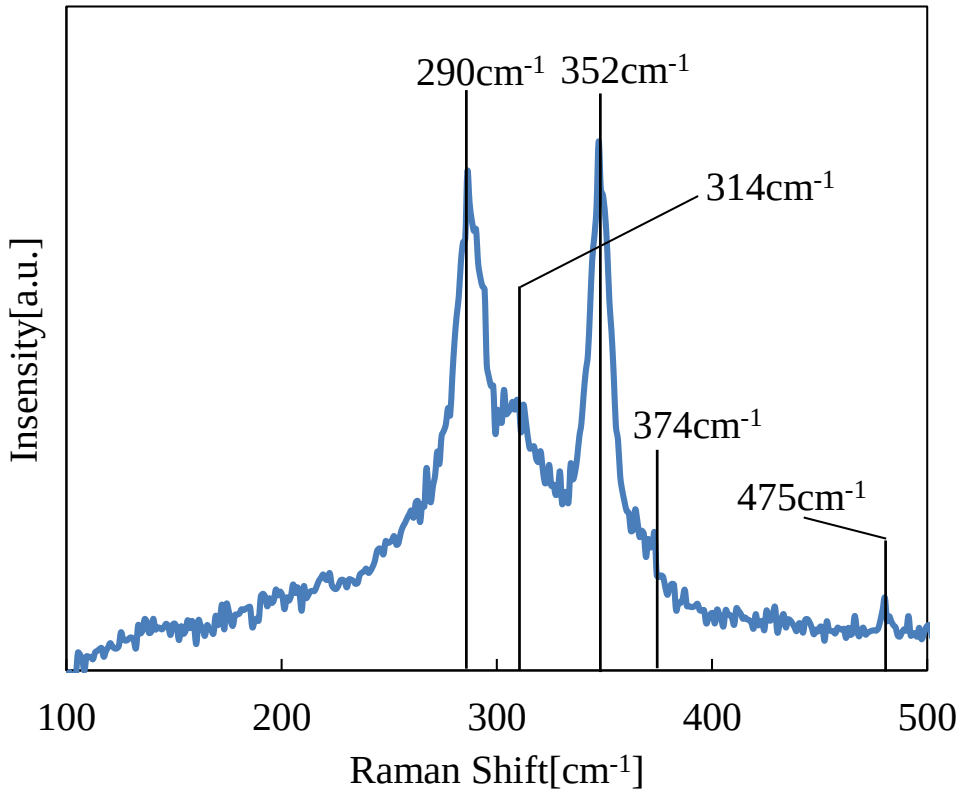

Figure 3.2 The Raman spectra for the sample of Cu/Sn molar ratio of 1.67.

3.4.3 Film morphologies

The surface morphologies of CTS thin films prepared at various Cu/Sn molar ratios of the evaporation materials are shown in Figure 3.3, and the cross-section morphologies are shown in Figure 3.4. It can be seen that the grain size in CTS thin films increased with increasing Sn molar ratio in the precursor until Cu/Sn molar ratio of 1.67, and then the grain size decreased with increasing Sn molar ratio. The film thickness was approximately around 1 μm, and the large column grains over 1 μm were formed at Cu/S molar ratio of 1.67. In all samples, some voids were seen in CTS thin films.

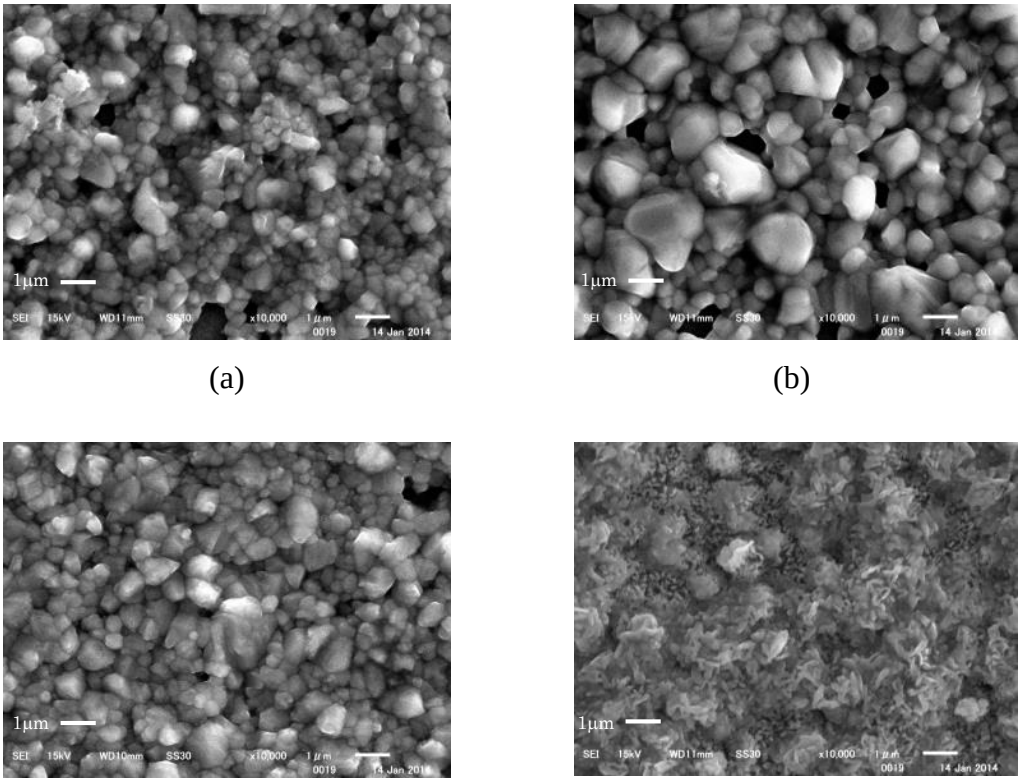

(a) (b)

(c) (d)

Figure 3.3 SEM micrographs of the surface of CTS thin films prepared at various Cu/Sn molar ratio of (a) 2.0, (b) 1.67, (c) 1.54, (d) 1.33.

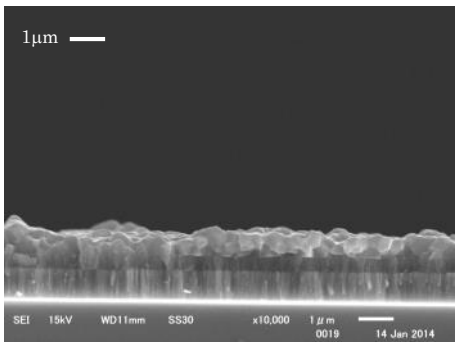

(a)

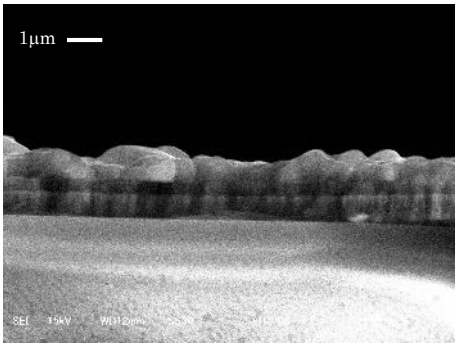

(b)

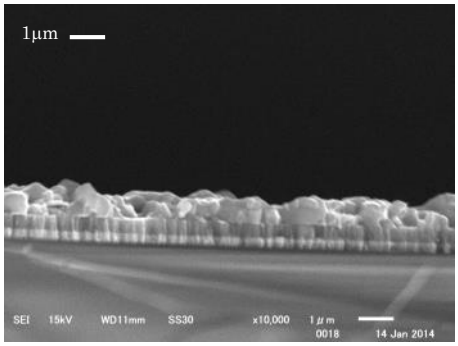

(c)

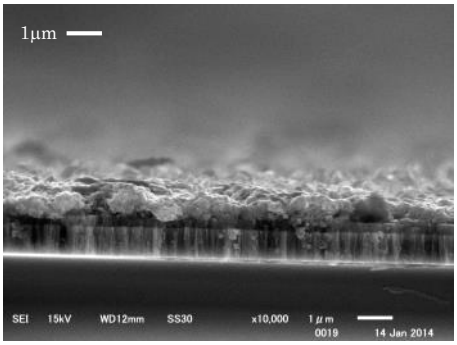

(d)

Figure 3.4 SEM micrographs of the cross-section of CTS thin films prepared at various Cu/Sn molar ratio of (a) 2.0, (b) 1.67, (c) 1.54, (d) 1.33.

3.4.4 Difference in composition of the depth direction of thin film

As seen in the cross section of thin films, it is considered that the thin films were formed in three layers. Figure 3.5 shows the cross-section morphologies of Cu/Sn molar ratio of 1.67 that was assigned four-points (A, B, C, and D) to each layer. Figure 3.6 is the result of point analysis at each point of Figure 3.5 measured by EDS (JEOL, JSM-6510A and JED-2300). It is considered that the measurements of point analysis were carried out exactly from the composition of each point which were clearly different. In the Point A, the composition of Mo was over 95 %, so the Mo layer was formed. In the Point D, the CTS was formed by Cu, Sn and S. For the near point of Mo layer (Point B), the composition of Mo was over 50 %. On the other hand, the composition of Mo was under 10 % in the near point of CTS layer (Point C). In addition, the S contents were not uniform in the second layer. It is considered that the composition inside of the thin films has gradation.

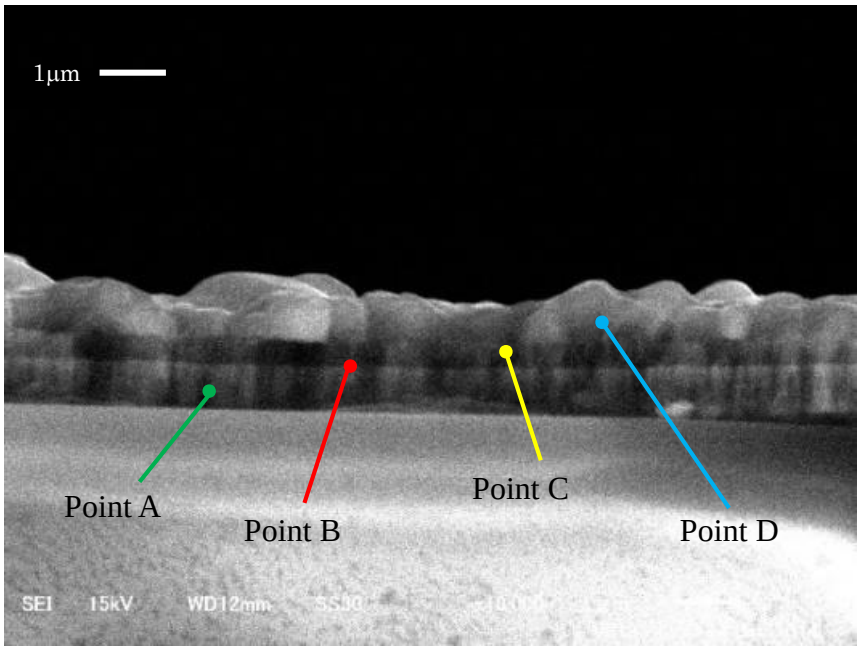

Figure 3.5 SEM micrographs of the cross-section of Cu/Sn molar ratio = 1.67 that was assigned four-points.

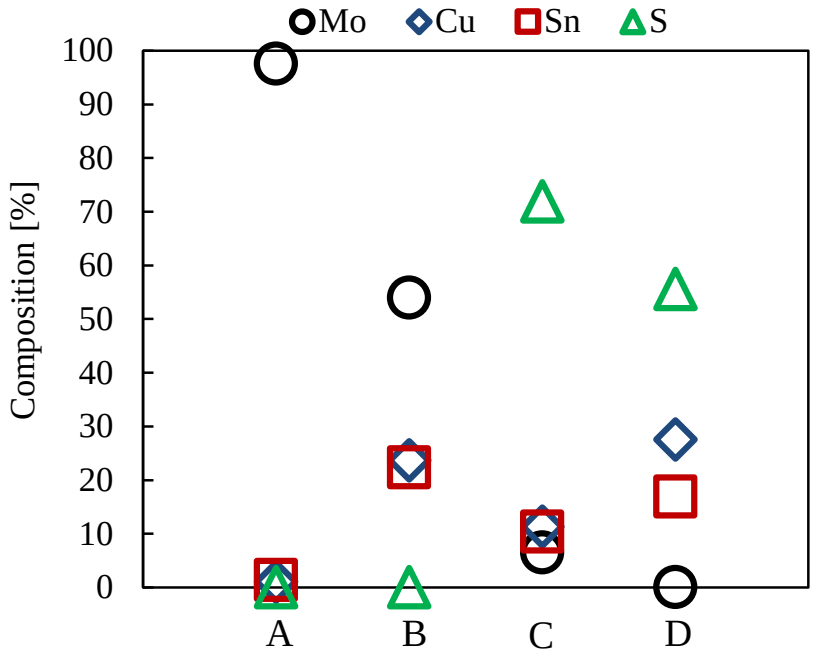

Figure 3.6 Dependence of the composition of each point (A, B, C, and D) in Figure 3.5.

3.4.5 Cell performances

Under the condition of house measurement, open–circuit voltages V_{oc} and short–circuit currents J_{sc} of the CTS thin film solar cells prepared at various Cu/Sn molar ratios of the evaporating materials are shown in Figure 3.7. The values of V_{oc} and J_{sc} in CTS solar cells increased with increasing Cu/Sn molar ratio. Figure 3.8 shows the J-V curve of the best solar cell in this study which was fabricated at Cu/Sn molar ratio of 1.67. This CTS thin film solar cell demonstrated V_{oc} of 247.5 mV, J_{sc} of 5.75 mA/cm^2, FF of 0.30 and η of 0.43%. The largest V_{oc} in this study is comparable with the V_{oc} of the early reported CTS thin film solar cell of 258 mV which demonstrated the good cell performances with Cu/Sn molar ratio of 1.87 **[12]**. In their report, they analyzed the composition of thin films by X-ray fluorescence (XRF) analysis,

as a result, their data of Cu/Sn molar ratio of 1.87 was obtained by measurement of the whole thin film including deep part **[12]**. On the other hand, we analyzed the composition of thin films by EDS which measures the composition of near the surface of thin film, and the largest V_{oc} in this study was obtained with the sample of the Cu/Sn molar ratio of 1.67. Therefore, it is considered that this difference of Cu/Sn molar ratio in spite of the V_{oc} at the same level occurred from difference of the measurement method. In the efficient chalcogenide-based solar cells, the composition of near the surface of thin films became Cu-poor **[22]**, and the CTS thin film solar cells which were fabricated in this study had same tendency. However, the conversion efficiency was low, because the J_{sc} was too small. It is considered that this cause is a small diffusion length of minority carrier by the defect of the CTS which is the absorber layer.

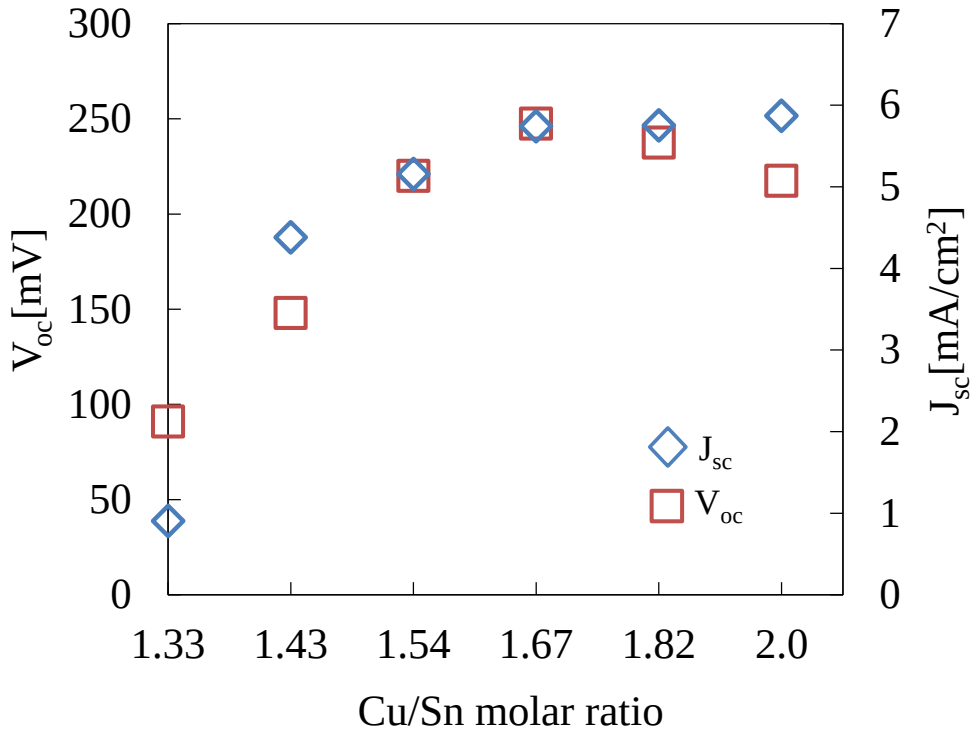

Figure 3.7 V_{oc} and J_{sc} of CTS thin film solar cells prepared at various Cu/Sn molar ratio of the evaporating materials.

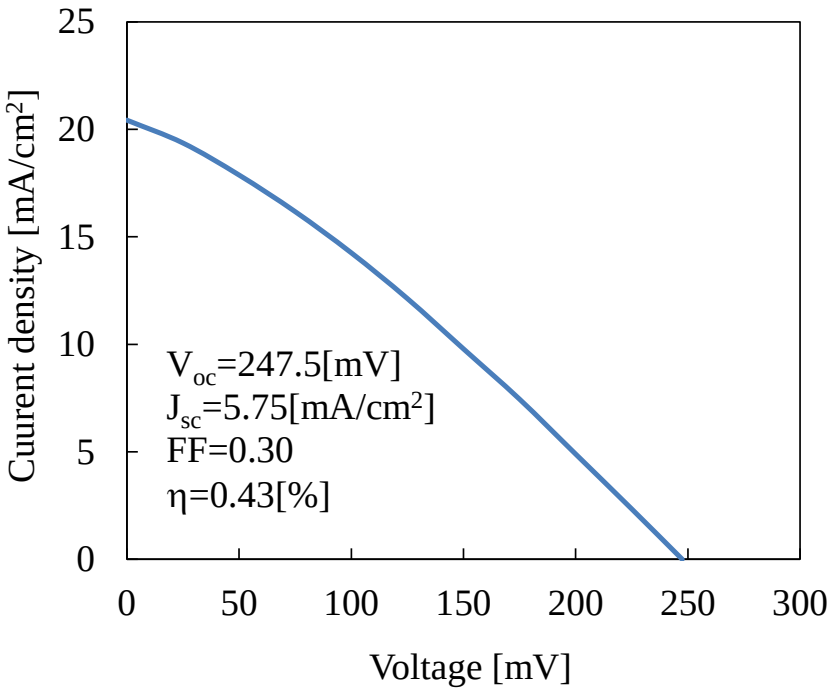

Figure 3.8 J-V curve of CTS thin film solar cell fabricated at Cu/Sn molar ratio of 1.67.

3.5 Conclusions

CTS thin films were successfully fabricated by thermal crystallization of evaporated Cu/Sn precursors in sulfur and tin mixing atmosphere. The CTS thin films fabricated in this study had a monoclinic structure. From EPMA analysis, the composition of surface was approximately constant with changing Sn molar ratio. However, the composition of inside of the thin films had gradation. Some voids were seen in the surface of the thin films at all samples. The largest V_{oc} of 247.5 mV was achieved in sample of Cu/Sn molar ratio of 1.67 using our fabrication method, which is comparable with early reported value of V_{oc}. However, J_{sc} is too small. From the results of this study, it is concluded that the optimum value of Cu/Sn molar ratio of the evaporation materials in our process is vicinity of 1.67.

REFERENCES

[1] T. A. Kuku, O. A. Fakolujo, Photovoltaic characteristics of thin films of Cu_2SnS_3, Sol. Energy Mater. **16**, 199 (1987).

[2] M. Bouaziz, M. Amlouk, S. Belgacem, Structural and optical properties of Cu_2SnS_3 sprayed thin films, Thin Solid Films **517**, 2527 (2009).

[3] M. Bouaziz, J. Ouerfelli, S. K. Srivastava, J. C. Bernède, M. Amlouk, Growth of Cu_2SnS_3 thin films by solid reaction under sulphur atmosphere, Vacuum **85**, 783 (2011).

[4] D. M. Berg, R. Djemour, L. Gütay, S. Siebentritt, P. J. Dale, X. Fontane, V. Izquierdo-Roca, A. Pérez-Rodriguez, Raman analysis of monoclinic Cu_2SnS_3 thin films, Appl. Phys. Lett. **100**, 192103 (2012).

[5] D. M. Berg, R. Djemour, L. Gutay, G. Zoppi, S. Siebentritt, P. J. Dale, Thin film solar cells based on the ternary compound Cu_2SnS_3, Thin Solid Films **520**, 6291 (2012).

[6] B. Li, Yi Xie, J. Huang, Y. Qian, Synthesis, Characterization, and Properties of Nanocrystalline Cu_2SnS_3, J. Solid State Chem. **153**, 170 (2000).

[7] M. Onoda, X. Chen, A. Sato, H. Wada, Crystal structure and twinning of monoclinic Cu_2SnS_3, Mater. Res. Bull. **35**, 1563 (2000).

[8] Q. Chen, X. Dou, Y. Ni, S. Cheng, and S. Zhuang, Study and enhance the photovoltaic properties of narrow-bandgap Cu_2SnS_3 solar cell by p-n junction interface modification, J. Colloid Interf. Sci. **376**, 327 (2012).

[9] P. A. Fernandes, P. M. Salomé, A. F. da Chnha, A study of ternary Cu_2SnS_3 and Cu_3SnS_4 thin films prepared by sulfurizing stacked metal precursors, J. Phys. D: Appl. Phys. **43**, 215403 (2010).

[10] N. Aihara, H. Araki, A. Takeuchi, K. Jimbo, H. Katagiri, Fabrication of Cu_2SnS_3 thin films by sulfurization of evaporated Cu-Sn precursors for solar cells, Phys. Status Solidi C **10**, 1086 (2013).

[11] N. Aihara, A. Kanai, K. Kimura, M. Yamada, K. Toyonaga, H. Araki, A. Takeuchi, H. Katagiri, Sulfurization temperature dependences of photovoltaic properties in Cu_2SnS_3-based thin-film solar cells, Jpn. J. Appl. Phys. **53**, 05FW13 (2014).

[12] A. Kanai, K. Toyonaga, K. Chino, H. Katagiri, H. Araki, Fabrication of Cu_2SnS_3 thin-film solar cells with power conversion efficiency of over 4%, Jpn. J. Appl. Phys. **54**, 08KC06 (2015).

[13] Y. Dong, J. He, L. Sun, Y. Chen, P. Yang, J. Chu, Effect of sulfurization temperature on properties of Cu_2SnS_3 thin films and solar cells prepared by sulfurization of stacked metallic precursors, Mater. Sci. Semicond. Process. **38**, 171 (2015).

[14] T. S. Reddy, R. Amiruddin, M. C. S. Kumar, Deposition and characterization of Cu_2SnS_3 thin films by co-evaporation for photovoltaic application, Sol. Energy Mater. Sol. Cells **143**, 128 (2015).

[15] T. Nomura, T. Maeda, T. Wada, Fabrication of Cu_2SnS_3 solar cells by screen-printing and high-pressure sintering process, Jpn. J. Appl. Phys. **53**, 05FW01 (2014).

[16] H. Dahman, S. Rabaoui, A. Alyamani, L. El Mir, Structural, morphological and optical properties of Cu_2SnS_3 thin film synthesized by spin coating technique, Vacuum **101**, 208 (2014).

[17] D. Avellaneda, M. T. S. Nair, P. K. Nair, Cu_2SnS_3 and Cu_4SnS_4 Thin Films via Chemical Deposition for Photovoltaic Application, J. Electrochem. Soc. **157**, D346 (2010).

[18] H. Hu, Z. Liub, B. Yang, X. Chen, Y. Qian, Template-mediated growth of Cu_3SnS_4 nanoshell tubes, J. Cryst. Growth **284**, 226 (2005).

[19] S. Fiechter, M. Martinez, G. Schmidt, W. Henrion, Y. Tomm, Phase relations and optical properties of semiconducting ternary sulfides in the system Cu-Sn-S, J. Phys. Chem. Solids **64**, 1859 (2003).

[20] A. Amlouk, K. Boubaker, M. Amlouk, A new procedure to prepare semiconducting ternary compounds from binary buffer materials and vacuum-deposited copper for photovoltaic applications, Vacuum **85**, 60 (2010).

[21] R. Suriakarthick, V. Nirmal Kumar, T. S. Shyju, R. Gopalakrishnan, Investigation on post annealed copper sulfide thin films from photochemical deposition technique, Mater. Sci. Semicon. Process. **26**, 155 (2014).

[22] K. M. Kim, K. H. Liao, H. Tampo, H. Shibata, S. Niki, $Cu_2ZnSnSe_4$ thin-film solar cells fabricated using Cu_2SnSe_3 and ZnSe bilayers, Appl. Phys. Express **8**, 042301 (2015).

CHAPTER 4

Cu_2SnS_3 thin film solar cells fabricated by sulfurization from NaF/Cu/Sn stacked precursor

4.1 Introduction

The condition of Cu/Sn molar ratio which demonstrated high V_{oc} in CTS thin film solar cells was presented in Chapter 3, and the largest V_{oc} of 247.5 mV was achieved in CTS thin film solar cell fabricated by sulfurization from Cu/Sn stacked precursor at Cu/Sn molar ratio of evaporation materials of 1.67. However, J_{sc} of it was too small. In recent years, the techniques of alkaline metals doping have been employed for improving the cell performance, and the high

conversion efficiencies were demonstrated in CIGS and CZTS-based solar cells by this techniques. **[1-16]** In particular, many papers have been published on research about sodium doping in the CIGS and CZTS-based solar cells, and several methods of sodium doping were reported, such as diffusion from a SLG substrate, **[1, 2]** the formation of a NaF layer on a Mo/SLG substrate, **[3]** the doping of Na_2S, Na_2Se, and NaF in precursors, **[4, 5]** and the postdeposition technique. **[6-11]** Recently, the techniques of alkaline metals doping helped set a new efficiency record of CIGS solar cells. **[10, 15]** The alkaline metals doping is regarded to decrease the concentration of Cu cations near the surface of the calcogenide film and passivate defects. **[7, 11, 17]** Therefore, it is considered to be a useful technique for improving the cell performance. However, the effect of alkaline metals addition on the conversion efficiency of the CTS thin film solar cell has not yet been reported.

4.2 Objective of this study

In CTS thin film solar cell, the alkaline metals doping which were effective in the improvement of film qualities and cell performances in CIGS and CZTS-based thin film solar cells may have the same effects of CIGS and CZTS-based thin film solar cells. In this study, CTS thin films were prepared by sulfurization from the stacked NaF/Cu/Sn precursors deposited by sequential evaporation of Sn, Cu elements and NaF, which was developed in addition of NaF to the fabrication method of Chapter 3. We have investigated the compositional, structural, morphological, optical, and electrical characterizations of these thin films and solar cells, and the effect of sodium addition on the conversion efficiency of CTS thin film solar cells fabricated by the sulfurization process have discussed.

4.3 Experimental procedure

The stacked NaF/Sn/Cu precursor was deposited on a Mo/soda lime glass substrate by the sequential evaporation of Sn and Cu elements and NaF using the ULVAC VPC-410 vacuum evaporation apparatus. The NaF/Cu molar ratio of the evaporation materials was changed from 0 to 0.12 while keeping constant the Cu and Sn ratios at 1.0 and 0.6, respectively. The stacked NaF/Sn/Cu precursor was set in a vacuum-sealed glass ampoule with an internal volume of 60 cm^3 with elemental sulfur and tin shots. The amounts of sulfur and tin were constant at 0.062 and 0.046 g, respectively. The precursor was crystallized by annealing in a sulfur/tin mixing atmosphere for 30 min at 570 °C. We fabricated solar cells with a configuration of Al grid contact/ Ga-doped ZnO transparent conducting layer/ non-doped ZnO/ CdS buffer layer/ CTS absorber layer/ Mo back contact/ SLG substrate. A CdS buffer layer of 70 nm thickness was deposited by the chemical bath deposition technique using a CdI_2-thiourea-ammonia aqueous solution during heating from room temperature to 65 °C. An i-ZnO buffer layer of 50 nm thickness was deposited by RF magnetron sputtering from a non-doped ZnO target in Ar and O_2 gases at room temperature. A transparent conductive ZnO : Ga film of 0.4 μm thickness was subsequently deposited by DC magnetron sputtering from a 3 wt. % Ga_2O_3-doped ZnO target in Ar gas at the substrate temperature of 100 °C. Al grids for the front electrode were formed by vacuum evaporation with a W boat using a metal mask. No antireflection coating was applied. The size of a solar cell is 5 × 5 mm^2. The composition of thin films was determined by electron probe microanalysis (EPMA) with an energy dispersive spectrometry (EDS) detector. The crystalline structure of the thin films was examined by X-ray diffraction (XRD) and Raman analysis. The surface morphology of the thin films was observed by scanning electron microscopy (SEM). The current-voltage (J-V) characteristics of the solar cells were obtained using a spectrophotometer (Nippon Bunkou YQ-250BX) under standard 1-sun (AM1.5, 100 mW/cm^2) illumination. With the same instrument, the quantum efficiencies (QEs) of the solar

cells were measured with illumination normalized against a calibrated photodiode (BS-520).

4.4 Results and discussions

4.4.1 Film compositions and crystal structure

From EPMA, the composition is approximately constant, and the Cu/Sn molar ratios were from 1.41 to 1.88, and the S/(Cu + Sn) molar ratios were from 1.37 to 1.93. The XRD patterns of the thin films prepared at various NaF/Cu molar ratios are shown in Figure 4.1. The XRD patterns showed several peaks corresponding to only the diffraction lines of the monoclinic structure with increasing NaF/Cu molar ratio. In addition, the XRD patterns showed unknown diffraction peaks such as those at 19, 29, and 39 °, which were observed for NaF/Cu molar ratios of 0 and 0.03. Those unknown diffraction peaks were similarly observed by Aihara et al. in their study of the sulfurization temperatures of the CTS thin film solar cell. **[18]** The CTS thin film that they fabricated at a sulfurization temperature of 580 °C showed unknown diffraction peaks, but the solar cell using this thin film has achieved a 2.7 % conversion efficiency. **[18]** Figure 4.2 shows the Raman spectra for CTS thin films. For all the samples including those that showed several unknown diffraction peaks in the XRD patterns, the spectra had peaks at 290, 314, 352, and 374 cm^{-1}. These peaks are in good agreement with those reported by Berg et al. **[19]** and Aihara et al. **[18]** From the XRD patterns and Raman spectra, it is considered that the CTS thin films fabricated by the addition of NaF have a monoclinic structure. Moreover, the Raman spectra of NaF/Cu = 0 had a dominant peak at 316 cm^{-1} than the peaks at 290, 314, 352, and 374 cm^{-1} of the monoclinic CTS structure. The identification of a dominant peak at 316 cm^{-1} with the characteristic of $Cu_2Sn_3S_7$ was reported by Cheng et al. **[20]** and Berg et al. **[19]** Thus, it is considered that a possible candidate of a dominant peak of NaF/Cu = 0 in this study is $Cu_2Sn_3S_7$.

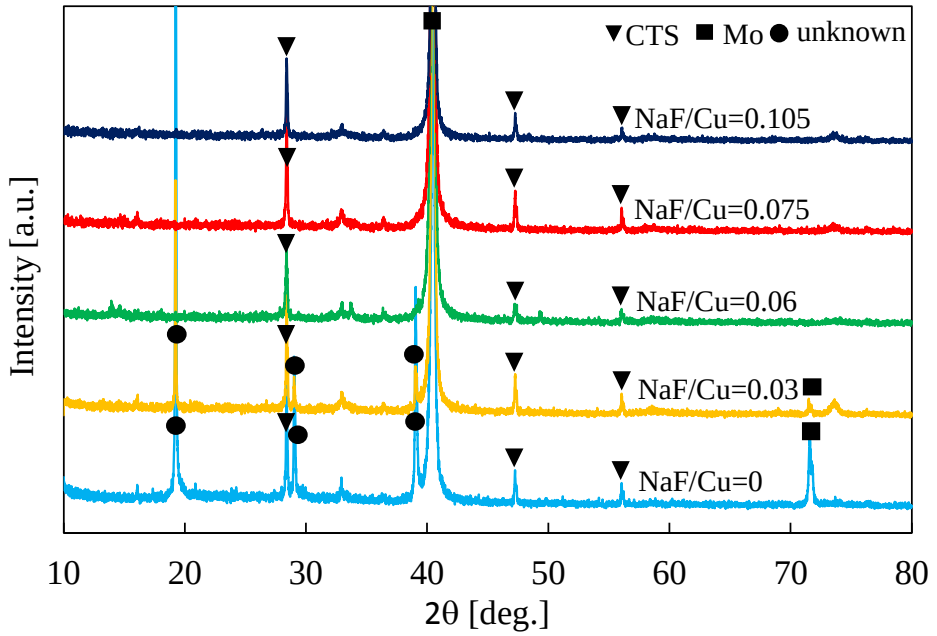

Figure 4.1 XRD patterns for the thin films prepared at various NaF/Cu molar ratio of the evaporating materials.

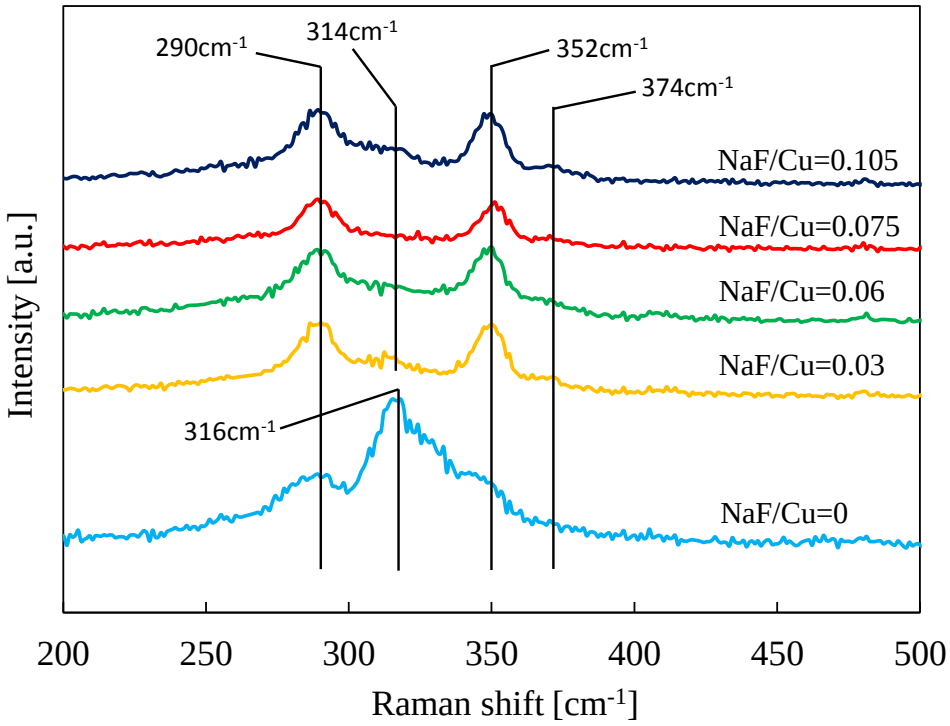

Figure 4.2 Raman spectra for the thin films prepared at various NaF/Cu molar ratio of the evaporating materials.

4.4.2 Film morphologies

The surface morphologies and cross-sectional morphologies of CTS thin films prepared at various NaF/Cu molar ratios of the evaporation materials are shown in Figure 4.3. It can be seen that the grain size of CTS thin films decreased with increasing NaF/Cu molar ratio in the precursor, and in particular, the close-packed structure was seen in NaF/Cu = 0.075. In the case of the CIGS thin films, Rudmann et al. have reported the improvement of conversion efficiency with the addition of Na in the precursor. **[21]** In that report, the grain size decreased with the addition of Na in the precursor and it decreased further with increasing amount of Na; a similar tendency was observed from the CTS thin films fabricated in this study.

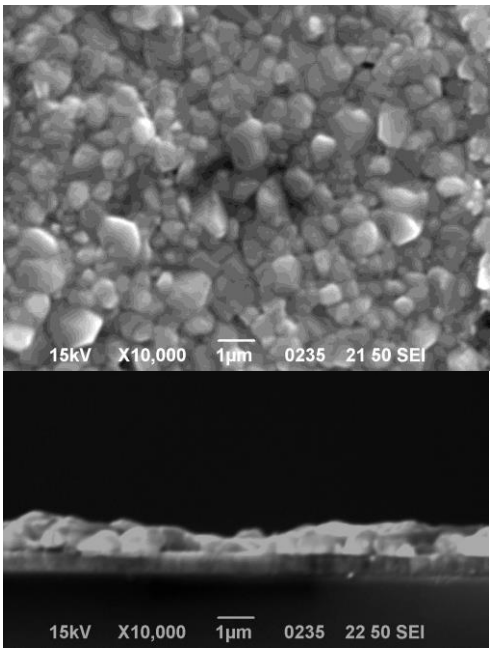

(a)

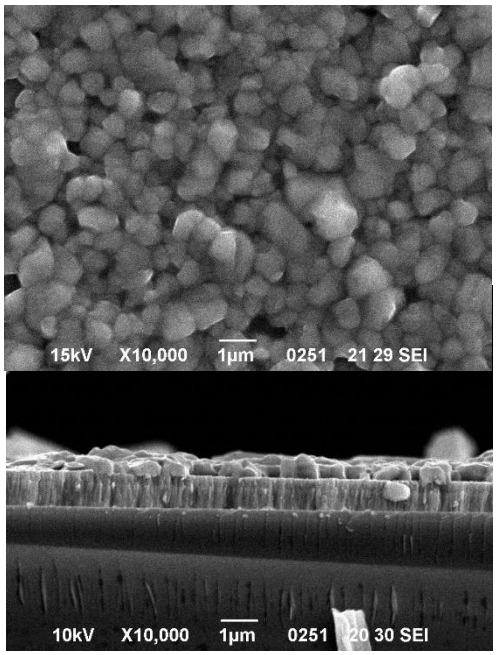

(b)

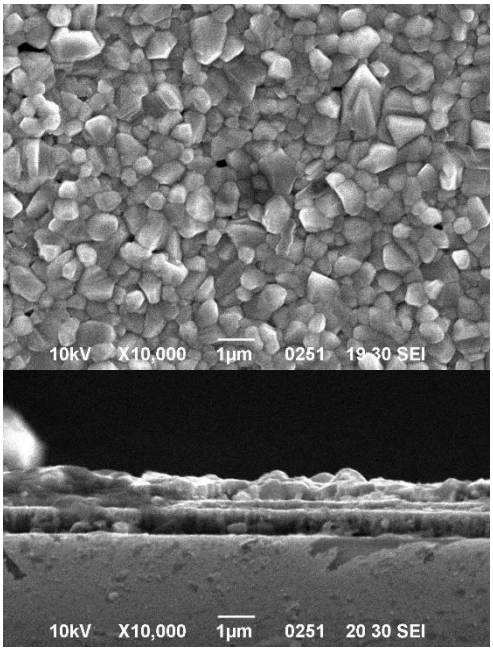

(c)

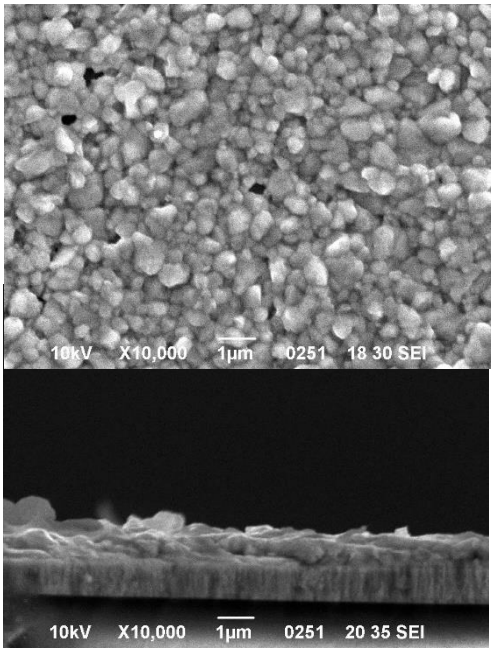

(d)

Figure 4.3 SEM micrographs of the surface and the cross-section of CTS thin films prepared at various NaF/Cu molar ratio, (a) NaF/Cu = 0, (b) NaF/Cu = 0.03, (c) NaF/Cu = 0.075, (d) NaF/Cu = 0.105.

4.4.3 Cell performances

Figure 4.4 shows the open-circuit voltage V_{oc}, the short-circuit current J_{sc}, the fill factor FF, and the conversion efficiency η of the CTS thin film solar cells prepared at various NaF/Cu molar ratios of the evaporation materials. From Figure 4.4, it can be seen that the values of all the characteristics of the CTS thin film solar cells had an upward trend with increasing NaF/Cu molar ratio in the precursor. In particular, the increase in V_{oc} with increasing NaF/Cu molar ratio can be observed. Niles et al. reported the increase in carrier concentration by Na incorporation into the CIGS, **[22]** and Keyas et al. reported an increase in V_{oc} with increasing carrier concentration in the CIGS. **[23]** In our study, similar results were observed. Therefore, it is considered that in the CTS, the addition of Na increased the carrier concentration, and from this result, V_{oc} increased. However, the performances of the CTS thin film solar cells were decreased with the samples of NaF/Cu molar ratio more than 0.09. It is considered that this results are due to the poor crystallinity of CTS which is the absorber layer of these samples by excessive decrease of grain size as seen in SEM micrographs. Therefore, it is considered that the optimum quantity of Na addition exists, and this study showed the optimum value of NaF/Cu = 0.075. The J‑V curve of the CTS thin film solar cell at NaF/Cu = 0.075 is shown in Figure 4.5, and this solar cell with the highest conversion efficiency in this study, which was fabricated at a NaF/Cu = 0.075 molar ratio, demonstrated V_{oc} = 283 mV, J_{sc} = 37.3 mA/cm^2, FF = 0.439, and η = 4.63 %. The conversion efficiency of 4.63% is the world record in the CTS thin film solar cell.

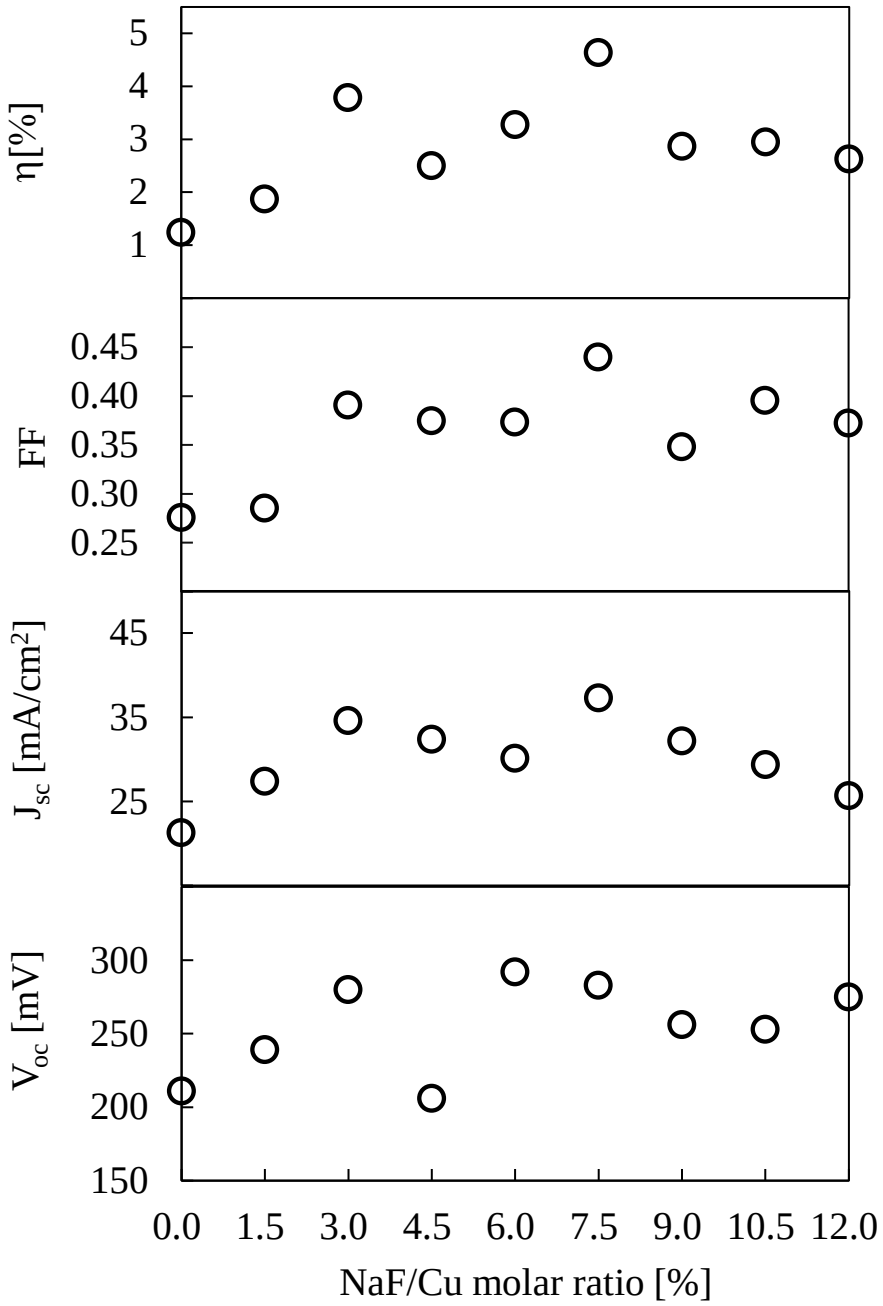

Figure 4.4 V_{oc}, J_{sc}, FF and η of CTS thin film solar cells prepared at various NaF/Cu molar ratio of the evaporating materials.

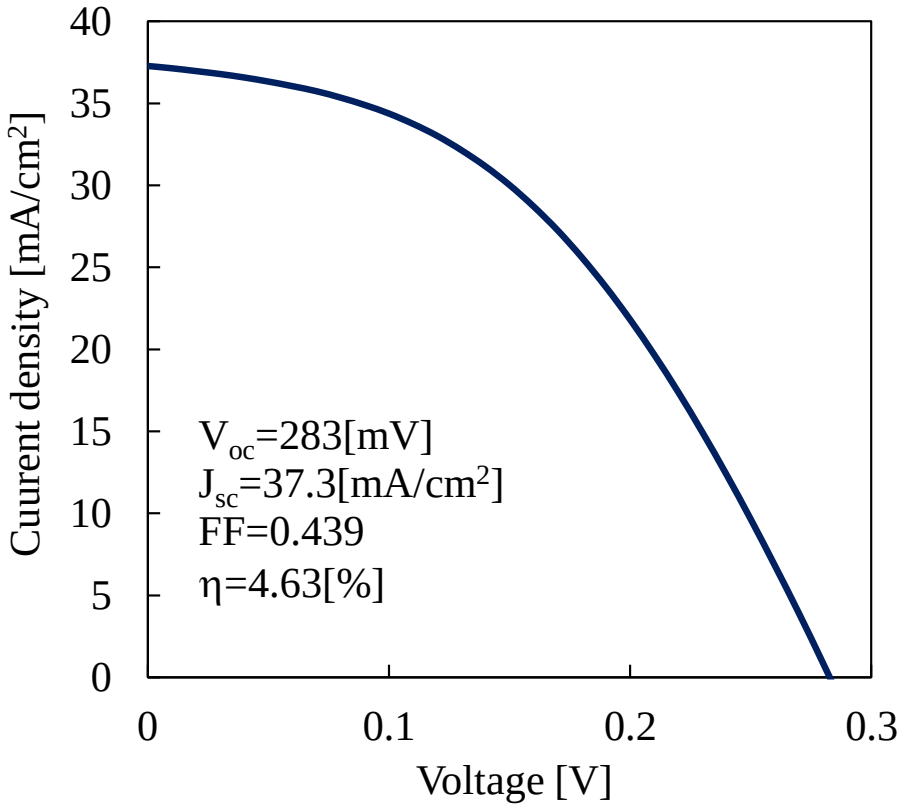

Figure 4.5 J-V characteristics of CTS thin film solar cell fabricated at NaF/Cu = 0.075.

4.4.4 Quantum efficiencies

Figure 4.6 shows the QE curves of the CTS thin film solar cell which demonstrated the highest conversion efficiency of 4.63% measured under two conditions, namely, without and with the white light bias of 1.57 mW/cm^2. The irradiation of the white light bias is to measure QE under the solar cell movement condition. In both curves, the absorption of the CdS buffer layer was observed in the vicinity of 520 nm. In the absence of white light bias, the QE was 37 % at 1100 nm, and it improved to 67 % under the white light bias of 1.57 mW/cm^2. Yamaguchi et al. have reported such a similar tendency in the CZTSe thin film solar cells fabricated by the selenization of the precursor evaporated from the CZTSe compound. **[24]** It is considered that the carrier which were generated by the white light bias compensated the carrier trap in the crystal grain boundary, and it is considered that the QE of long wavelength regions were improved. In addition, two steps of the sharp optical absorptions around 1200 and 1300 nm are seen in Figure 4.6. These two steps of the optical absorptions were reported by other groups. **[18, 25]** Assuming a very short minority carrier diffusion length, for a direct transition, a plot of $[h\nu \times \ln(1-QE)]^2$ versus $h\nu$ can be used to extrapolate the band-gap energy. **[26]** Figure 4.7 shows the transition energies estimated by extrapolating from the QE, and the band-gap energies were estimated to be 0.93 and 1.02 eV. Our values are approximately in agreement with the band-gap energies of 0.93 and 0.99 eV reported by Berg et al. **[25]**, and the band-gap energies of 0.92 and 0.99 eV estimated from absorption spectrum reported by Aihara et al. **[18]**

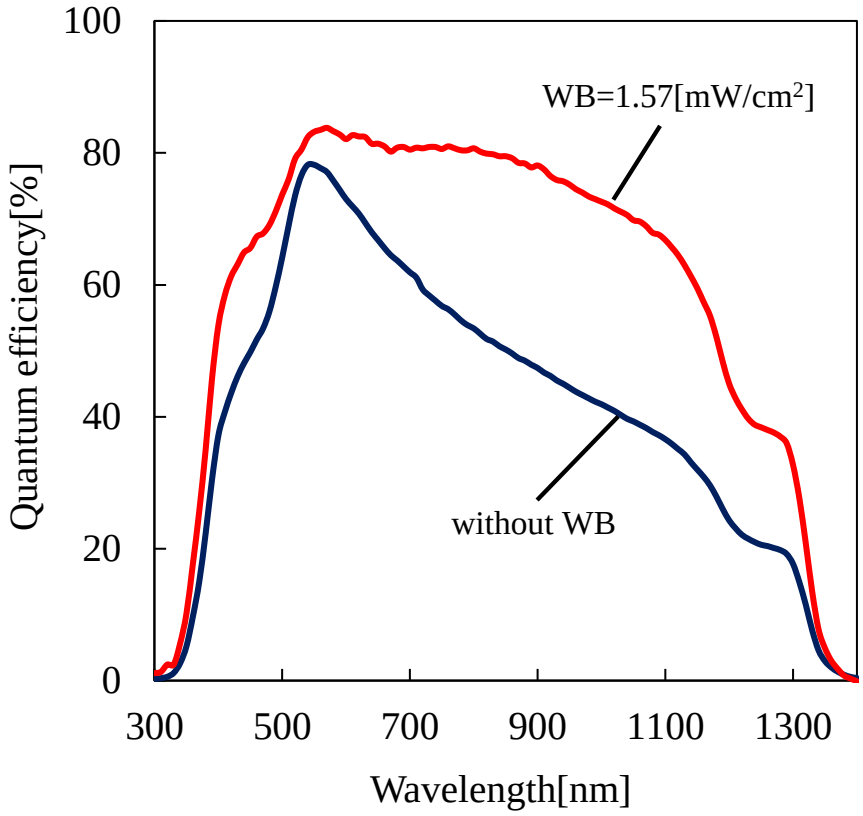

Figure 4.6 QE of CTS thin film solar cell which demonstrated 4.63% conversion efficiency.

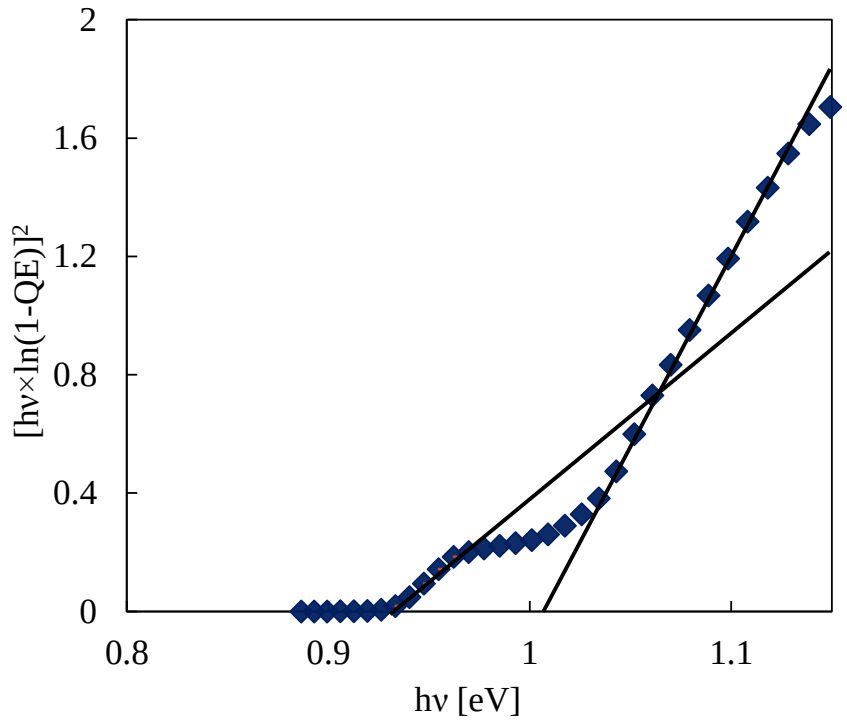

Figure 4.7 $[h\nu \times \ln(1\text{-}QE)]^2$ versus $h\nu$ plot (WB = 1.57[mW/cm^2])

4.5 Conclusions

In this study, CTS thin films were successfully fabricated by the thermal crystallization of evaporated NaF/Cu/Sn precursors in a sulfur and tin mixing atmosphere. XRD patterns showed several peaks corresponding to diffraction lines of the monoclinic structure in CTS, and a few unknown peaks were also observed. The unknown peaks disappeared with increasing NaF/Cu molar ratio. Furthermore, Raman spectra showed the estimated peaks of a monoclinic structure. The grain size of CTS thin films decreased with increasing NaF/Cu molar ratio. The characteristics of the CTS thin film solar cells fabricated in this study improved with increasing NaF/Cu molar ratio, and the best solar cell fabricated at the NaF/Cu molar ratio of 0.075 showed Voc = 283 mV, Isc = 37.3 mA/cm^2, FF = 0.439, and η = 4.63 %, which includes the highest conversion efficiency in CTS thin film solar cells. From QE measurement, the carrier trap in the crystal grain boundary was compensated by white light bias, and two steps of the sharp optical absorptions were observed. The band-gap energies of the CTS thin film were estimated to be 0.93 and 1.02 eV.

REFERENCES

[1] W. N. Shafarman, J. Zhu, Effect of substrate temperature and deposition profile on evaporated Cu(InGa)Se_2 films and devices, Thin Solid Films **361-362**, 473 (2000).

[2] S. Nishiwaki, T. Saitoh, Y. Hashimoto, T. Negami, T. Wada, Preparation of Cu(In,Ga)Se_2 thin films at low substrate temperatures, J. Mater. Res. **16**, 394 (2001).

[3] I. Repins, C. Beall, N. Vora, C. DeHart, D. Kuciauskas, P. Dippo, B. To, J. Mann, W. C. Hsu, A. Goodrich, R. Noufi, Co-evaporated $Cu_2ZnSnSe_4$ films and devices, Sol. Energy Mater. Sol. Cells **101**, 154 (2012).

[4] C. M. Sutter-Fella, J. A. Stückelberger, H. Hagendorfer, F. La Mattina, L. Kranz, S. Nishiwaki, A. R. Uhl, Y. E. Romanyuk, A. N. Tiwari, Sodium Assisted Sintering of Chalcogenides and Its Application to Solution Processed $Cu_2ZnSn(S,Se)_4$ Thin Film Solar Cells, Chem. Mater. **26**, 1420 (2014).

[5] A. Nagaoka, H. Miyake, T. Taniyama, K. Kakimoto, Y. Nose, M.A. Scarpulla, K. Yoshino, Effects of sodium on electrical properties in Cu_2ZnSnS_4 single crystal, Appl. Phys. Lett. **104**, 152101 (2014).

[6] D. Rudmann, A. F. da Cunha, M. Kaelin, F. Kurdesau, H. Zogg, A. N. Tiwari, G. Bilger, Efficiency enhancement of Cu(In,Ga)Se_2 solar cells due to post-deposition Na incorporation, Appl. Phys. Lett. **84**, 1129 (2004).

[7] A. Chirilă, P. Reinhard, F. Pianezzi, P. Bloesch, A. R. Uhl, C. Fella, L. Kranz, D. Keller, C. Gretener, H. Hagendorfer, D. Jaeger, R. Erni, S. Nishiwaki, S. Buecheler, A. N. Tiwari, Potassium-induced surface modification of $Cu(In,Ga)Se_2$ thin films for high-efficiency solar cells, Nat. Mater. **12**, 1107 (2013).

[8] P. Jackson, D. Hariskos, R.Wuerz, O. Kiowski, A. Bauer, T.M. Friedlmeier, M. Powalla, Properties of $Cu(In,Ga)Se_2$ solar cells with new record efficiencies up to 21.7%, Phys. Status Solidi Rapid Res. Lett. **9**, 28 (2015).

[9] T. Mise, S. Tajima, T. Fukano, K. Higuchi, T. Washio, K. Jimbo, H. Katagiri, Improving the photovoltaic performance of co-evaporated Cu_2ZnSnS_4 thin-film solar cells by incorporation of sodium from NaF layers, Prog. Photovoltaics **24**, 1009 (2016).

[10] P. Jackson, R. Wuerz, D. Hariskos, E. Lotter, W. Witte, M. Powalla, Effect of heavy alkali elements in $Cu(In,Ga)Se_2$ solar cells with efficiencies up to 22.6%, Phys. Status Solidi: Rapid Res. Lett. **10**, 583 (2016).

[11] I. Khatri, H. Fukai, H. Yamaguchi, M. Sugiyama, T. Nakada, Effect of potassium fluoride post-deposition treatment on $Cu(In,Ga)Se_2$ thin films and solar cells fabricated onto sodalime glass substrates, Sol. Energy Mater. Sol. Cells **155**, 280 (2016).

[12] A. Laemmle, R. Wuerz, M. Powalla, Efficiency enhancement of $Cu(In,Ga)Se_2$ thin-film solar cells by a post-deposition treatment with potassium fluoride, Phys. Status Solidi: Rapid Res. Lett. **7**, 631 (2013).

[13] Z. Tong, C. Yan, Z. Su, F. Zeng, J. Yang, Y. Li, L. Jiang, Y. Lai, F. Liu, Effects of potassium doping on solution processed kesterite Cu_2ZnSnS_4 thin film solar cells, Appl. Phys. Lett. **105**, 223903 (2014).

[14] A. Laemmle, R. Wuerz, M. Powalla, Investigation of the effect of potassium on $Cu(In,Ga)Se_2$ layers and solar cells, Thin Solid Films **582**, 27 (2015).

[15] P. Jackson, D. Hariskos, R. Wuerz, W. Wischmann, M. Powalla, Compositional investigation of potassium doped $Cu(In,Ga)Se_2$ solar cells with efficiencies up to 20.8%, Phys. Status Solidi: Rapid Res. Lett. **8**, 219 (2014).

[16] P. Reinhard, B. Bissig, F. Pianezzi, E. Avancini, H. Hagendorfer, D. Keller, P. Fuchs, M. Döbeli, C. Vigo, P. Crivelli, S. Nishiwaki, S. Buecheler, A. N. Tiwari, Features of KF and NaF Postdeposition Treatments of $Cu(In,Ga)Se_2$ Absorbers for High Efficiency Thin Film Solar Cells, Chem. Mater. **27**, 5755 (2015).

[17] M. Sugiyama, T. Yokoi, A. Henmi, T. Asano, Effect of Na on sulfurization growth of SnS thin films and solar cells using NaF/Sn-S precursor, Thin Solid Films **615**, 25 (2016).

[18] N. Aihara, A. Kanai, K. Kimura, M. Yamada, K. Toyonaga, H. Araki, A. Takeuchi, H. Katagiri, Sulfurization temperature dependences of photovoltaic properties in Cu_2SnS_3-based thin-film solar cells, Jpn. J. Appl. Phys. **53**, 05FW13 (2014).

[19] D. M. Berg, R. Djemour, L. Gütay, S. Siebentritt, P. J. Dale, X. Fontane, V. Izquierdo-Roca, A. Pérez-Rodriguez, Raman analysis of monoclinic Cu_2SnS_3 thin films, Appl. Phys. Lett. **100**, 192103 (2012).

[20] A.-J. Cheng, M. Manno, A. Khara, C. Leighton, S. A. Campbell, E. S. Aydil, Imaging and phase identification of Cu_2ZnSnS_4 thin films using confocal Raman spectroscopy, J. Vac. Sci. Technol. A **29**, 051203 (2011).

[21] D. Rudmann, G. Bilger, M. Kaelin, F.-J. Haug, H. Zogg, A. N. Tiwari, Effects of NaF coevaporation on structural properties of Cu(In,Ga)Se_2 thin films, Thin Solid Films **431–432**, 37 (2003).

[22] D. W. Niles, K. Ramanathan, F. Hasoon, R. Noufi, B. J. Tielsch, J. E. Fulghum, Na impurity chemistry in photovoltaic CIGS thin films: Investigation with x-ray photoelectron spectroscopy, J. Vac. Sci. Technol. A **15**, 3044 (1997).

[23] B. M. Keyes, F. Hasoon, P. Dippo, A. Balcioglu, F. Abulfotuh, Influence of Na on the electro-optical properties of Cu(In,Ga)Se_2, Proceedings of the 26th IEEE Photovoltaic Specialists Conference (PVSC), 479 (1997).

[24] T. Yamaguchi, K. Kawamoto, S. Oura, S. Niiyama, T. Imanishi, Preparation of $Cu_2ZnSnSe_4$ thin films by selenization of precursor evaporated from $Cu_2ZnSnSe_4$ compound, Phys. Status Solidi C **10**, 1071 (2013).

[25] D. M. Berg, R. Djemour, L. Gutay, G. Zoppi, S. Siebentritt, P. J. Dale, Thin film solar cells based on the ternary compound Cu_2SnS_3, Thin Solid Films **520**, 6291 (2012).

[26] G. Zoppi, I. Forbes, R. W. Miles, P. J. Dale, J. J. Scragg, L. M. Peter, $Cu_2ZnSnSe_4$ thin film solar cells produced by selenisation of magnetron sputtered precursors, Prog. Photovolt. Res. Appl. **17**, 315 (2009).

CHAPTER 5

Cu_2SnS_3 thin film solar cells with KF addition fabricated by sulfurization

5.1 Introduction

The CTS thin film solar cells fabricated by sulfurization from NaF/Cu/Sn stacked precursors were presented in Chapter 4, and the high cell performances including highest conversion efficiency in CTS thin film solar cells of 4.63 % were obtained with NaF/Cu molar ratio of the evaporation materials of 0.075. As we mentioned in an introduction of Chapter 4, many researches of the techniques of alkaline metals doping were carried out by the researchers of

CIGS and CZTS-based solar cells, and the high cell performances were obtained by those techniques. The representative alkaline metal which were used in the techniques of the alkaline metals doping were sodium **[1-9]**. In addition, the potassium doping technique was reported as one of the methods of improving the cell performance. **[10-14]** Most recently, the technique of combined sodium and potassium doping has been reported, **[13-16]** and it helped set a new efficiency record of CIGS solar cells. **[13, 16]** Similarly, the conversion efficiency of CZTS thin film solar cells was improved by potassium and sodium doping. **[11]** However, the effect of potassium addition to the CTS thin film solar cell has not yet been reported.

5.2 Objective of this study

The technique of combined sodium and potassium doping was effective for improvement of the conversion efficiency in CIGS thin film solar cells, and it may be effective in CTS thin film solar cell. In this study, CTS thin films were fabricated by sulfurization with the addition of NaF and KF, and applied to photovoltaic devices. We carried out several KF addition experiments and investigated the compositional, structural, morphological, and electrical characterizations of the CTS thin films and solar cells. Moreover, the effective method of KF addition of CTS thin film solar cells were investigated.

5.3 Experimental procedure

We carried out two experiments of KF addition. In the first experiment, the CTS thin films were fabricated by two-stage annealing. The stacked NaF/Cu/Sn precursors were deposited on Mo/SLG substrates using an ULVAC VPC-410 vacuum evaporation apparatus. The molar ratio of the evaporation materials was Cu : Sn : NaF = 1:0 : 0:6 : 0:075. The precursors were set in vacuum-sealed glass ampoules with an internal volume of 60 cm^3 with elemental sulfur and tin shots. The amounts of sulfur and tin were constant at 0.062 and 0.046 g, respectively. The precursors were crystallized by annealing in sulfur/tin mixed atmosphere for 30 min at 570 °C. Then, KF was deposited on the crystallized thin film in the vacuum chamber at room temperature using the ULVAC VPC-410 vacuum evaporation apparatus. The KF/film-bilayer samples were annealed again in sulfur/tin mixed atmosphere for 30 min. The amounts of sulfur and tin were the same as in the first annealing. This time, the KF/Cu molar ratios were 0.02 and 0.05, and the second annealing temperatures were 350 and 500 °C. In the second experiment, the four-layer KF/NaF/Cu/Sn precursors, which were prepared in the same evaporation apparatus as in the first experiment, were employed. These four-layer precursors were crystallized by annealing in sulfur/tin mixed atmosphere for 30 min at 570 °C. The molar ratio of the evaporation materials was Cu : Sn : NaF : KF = 1:0 : 0:6 : 0:075 : x (x = 0.02 and 0.05). Next, the molar ratio of the evaporation materials was Cu : Sn : NaF : KF = 1:0 : 0:6 : y : 0:02 (y = 0 to 0.075). We fabricated solar cells with the configuration of Al grid contact/ Ga-doped ZnO transparent conducting layer/ non-doped ZnO/ CdS buffer layer/ CTS absorber layer/ Mo back contact/ SLG substrate by the following steps. CdS buffer layers with a thickness of 70 nm were deposited by chemical bath deposition, and i-ZnO buffer layers with a thickness of 50 nm were produced by RF magnetron sputtering. Transparent conductive ZnO:Ga films with a thickness of 0.4 μm were subsequently deposited by the DC magnetron sputtering of 3 wt. % Ga_2O_3-doped ZnO targets at a substrate temperature of 100 °C, and Al grids for the front

electrode were produced by vacuum evaporation using metal masks. The dimensions of the obtained solar cells without antireflection coatings were 5 × 5mm^2. The compositions of the obtained thin films were determined from the results of electron probe microanalysis (EPMA) performed by energy-dispersive spectrometry (EDS); the crystalline structure was examined by X-ray diffraction (XRD) analysis and Raman spectroscopy, while the morphologies were studied by scanning electron microscopy (SEM). Current–voltage (J–V) characteristics of the fabricated solar cells were measured using standard 1 sun (AM1.5, 100 mW/cm^2) illumination.

5.4 Results and discussions

5.4.1 Summary of characteristics of CTS thin films and solar cells in this study

Table 5.1 shows the summary of the fabrication conditions and the characteristics of CTS thin films and solar cells in this study. In the fabrication method of Chapter 4, the four-layer KF/NaF/Cu/Sn precursor was equivalent to KF/Cu = 0.0, and it means K-free. By EPMA analysis, the Cu/Sn molar ratio was found to range from 0.81 to 1.51. In the CTS thin film solar cells that achieved conversion efficiencies higher than 4% without KF, Cu/Sn molar ratio of 1.87 was reported, **[17]** and Cu/Sn molar ratio of 1.64 was shown in Chapter 4. In this study, the CTS thin films became Cu-poor upon the addition of KF. A similar tendency was reported in the CIGS thin film. **[15]** Therefore, it is considered that the content of Cu near the surface of the CTS thin film was decreased by KF addition.

Table 5.1 Fabrication conditions and characteristics of CTS thin films and solar cells.

Fabrication method	Sample No.	NaF/Cu (%)	KF/Cu (%)	Annealing temp. 1st/2nd (^{o}C)	Cell performance				Composition in film			
					V_{oc} (mV)	J_{sc} (mA/cm^2)	FF	η (%)	Cu (%)	Sn (%)	S (%)	Cu/Sn
Two-stage annealing	1a	7.5	2.0	570 / 350	293	24.71	0.41	2.93	19.60	14.20	66.20	1.38
	1b	7.5	2.0	570 / 500	270	25.69	0.36	2.48	21.02	14.06	64.92	1.50
	1c	7.5	5.0	570 / 350	188	3.02	0.00	0.00	21.10	14.60	64.30	1.45
	1d	7.5	5.0	570 / 500	239	15.27	0.25	0.92	19.60	15.30	65.10	1.28
Four-layer KF/NaF/Cu/Sn precursor	2a	7.5	2.0	570 / —	220	13.78	0.27	0.82	19.60	16.30	64.10	1.20
	2b	7.5	5.0	570 / —	259	21.45	0.32	1.78	21.70	15.40	62.90	1.41
	3a	0.0	2.0	570 / —	255	14.02	0.26	0.93	19.03	13.32	67.65	1.43
	3b	3.0	2.0	570 / —	262	17.92	0.27	1.26	20.07	24.73	55.21	0.81
	3c	4.5	2.0	570 / —	248	23.18	0.34	1.97	16.40	15.91	67.69	1.03
	3d	6.0	2.0	570 / —	249	25.03	0.41	2.57	17.38	15.07	67.56	1.15
	3e	7.5	2.0	570 / —	220	13.78	0.27	0.82	19.60	16.30	64.10	1.20

5.4.2 Crystal structure

The XRD patterns of the CTS thin films are shown in Figure 5.1. The XRD patterns showed several peaks corresponding to the diffraction line of the monoclinic CTS structure. Moreover, the peaks of Mo_xS_y were seen for some samples. Figure 5.2 shows the Raman spectra for CTS thin films. For all samples, the spectra had peaks at 290, 314, 352, and 374 cm^{-1}. These Raman peaks are in good agreement with the peaks of the monoclinic CTS structure reported by Berg et al., **[18]** Aihara et al., **[19]** and Chapter 4 of this thesis of K-free films. On the basis of the results of the XRD patterns and Raman spectra, it is considered that the addition of KF to a CTS thin film does not affect the crystal structure. Moreover, no Raman peaks of Mo_xS_y were observed, indicating that Mo_xS_y was formed in the vicinity of the Mo layer.

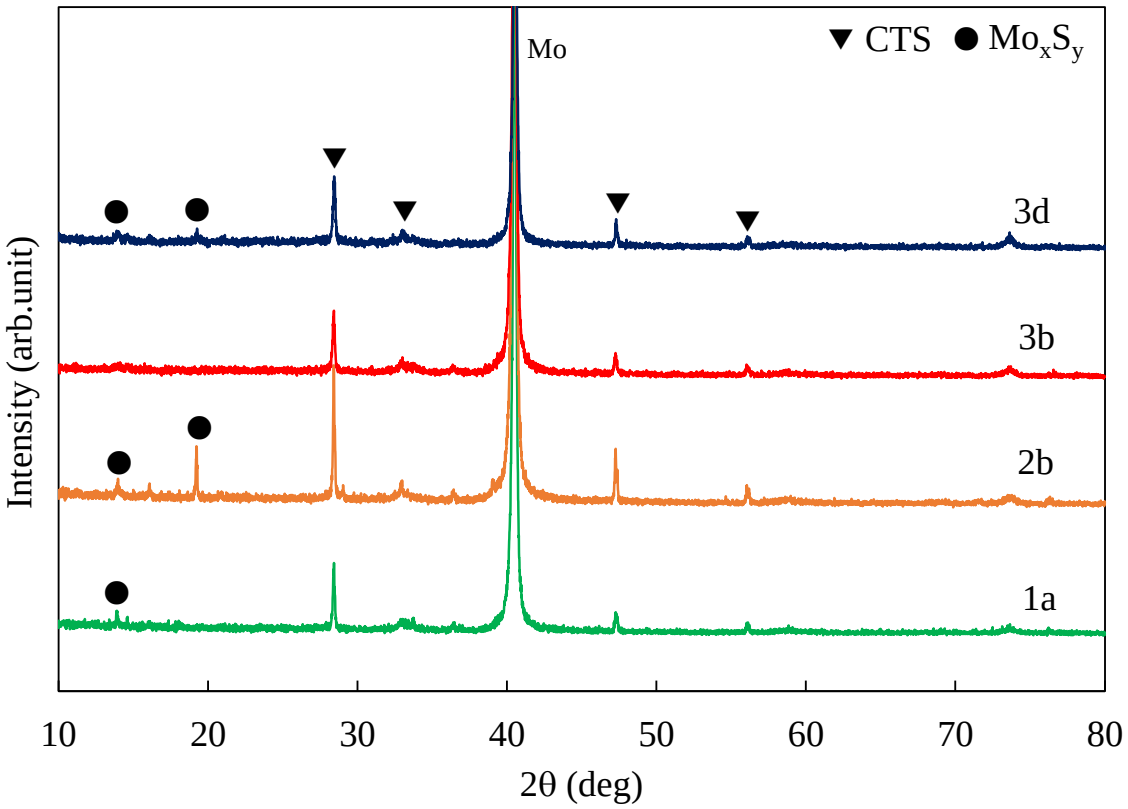

Figure 5.1 XRD patterns of the CTS thin films with KF addition.

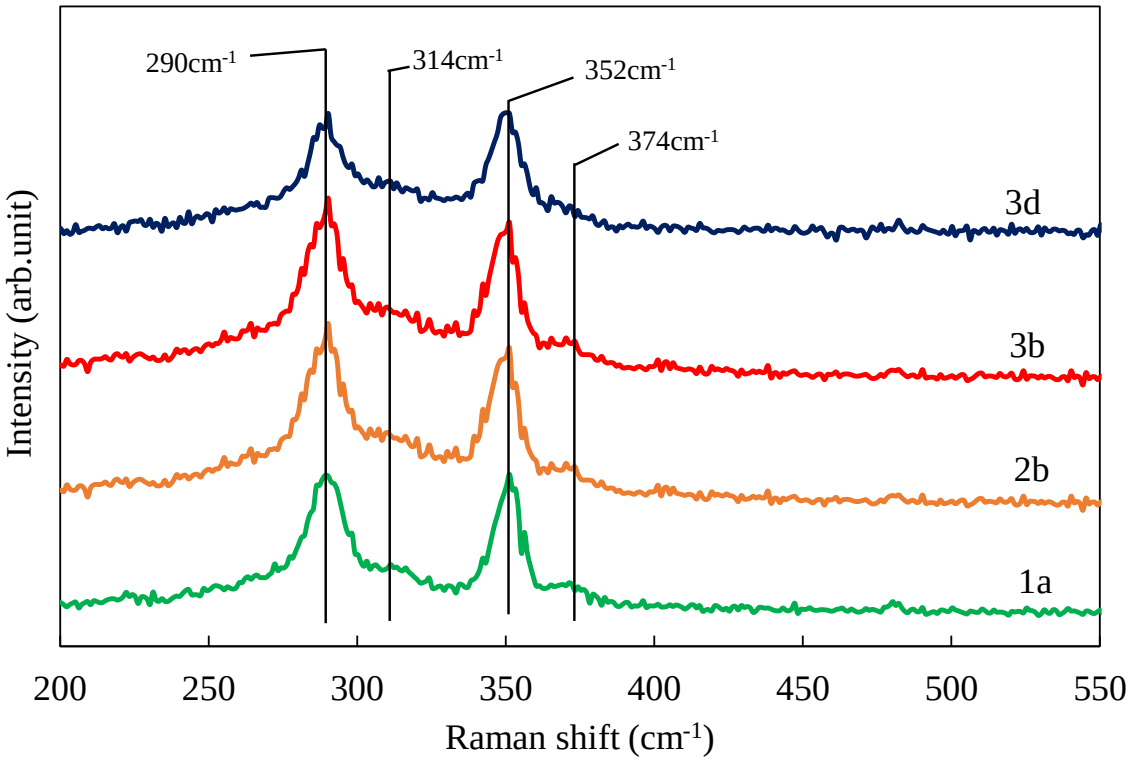

Figure 5.2 Raman spectra of the CTS thin films with KF addition.

5.4.3 Film morphologies

The surface and cross-sectional morphologies of CTS thin films are shown in Figure 5.3. The grain sizes and film thickness were approximately the same in all samples. As seen in Figure 5.3, sample 1a, fabricated by two-stage annealing, had a close-packed structure and a pinhole-free surface morphology in comparison with other samples.

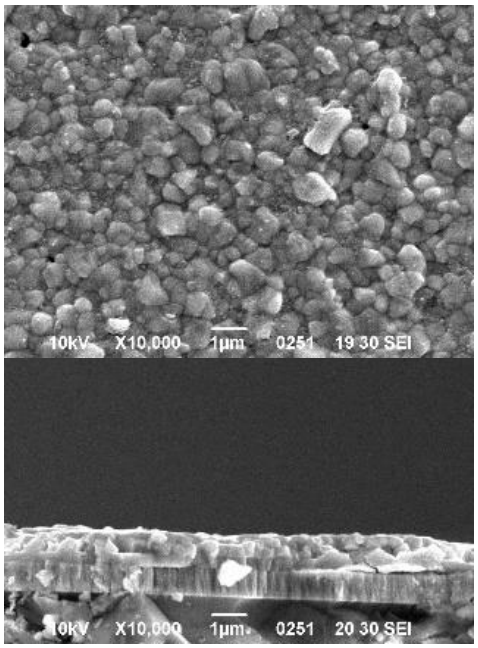

(a)

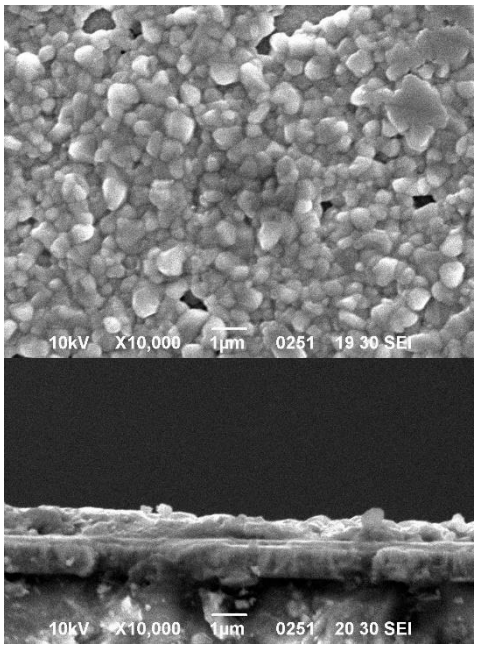

(b)

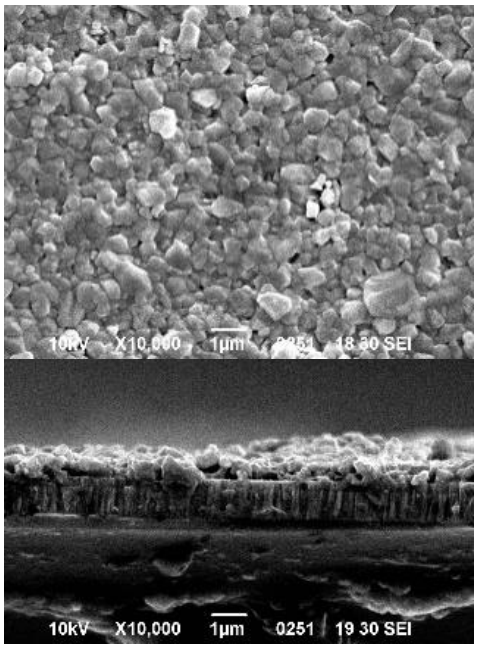

(c)

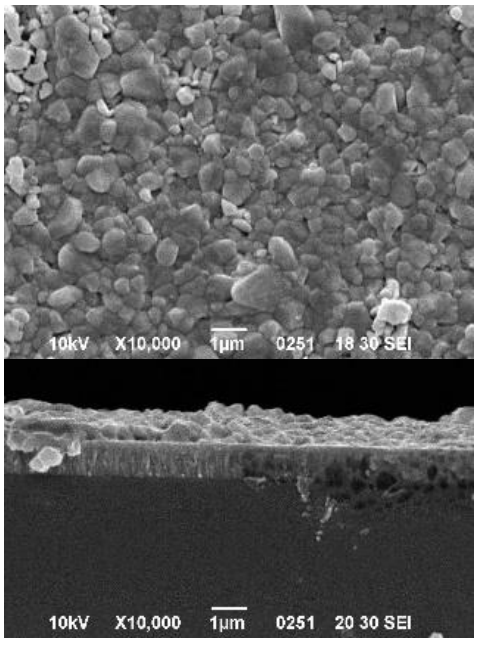

(d)

Figure 5.3 SEM images of the surface and cross section of CTS thin films with KF addition: (a) 1a, (b) 2b, (c) 3b, and (d) 3d.

5.4.4 Cell performances

Figure 5.4 shows the relationship between the V_{oc} of the CTS thin film solar cells and the Cu/Sn molar ratio of the CTS thin films. From Figure 5.4, it can be seen that the Cu/Sn molar ratios of the samples fabricated by two-stage annealing were approximately stable, whereas the samples prepared using KF/NaF/Cu/Sn precursor had various Cu/Sn molar ratios. The best solar cell in this study showed V_{oc} of 293 mV, J_{sc} of 24.71 mA/cm^2, FF of 0.41, and η of 2.93 %; it was fabricated by two-stage annealing with NaF/Cu = 0.075 and KF/Cu = 0.02 (sample 1a). In particular, this highest V_{oc} surpassed the values which were shown in Chapter 4 of this thesis (V_{oc} of 292 mV with NaF/Cu = 0.06 and 283 mV with NaF/Cu = 0.075) including that of the CTS thin film solar cell having the record conversion efficiency without KF addition. Moreover, in the CTS thin film solar cells that attained high V_{oc} values of 292 mV (in Chapter 4) and 293 mV (sample 1a in this study), the Cu/Sn molar ratios were 1.41 and 1.38, respectively. On the other hand, the Cu/Sn molar ratio of the CTS thin film solar cell in Chapter 4 of this thesis that showed the record conversion efficiency at V_{oc} of 283 mV was 1.64. From the above, it is considered that V_{oc} increased under Cu-poor composition. In CIGS thin film solar cells, the increase in V_{oc} with increasingly Cu-poor composition near the surface of the thin film and the increase in the carrier concentration upon KF incorporation have been reported. **[7, 10, 12, 14]** In this study, the CTS thin films became Cu-poor as shown in table 5.1 and figure 5.4 and V_{oc} was increased by KF addition; therefore, it is hypothesized that the addition of KF in the CTS thin films increases the carrier concentration. A future agenda is to investigate the effect of KF addition on the carrier concentration of CTS thin films. However, the increase in V_{oc} occurred only in one sample; therefore, it is considered that an optimum amount of added KF exists for two-stage annealing, and it is related to the Cu/Sn molar ratio of the thin film.

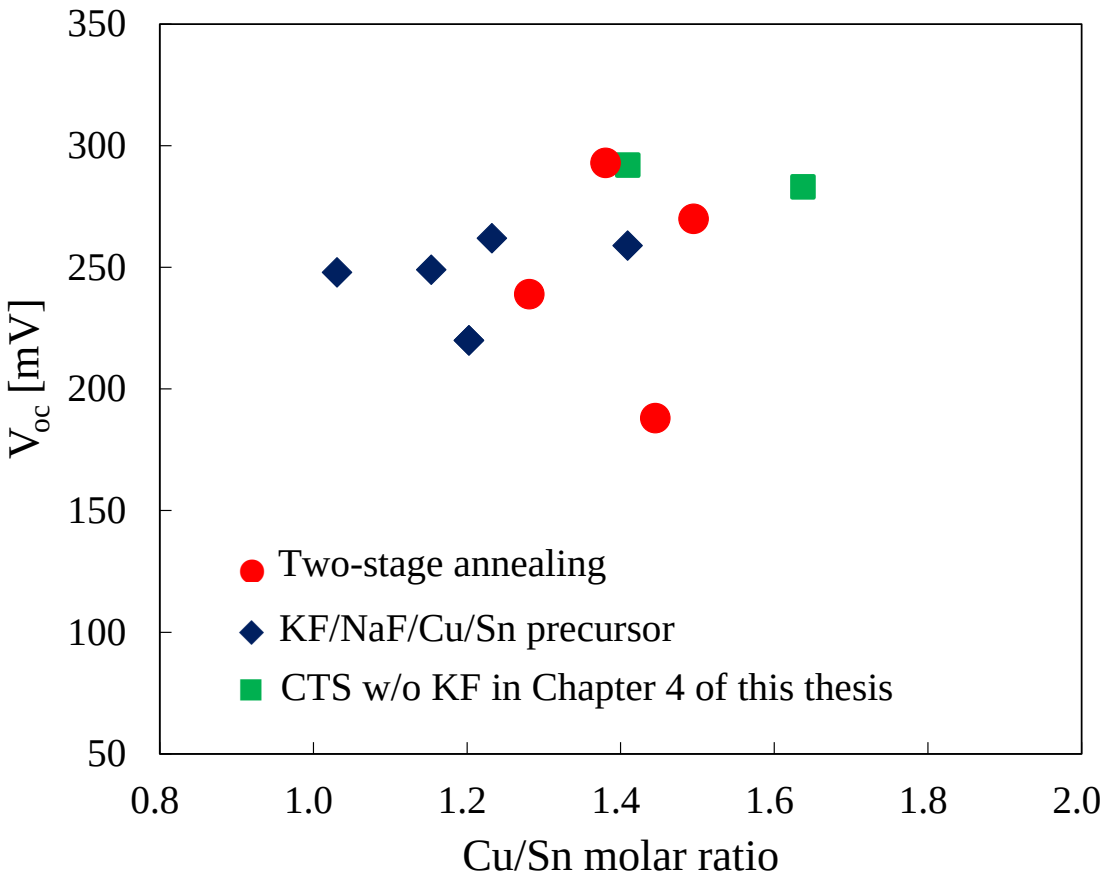

Figure 5.4 V_{oc} of CTS thin film solar cells with KF addition.

5.4.5 Relationship between band-gap energy and V_{oc}

Figure 5.5 shows the relationship between V_{oc} and the band-gap energy (E_g) of the various thin film solar cells in the recent research, and also shows V_g ($E_g/q - V_{oc}$, q is the electron charge). A low V_g indicates good solar cell performance. For the improvement of cell performance, increasing V_{oc} and decreasing V_g are very important. V_g of the CIGS thin film solar cell that attained a conversion efficiency of 21.7% **[7]** was as low as 0.38 V, and that of the CZTSSe thin film solar cell that demonstrated a conversion efficiency of 12.6% **[20]** was 0.62 V. Furthermore, V_g of the CZTSe thin film solar cell with 11.6% efficiency **[21]** was 0.58

V. On the other hand, V_g of the CTS thin film solar cell improved from 0.65 V in Chapter 4 of this thesis to 0.64 V in this study. However, it can be seen that V_g of the CTS thin film solar cell is higher than those of other thin film solar cells. For further improvement of the performance of CTS thin film solar cells, it is important to investigate the technique of fabrication process which is effective for increase in V_{oc}, such as the more increase of the carrier concentrations and the expansion of the band-gap energy.

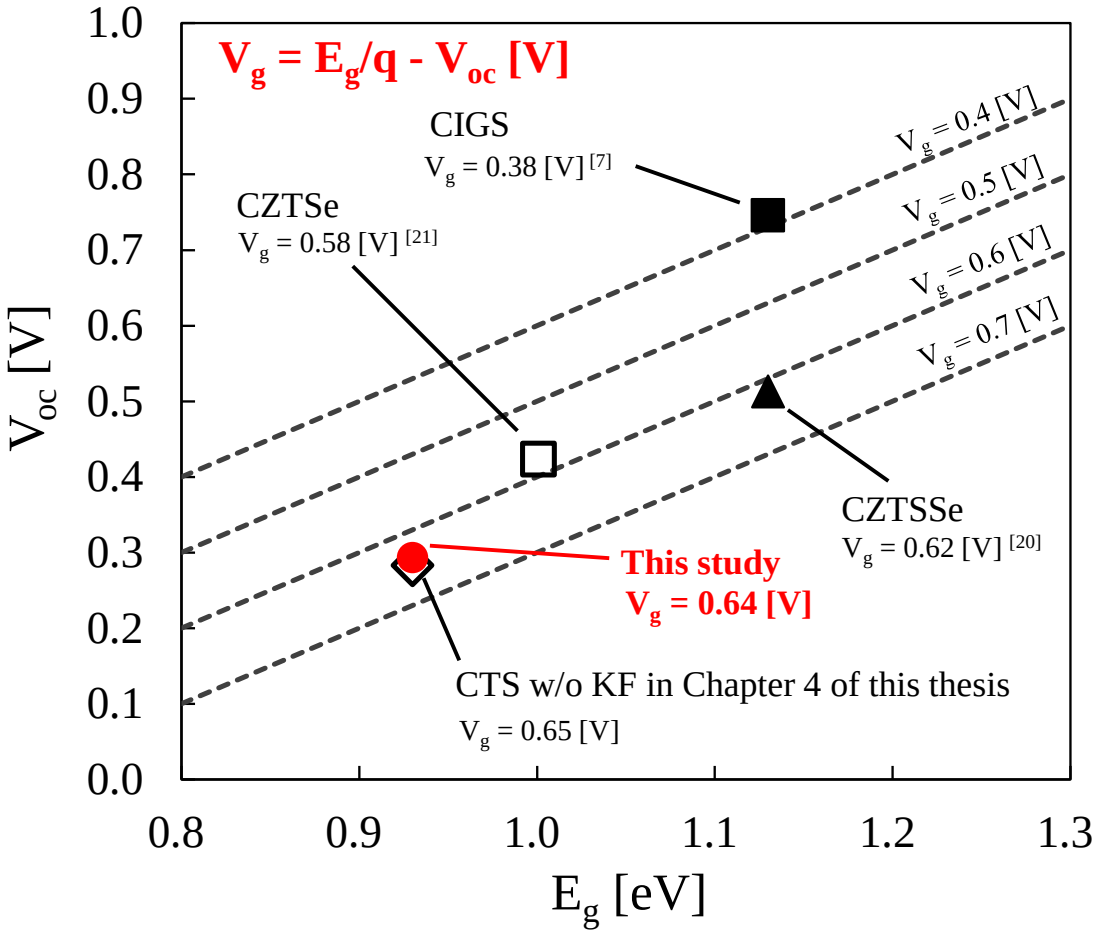

Figure 5.5 Relationship between E_g and V_{oc} of the thin-film solar cells in recent research.

5.5 Conclusions

In this study, CTS thin films were successfully fabricated in two KF-addition experiments. The composition of CTS thin films fabricated in this study was Cu-poor owing to the addition of KF. XRD patterns exhibited several peaks corresponding to diffraction lines of the monoclinic CTS structure. Furthermore, Raman spectra exhibited the peaks of the monoclinic CTS structure. The sample fabricated by two-stage annealing had a pinhole-free surface morphology and a close-packed structure in comparison with other samples. V_{oc} of the CTS thin film solar cell fabricated at NaF/Cu = 0.075 and KF/Cu = 0.02 by two-stage annealing was 293 mV, which surpassed the previously reported value, and it is considered that the carrier concentrations were more increased by KF addition to the CTS thin film which added NaF. V_g of the CTS thin film solar cell, i.e., the difference between the band-gap energy and V_{oc}, was improved to 0.64 V in this work.

REFERENCES

[1] W. N. Shafarman, J. Zhu, Effect of substrate temperature and deposition profile on evaporated Cu(InGa)Se_2 films and devices, Thin Solid Films **361-362**, 473 (2000).

[2] S. Nishiwaki, T. Saitoh, Y. Hashimoto, T. Negami, T. Wada, Preparation of Cu(In,Ga)Se_2 thin films at low substrate temperatures, J. Mater. Res. **16**, 394 (2001).

[3] I. Repins, C. Beall, N. Vora, C. DeHart, D. Kuciauskas, P. Dippo, B. To, J. Mann, W. C. Hsu, A. Goodrich, R. Noufi, Co-evaporated $Cu_2ZnSnSe_4$ films and devices, Sol. Energy Mater. Sol. Cells **101**, 154 (2012).

[4] C. M. Sutter-Fella, J. A. Stückelberger, H. Hagendorfer, F. La Mattina, L. Kranz, S. Nishiwaki, A. R. Uhl, Y. E. Romanyuk, A. N. Tiwari, Sodium Assisted Sintering of Chalcogenides and Its Application to Solution Processed $Cu_2ZnSn(S,Se)_4$ Thin Film Solar Cells, Chem. Mater. **26**, 1420 (2014).

[5] A. Nagaoka, H. Miyake, T. Taniyama, K. Kakimoto, Y. Nose, M.A. Scarpulla, K. Yoshino, Effects of sodium on electrical properties in Cu_2ZnSnS_4 single crystal, Appl. Phys. Lett. **104**, 152101 (2014).

[6] D. Rudmann, A. F. da Cunha, M. Kaelin, F. Kurdesau, H. Zogg, A. N. Tiwari, G. Bilger, Efficiency enhancement of Cu(In,Ga)Se_2 solar cells due to post-deposition Na incorporation, Appl. Phys. Lett. **84**, 1129 (2004).

[7] P. Jackson, D. Hariskos, R.Wuerz, O. Kiowski, A. Bauer, T.M. Friedlmeier, M. Powalla, Properties of Cu(In,Ga)Se_2 solar cells with new record efficiencies up to 21.7%, Phys. Status Solidi Rapid Res. Lett. **9**, 28 (2015).

[8] T. Mise, S. Tajima, T. Fukano, K. Higuchi, T. Washio, K. Jimbo, H. Katagiri, Improving the photovoltaic performance of co-evaporated Cu_2ZnSnS_4 thin-film solar cells by incorporation of sodium from NaF layers, Prog. Photovoltaics **24**, 1009 (2016).

[9] I. Khatri, H. Fukai, H. Yamaguchi, M. Sugiyama, T. Nakada, Effect of potassium fluoride post-deposition treatment on Cu(In,Ga)Se_2 thin films and solar cells fabricated onto sodalime glass substrates, Sol. Energy Mater. Sol. Cells **155**, 280 (2016).

[10] A. Laemmle, R. Wuerz, M. Powalla, Efficiency enhancement of Cu(In,Ga)Se_2 thin-film solar cells by a post-deposition treatment with potassium fluoride, Phys. Status Solidi: Rapid Res. Lett. **7**, 631 (2013).

[11] Z. Tong, C. Yan, Z. Su, F. Zeng, J. Yang, Y. Li, L. Jiang, Y. Lai, F. Liu, Effects of potassium doping on solution processed kesterite Cu_2ZnSnS_4 thin film solar cells, Appl. Phys. Lett. **105**, 223903 (2014).

[12] A. Laemmle, R. Wuerz, M. Powalla, Investigation of the effect of potassium on Cu(In,Ga)Se_2 layers and solar cells, Thin Solid Films **582**, 27 (2015).

[13] P. Jackson, D. Hariskos, R. Wuerz, W. Wischmann, M. Powalla, Compositional investigation of potassium doped Cu(In,Ga)Se_2 solar cells with efficiencies up to 20.8%, Phys. Status Solidi: Rapid Res. Lett. **8**, 219 (2014).

[14] P. Reinhard, B. Bissig, F. Pianezzi, E. Avancini, H. Hagendorfer, D. Keller, P. Fuchs, M. Döbeli, C. Vigo, P. Crivelli, S. Nishiwaki, S. Buecheler, A. N. Tiwari, Features of KF and NaF Postdeposition Treatments of Cu(In,Ga)Se_2 Absorbers for High Efficiency Thin Film Solar Cells, Chem. Mater. **27**, 5755 (2015).

[15] A. Chirilă, P. Reinhard, F. Pianezzi, P. Bloesch, A. R. Uhl, C. Fella, L. Kranz, D. Keller, C. Gretener, H. Hagendorfer, D. Jaeger, R. Erni, S. Nishiwaki, S. Buecheler, A. N. Tiwari, Potassium-induced surface modification of Cu(In,Ga)Se_2 thin films for high-efficiency solar cells, Nat. Mater. **12**, 1107 (2013).

[16] P. Jackson, R. Wuerz, D. Hariskos, E. Lotter, W. Witte, M. Powalla, Effect of heavy alkali elements in Cu(In,Ga)Se_2 solar cells with efficiencies up to 22.6%, Phys. Status Solidi: Rapid Res. Lett. **10**, 583 (2016).

[17] A. Kanai, K. Toyonaga, K. Chino, H. Katagiri, H. Araki, Fabrication of Cu_2SnS_3 thin-film solar cells with power conversion efficiency of over 4%, Jpn. J. Appl. Phys. **54**, 08KC06 (2015).

[18] D. M. Berg, R. Djemour, L. Gütay, S. Siebentritt, P. J. Dale, X. Fontane, V. Izquierdo-Roca, A. Pérez-Rodriguez, Raman analysis of monoclinic Cu_2SnS_3 thin films, Appl. Phys. Lett. **100**, 192103 (2012).

[19] N. Aihara, A. Kanai, K. Kimura, M. Yamada, K. Toyonaga, H. Araki, A. Takeuchi, H. Katagiri, Sulfurization temperature dependences of photovoltaic properties in Cu_2SnS_3-based thin-film solar cells, Jpn. J. Appl. Phys. **53**, 05FW13 (2014).

[20] W. Wang, M. T. Winkler, O. Gunawan, T. Gokmen, T. K. Todorov, Y. Zhu, D. Mitzi, Device Characteristics of CZTSSe Thin-Film Solar Cells with 12.6% Efficiency, Ext. Abstr. Adv. Energy Mater. **4**, 1301465 (2014).

[21] Y. S. Lee, T. Gershon, O. Gunawan, T. K. Todorov, T. Gokmen, Y. Virgus, S. Guha, $Cu_2ZnSnSe_4$ Thin-Film Solar Cells by Thermal Co-evaporation with 11.6% Efficiency and Improved Minority Carrier Diffusion Length, Adv. Energy Mater. **5**, 1401372 (2015).

CHAPTER 6

$(Cu,Ag)_2SnS_3$ thin film solar cells fabricated by sulfurization

6.1 Introduction

As we mentioned in Chapter 4, the CTS thin film solar cells fabricated by sulfurization using NaF added precursors have achieved a record conversion efficiency equal to 4.63 %. The open-circuit-voltage (V_{oc}) of this CTS thin film solar cell was 283 mV. In addition, the CTS thin film solar cells fabricated by sulfurization with the addition of NaF and KF demonstrated the V_{oc} of 293 mV in Chapter 5.On the other hand, the V_{oc} of CZTSSe which achieved the highest conversion efficiency in CZTS-based of 12.6% was 513.4 mV, **[1]** and this V_{oc} was very large

in comparison with the value of CTS. The band-gap energy of the CTS presented in Chapter 4 of 0.93eV is slightly smaller than the ideal value of around 1.4 eV **[2]** for solar spectrum absorption material, and it is considered that it is one of the reason of low V_{oc}. One promising approach to expand the band-gap energy of an absorber is to partially replace the elements. Morihama et al. reported the band-gap energy of CZTSe increased after some of the Sn was replaced with Ge **[3]**. In their study, they synthesized $Cu_2Zn(Sn,Ge)Se_4$ (CZTGSe) solid solution powders, and were able to control the band-gap energy from 1.0 eV for CZTSe to 1.35 eV for $Cu_2ZnGeSe_4$ **[3]**. Furthermore, Gong et al. reported $(Cu,Ag)_2ZnSnS_4$ (CAZTS) and $(Cu,Ag)_2ZnSnSe_4$ (CAZTSe), which incorporated Ag into CZTS and CZTSe, respectively **[4]**. In their report, the band-gap energies of CAZTS and CAZTSe ranged from 1.49 eV to 2.01 eV, and from 0.98 eV to 1.34 eV, respectively. In addition, the band-gap energies of CAZTS and CAZTSe exhibited bowing as the Ag content increased. The band-gap energy bowing of compound semiconductors has also been reported by other groups **[5–7]**. Most recently, conversion efficiencies of CAZTSe solar cells have increased above 10% **[8]**. Based on the above, we expect that the band-gap energy of CTS may be expanded by incorporating Ge and/or Ag, which also may help improve the performance of the cell. Umehara et al. replaced some of the Sn in the CTS with Ge in a $Cu_2(Sn,Ge)S_3$ thin film solar cell, and achieved a conversion efficiency of 6.01% with Ge / (Ge+ Sn) = 0.17 **[9]**. In their report, with the addition of Ge, the band-gap energy increased from 0.93 eV to 1.02 eV and the cell performance improved. In particular, the V_{oc} increased by > 100 mV, and the conversion efficiency improved by > 3%. Belandria et al. **[10]** and Fedorchuk et al. **[11]** reported a band-gap energy of 1.26 eV in Ag_2SnS_3 (ATS) when Cu was substituted for Ag in the CTS. Therefore, based on these results, we expect that the band-gap energy of alloyed $(Cu,Ag)_2SnS_3$ (CATS) may be controllable to 1.26 eV and, in comparison with the CTS thin film solar cells, we expect a high V_{oc} and high conversion efficiency. To the best of our knowledge, there are no reports describing the preparation of

alloyed CATS thin films and solar cells.

6.2 Objective of this study

It is considered that the CATS thin film fabricated by Ag doping for CTS thin film expand the band-gap energy in comparison with CTS thin film, and V_{oc} and the conversion efficiency may improve. In this study, CATS thin films and solar cells varying the Ag/(Ag+Cu) molar ratio and sulfurization temperature were fabricated by sulfurization. We have investigated the compositional, structural, morphological, optical, and electrical characterizations of these thin films and solar cells, and the effects of Ag doping on the band-gap energy and V_{oc} of CATS thin film solar cells fabricated by the sulfurization process have discussed.

6.3 Experimental procedure

In the experiments, stacked NaF/Sn/(Ag+Cu) precursors were deposited on Mo/SLG substrates by sequential evaporation using an ULVAC VPC-410 vacuum evaporation apparatus with Ag, Cu and Sn elements and NaF. The mole ratio of the evaporation materials was held constant at (Ag+Cu) : Sn : NaF = 1.0 : 0.6 : 0.075, which are the same conditions as those used to fabricate the high performance CTS thin film solar cells in Chapter 4 of this thesis. The Ag/(Ag+Cu) molar ratio of the evaporation materials was varied from 0 to 0.2, the precursors were set in vacuum-sealed glass ampoules with an internal volume of 60 cm^3 with elemental sulfur and tin shots, and the amounts of sulfur and tin were maintained constant at 0.062 and 0.046 g, respectively. The precursors were crystallized by annealing in a mixed sulfur/tin

atmosphere for 30 min at T °C (T =530 and 570 °C). Solar cells with a configuration of Al grid contact/ Ga-doped ZnO transparent conducting layer/ non-doped ZnO/ CdS buffer layer/ CATS absorber layer/ Mo back contact/SLG substrate were fabricated using the following steps. CdS buffer layers of n-type semiconductor with thicknesses of 70 nm were deposited while the solution temperature was raised from 35 °C to 65 °C by chemical bath deposition, while i-ZnO buffer layers with thicknesses of 50 nm were produced by RF magnetron sputtering. Transparent conductive ZnO:Ga films with thicknesses of 0.4 μm were subsequently deposited by DC magnetron sputtering of 3 wt. % Ga_2O_3-doped ZnO targets at a substrate temperature of 100 °C to obtain a low resistive TCO film, and Al grids for the front electrode were produced using metal masks by vacuum evaporation. The dimensions of the obtained solar cells without antireflection coatings were 5 × 5 mm^2. The compositions of the obtained thin films were determined from the results of an electron probe microanalysis (EPMA) performed by energy-dispersive spectrometry (EDS). The crystalline structure was examined by X-ray diffraction (XRD) analysis and Raman spectroscopy, while the morphologies were studied by scanning electron microscopy (SEM). The quantum efficiencies (QE) and current-voltage (J−V) characteristics of the fabricated solar cells were measured using standard 1 sun (AM1.5, 100 mW/cm^2) illumination.

6.4 Results and discussions

6.4.1 Film compositions

Based on the results of the EPMA analysis, the relationship between the Ag/(Ag+Cu) molar ratio in thin films and that in the evaporation materials is shown in Figure 6.1. The Ag/(Ag+Cu) molar ratio in the thin films increased as the Ag/(Ag+Cu) molar ratio in the evaporation materials increased. The relationships between the (Ag+Cu)/Sn molar ratio in the thin films and that in the evaporation materials are shown in Figure 6.2. The (Ag+Cu)/Sn molar ratio in the thin films fabricated at 530 °C and 570 °C were in the range from 1.38 to 1.73 and 1.26 to 2.03, respectively. In the CTS thin film solar cells that achieved conversion efficiencies above 4% including the CTS thin film solar cell which was shown in Chapter 4 of this thesis, the reported Cu/Sn molar ratios were lower than a stoichiometric composition ratio of 2.0, which indicated a Cu-poor composition **[12]**. Although the (Ag+Cu)/Sn molar ratio of the thin film prepared at Ag/(Ag+Cu) = 0 and T = 570 °C was 2.03, all other samples in this study became (Ag+Cu)-poor. This tendency of the film composition ratios was similar to that of the CTS thin film solar cells that obtained high conversion efficiencies. In addition, the (Ag+Cu)/Sn molar ratio in the thin films decreased as Ag/(Ag+Cu) molar ratio in the evaporation materials increased, and the samples fabricated at high sulfurization temperatures in particular strongly exhibited this tendency. It was observed that the quantity of re-evaporated Sn had a tendency to decrease as the quantity of additional Ag increased.

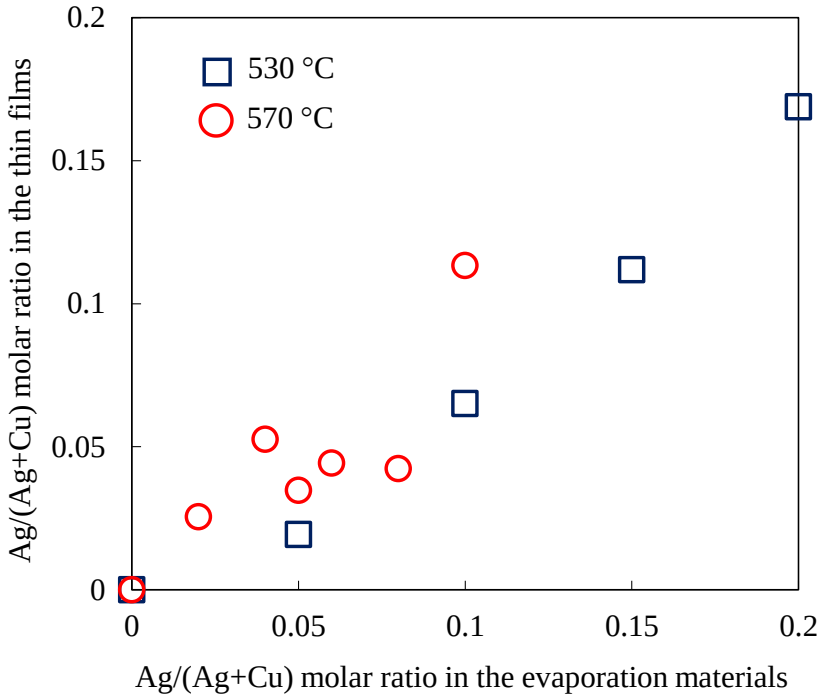

Figure 6.1 Relationship between the Ag/(Ag+Cu) molar ratio in the thin films and that in the evaporation materials.

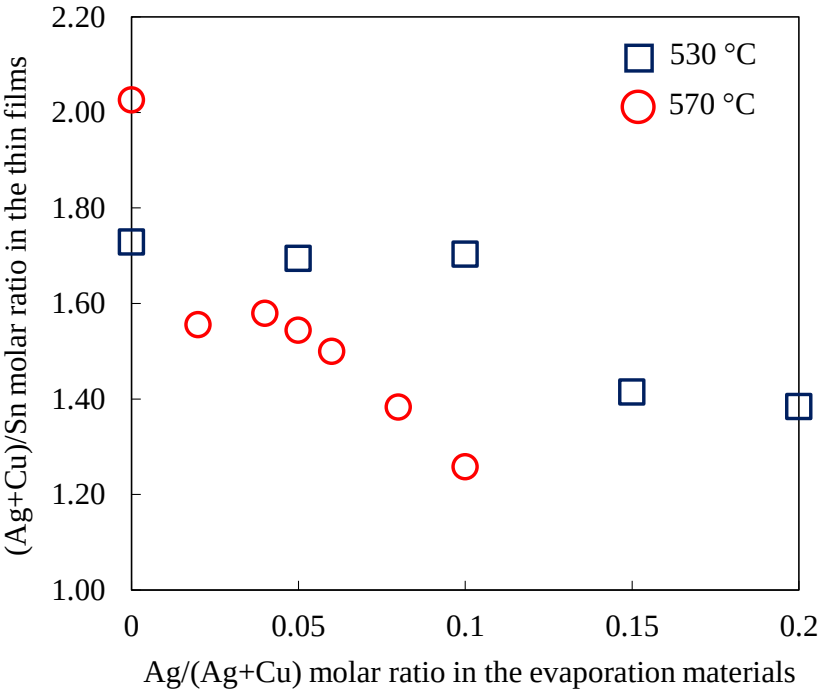

Figure 6.2 Relationship between the (Ag+Cu)/Sn molar ratio in the thin films and that in the evaporation materials.

6.4.2 Crystal structure

Figure 6.3 displays the XRD patterns for the CATS thin films. For all samples, the XRD patterns showed several peaks near the diffraction line of the monoclinic CTS structure. Moreover, the foreign phases of Na_9Sn_4 (indicated by the diamond markers in Figure 6.3. PDF#03-065- 6193) and MoS_2 (indicated by the square markers in Figure 6.3. PDF#01-089-5112) were seen in almost all of the samples at T = 570 °C. In addition, the strong diffraction peaks of Na_9Sn_4 were seen with high values of the Ag/(Ag+Cu) molar ratio. Based on the above, when the Na_9Sn_4 was formed with a high sulfurization temperature, the (Ag+Cu)/Sn molar ratio in the thin film decreased, as shown in Figure 6.2.

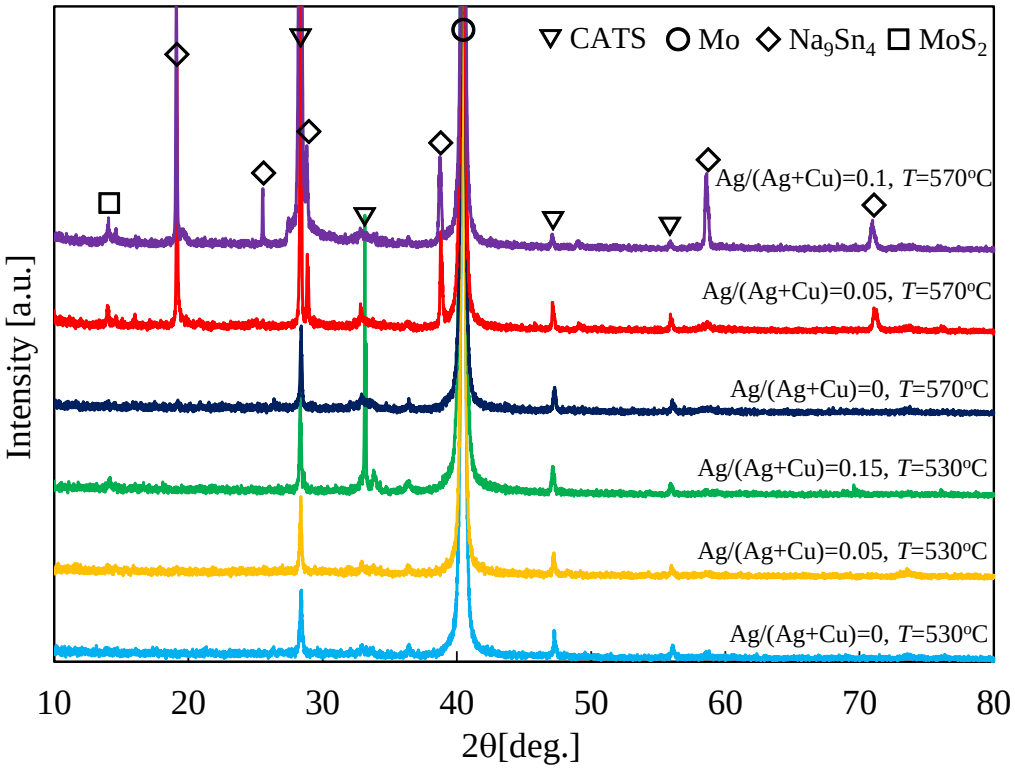

Figure 6.3 XRD patterns for the thin films prepared at various Ag/(Ag+Cu) molar ratios of evaporation materials with two sulfurization temperatures.

Figure 6.4 shows the relationship between the position of the 200 peak (around 2θ = 28°) of XRD patterns and the Ag/(Ag+Cu) molar ratio in the films. The 200 peak of the CTS is at 28.409°, and that of the ATS is at 27.165°. It can be seen that the position of the 200 peak shifted lower as the Ag/(Ag+Cu) molar ratio increased. In addition, the relationship between the lattice spacing calculated from Bragg's equation (2dsinθ = nλ) and the Ag/(Ag+Cu) molar ratio in the films are shown in Figure 6.5. The straight dotted line in Figure 6.5 refers to the connection between the CTS (3.1392 Å) and ATS (3.2800 Å) values. The lattice spacing increased along the dotted line as the Ag/(Ag+Cu) molar ratio in films increased up to a value of approximately 0.05, and became saturated at values over 0.1. Therefore, we concluded that the CATS was fabricated by gradual substitution of Cu for Ag until around Ag/(Ag+Cu) = 0.05, and that quantities of Ag higher than Ag/(Ag+Cu) = 0.1 did not contribute to the formation of the alloyed CATS crystals.

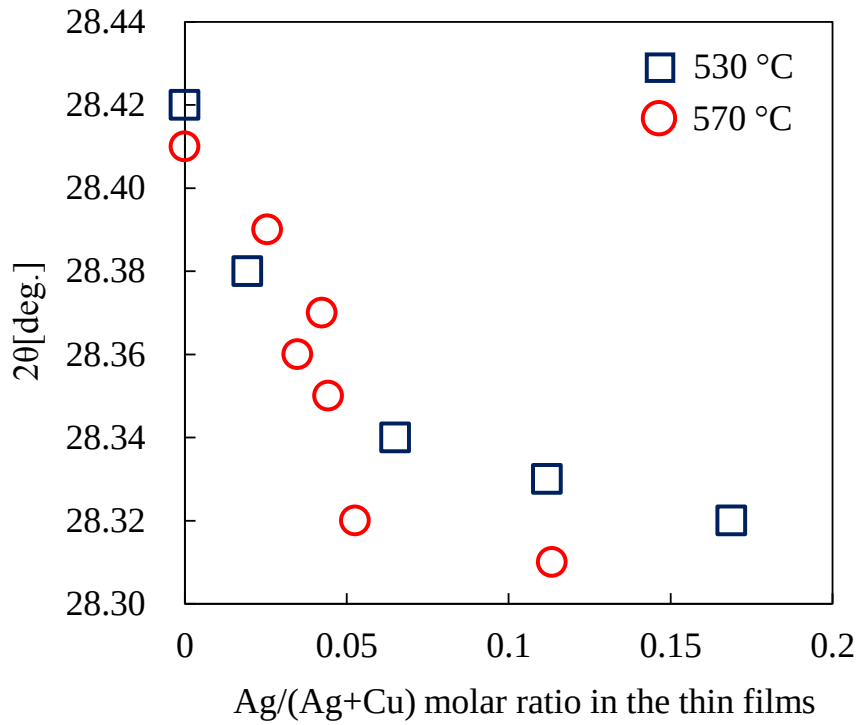

Figure 6.4 Relationship between the position of the 200 peak of the XRD patterns and the Ag/(Ag+Cu) molar ratio in the thin films.

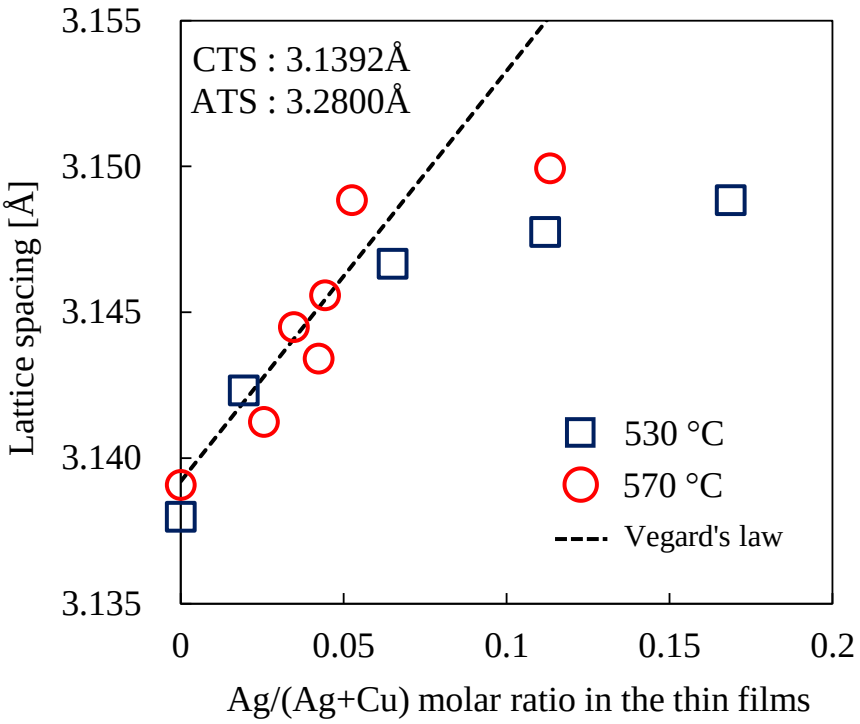

Figure 6.5 Relationship between the lattice spacing and the Ag/(Ag+Cu) molar ratio in the thin films.

Furthermore, we investigated in detail the foreign phases of the XRD patterns, such as Na_9Sn_4 and MoS_2. Specifically, we measured several XRD patterns at each stage of the fabrication of the CATS thin film solar cell that employed CATS thin film with Ag/(Ag+Cu) = 0.05 and T = 570 °C, and investigated the changes in the foreign phases. The XRD patterns of the thin films that were rinsed with H_2O, the thin films that were rinsed with an H_2O and ammonium solution, and the solar cells fabricated using the thin films that were rinsed with the H_2O and ammonium solution are shown in Figure 6.6. As can be seen from the figure, the foreign phases of Na_9Sn_4 and MoS_2 existed in films at all stages, as well as in the solar cell device. Other researchers have reported that the diffraction peaks thought to be Na_9Sn_4 were observed with monoclinic CTS diffraction peaks for sulfurized films fabricated at high sulfurization temperatures directly

on SLG substrates **[13, 14]**. These peaks were assigned as "unknown," and a compound consisting of sodium eluted from the SLG substrate was thought to have formed **[13]**. Based on the above, it was estimated that the Na_9Sn_4 observed in this study was formed by sodium that diffused from the SLG, and the Sn of the evaporation material.

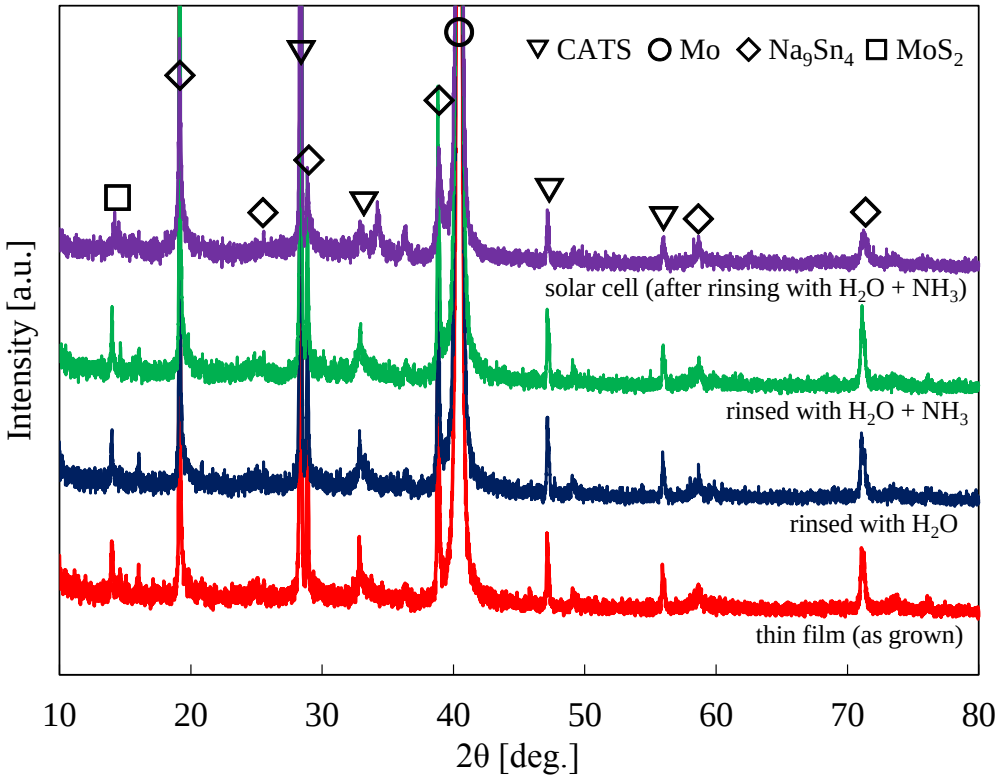

Figure 6.6 XRD patterns for the thin films and solar cells.

Figure 6.7 shows the Raman spectra for the CATS thin films. For all samples, the spectra had peaks at 290 cm^{-1}, 314 cm^{-1}, 352 cm^{-1}, and 374 cm^{-1}. These Raman peaks were in good agreement with the peaks of the monoclinic CTS structure reported by CTS researchers **[13, 15]**. The detection depth of the Raman measurement was about 250 nm; therefore, it was determined that the CTS formed near the surface of the thin films. In addition, the weak peak at about 470 cm^{-1} that was seen in some samples was Cu_2S. **[16]** On the other hand, no Raman

peaks corresponding to the foreign phases of Na_9Sn_4 and MoS_2 were observed in Figure 6.7. This may have been because the foreign phases of Na_9Sn_4 and MoS_2 formed in the middle of the thin film and/or in the vicinity of the Mo layer.

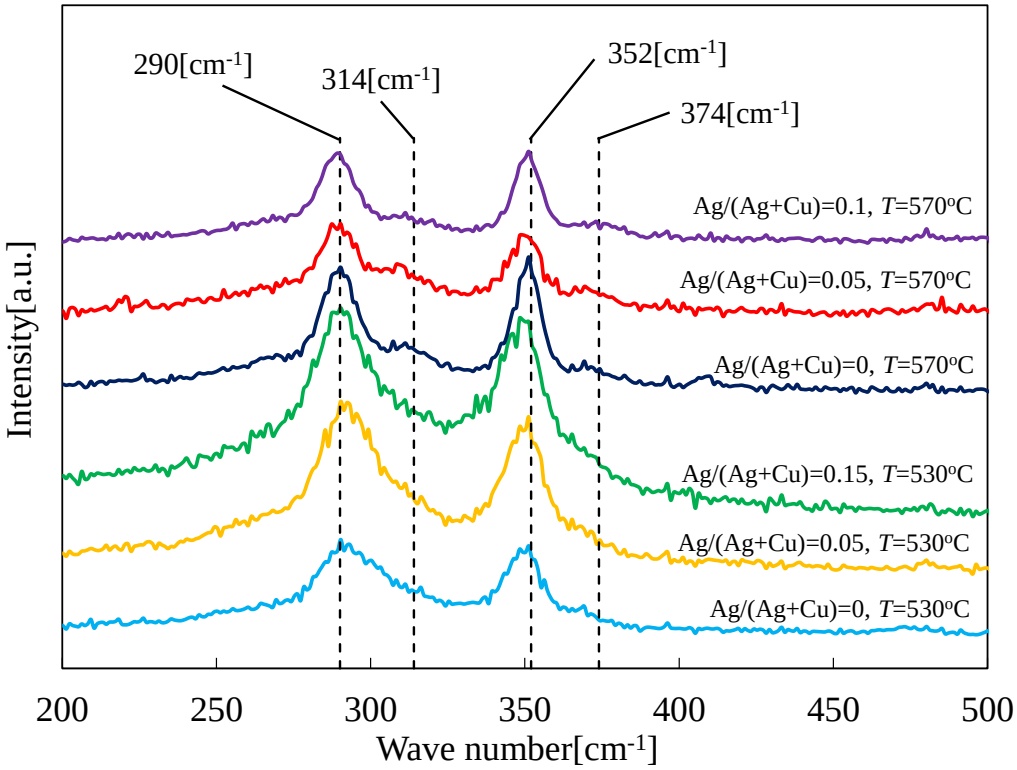

Figure 6.7 Raman spectra for the thin films prepared at various Ag/(Ag+Cu) molar ratios of evaporation materials with two sulfurization temperatures.

6.4.3 Film morphologies

The surface and cross-sectional morphologies of the CATS thin films are shown in Figure 6.8. The grain size in the thin films increased as the Ag/(Ag+Cu) molar ratio increased, and the sample of the Ag/(Ag+Cu) = 0.05 with T = 570 °C (Figure 6.8 (d)) had a close-packed structure and large crystal grains in comparison to that of the other samples including Ag-free CTS.

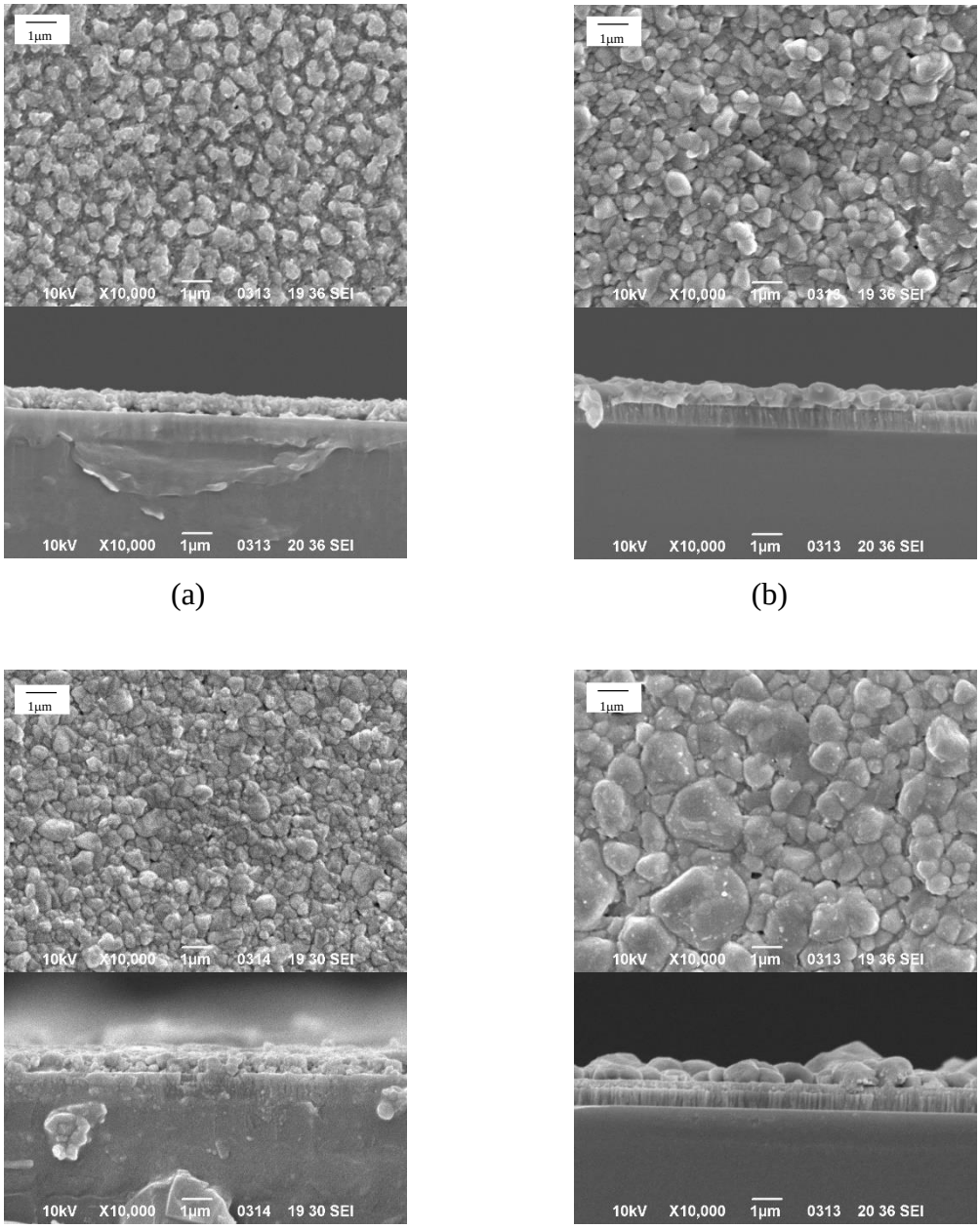

Figure 6.8 SEM images of the surface and cross-sections of the CATS thin films prepared at various Ag/(Ag+Cu) molar ratios of evaporation materials with two sulfurization temperatures: (a) Ag/(Ag+Cu) = 0 (T = 530 °C), (b) Ag/(Ag+Cu) = 0.1 (T = 530 °C), (c) Ag/(Ag+Cu) = 0 (T = 570 °C), and (d) Ag/(Ag+Cu) = 0.05 (T = 570 °C).

6.4.4 Cell performances

Figure 6.9 shows the V_{oc}, short-circuit current density (J_{sc}), fill factor (FF), and conversion efficiency (η) for the CATS thin film solar cells prepared at various Ag/(Ag+Cu) molar ratios of the evaporating materials. From Figure 6.9, it can be seen that the values of all characteristics in the CATS thin film solar cells had upward trends until the Ag/(Ag+Cu) molar ratio in the evaporation materials reached 0.05. Based on the increase in V_{oc}, it was apparent that that the band-gap energy of the CATS thin films changed with the Ag/(Ag+Cu) molar ratio. Moreover, a large increase in J_{sc} was obtained with the increase in the diffusion length of the minority carrier caused by the improvements in the thin film morphology, such as the formation of large crystal grains and close-packed structure, as shown in Figure 6.8. The CATS thin film solar cell that had the highest conversion efficiency in this study was fabricated with Ag/(Ag+Cu) = 0.05 and T = 570 °C. The measured parameters for this solar cell were V_{oc} = 244 mV, J_{sc} = 36.9 mA/cm^2, FF = 0.45, and η = 4.07 %.

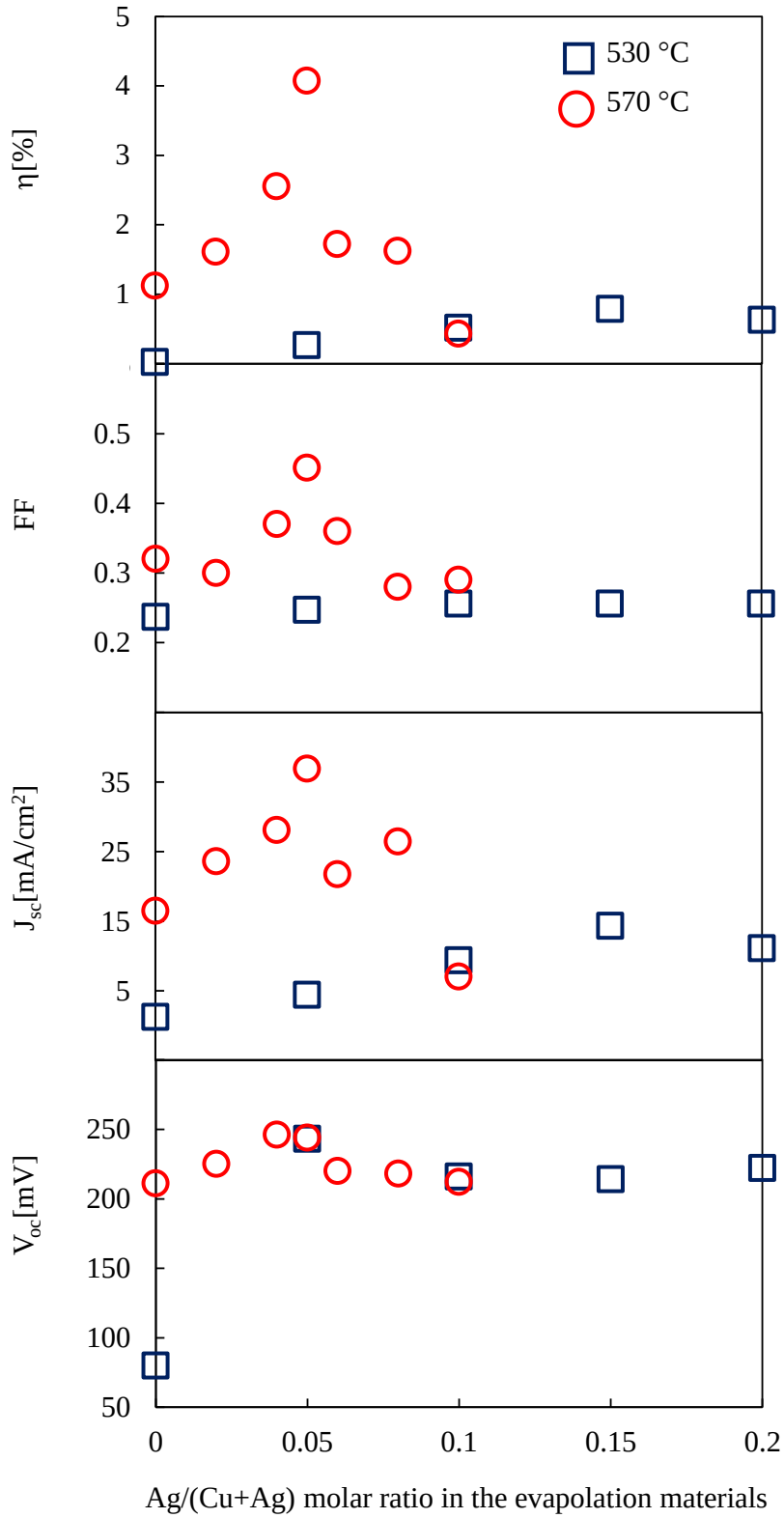

Figure 6.9 V_{oc}, J_{sc}, FF, and η of CATS thin film solar cells prepared at various Ag/(Ag+Cu) molar ratios of evaporation materials with two sulfurization temperatures.

6.4.5 Quantum efficiencies

Figure 6.10 shows the QE curves of the CATS thin film solar cells, which were fabricated at T = 570 °C and measured under practical use conditions with a white light irradiation density of 100 mW/cm^2. The QE of the long-wavelength range (> 500 nm) increased as the Ag/(Ag+Cu) molar ratio of the evaporation materials increased. However, the QE of long-wavelength range was the largest when Ag/(Ag+Cu) = 0.05, and decreased beyond this point. This phenomenon was in good agreement with the increase of J_{sc}; therefore, we reasoned that the high QE of the long-wavelength range were obtained due to the increase in the diffusion length of the minority carrier as a result of the improvements in the thin film morphology. In addition, the QE of the short-wavelength range (< 500 nm) of all samples, except the sample of Ag/(Ag+Cu) = 0.05, were very high compared to the sample of Ag/(Ag+Cu) = 0.05; however, further investigation will be necessary to determine the cause. Furthermore, two steps of sharp optical absorptions around 1200 nm and around 1300 nm were seen in all samples. This has also been reported by other CTS thin film solar cell research groups **[9, 13]**. In their reports, it was thought that the optical absorption around 1300 nm was the band edge absorption corresponding to the band-gap energy. However, an explanation for the optical absorption around 1200 nm has not yet been determined, and further investigation is necessary.

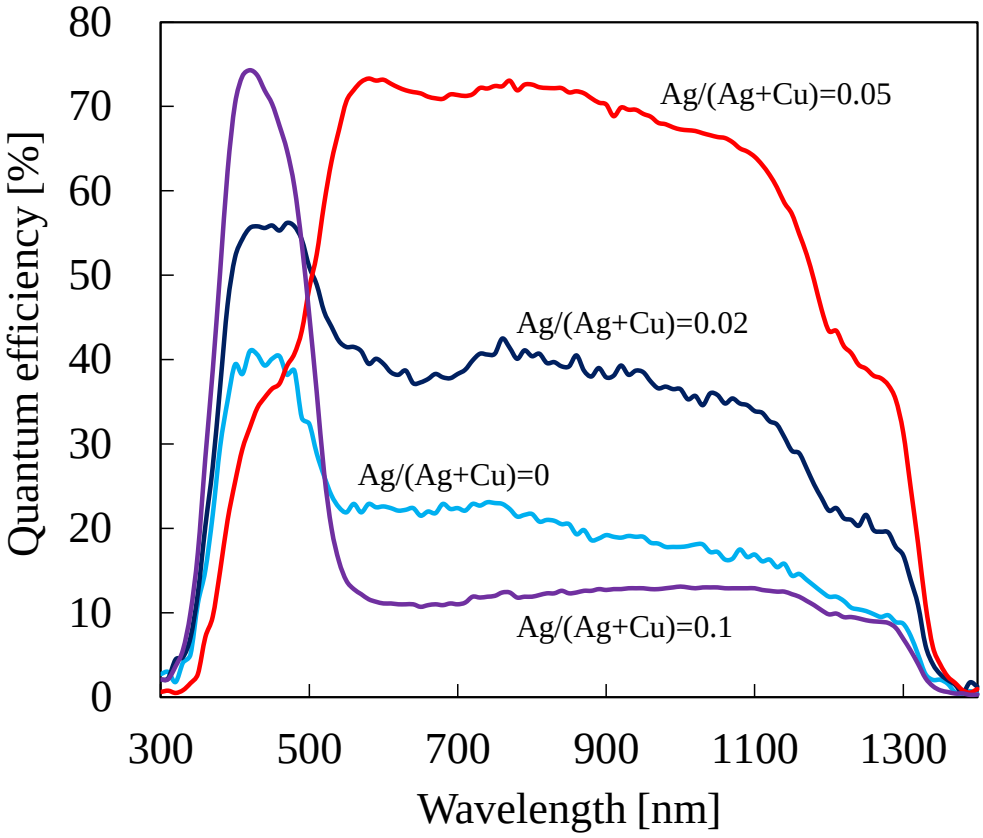

Figure 6.10 QE of the CATS thin film solar cells fabricated at various Ag/(Ag+Cu) molar ratios of evaporation materials with a sulfurization temperature of 570 °C.

6.4.6 Relationship between band-gap energy and V_{oc}

Assuming a very short minority carrier diffusion length, for a direct transition, a plot of $[h\nu \times \ln(1-QE)]^2$ versus $h\nu$ can be used to extrapolate the band-gap energy. **[17]** The sample transition energies in this study were estimated by extrapolating the measured QE values, and the relationship between the obtained band-gap energy for the CATS thin film solar cells and Ag/(Ag+Cu) molar ratio in thin films is shown in Figure 6.11. In addition, the value of V_{oc} of the CATS thin film solar cells is shown in Figure 6.11. The band-gap energies of CATS ranged

from 0.928 eV to 0.934 eV, and a slight increase in the band-gap energies was seen as the Ag/(Ag+Cu) molar ratio increased. Furthermore, the value of V_{oc} improved as the Ag/(Ag+Cu) molar ratio increased, which was the same tendency as that of the band-gap energies. Therefore, it was evident that the V_{oc} were improved by the expansion of the band-gap energy of the CATS thin film solar cells. However, further investigation will be necessary into the fabrication conditions of CATS thin films to further increase the band-gap energy beyond the saturation point at approximately 0.93 eV.

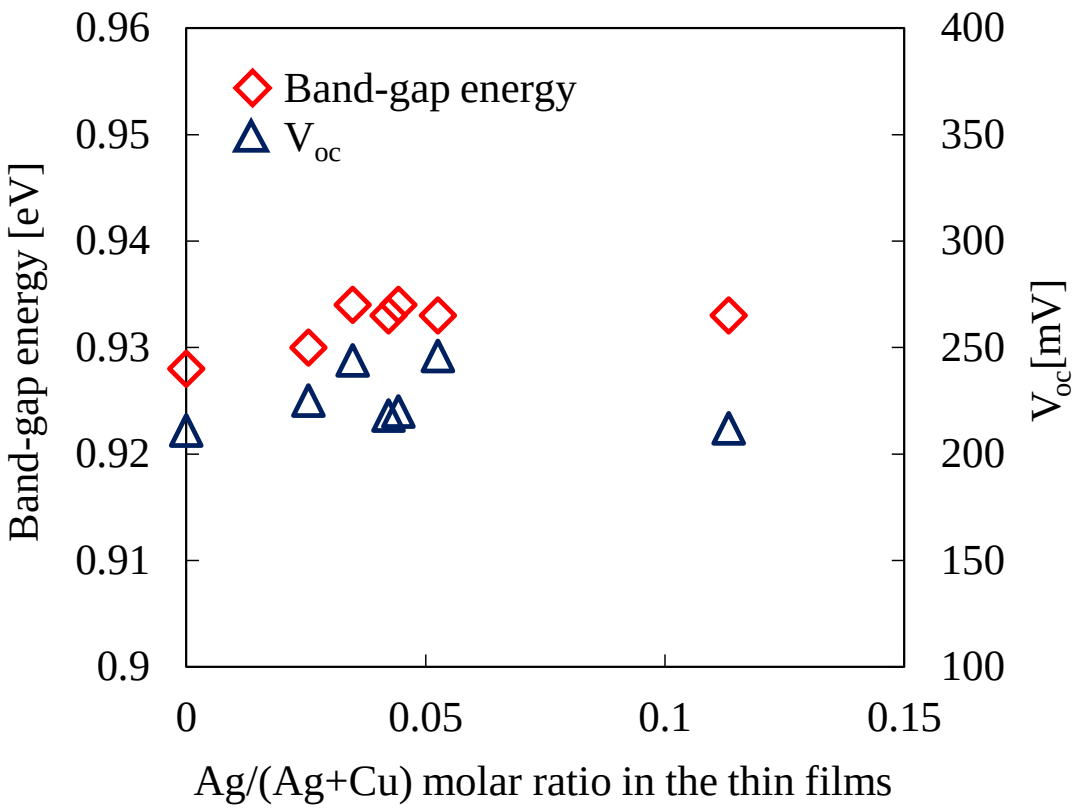

Figure 6.11 Relationship between the band-gap energies, V_{oc} and the Ag/(Ag+Cu) molar ratios in the thin films.

6.5 Conclusions

In this study, CATS thin films were successfully fabricated by sulfurization. The Ag/(Ag+Cu) molar ratio in the thin films increased along with that in the evaporation materials. The position of the 200 peak of the XRD pattern shifted to lower angles and the lattice spacing increased as the Ag/(Ag+Cu) molar ratio increased in the films. Moreover, foreign phases of Na_9Sn_4 and MoS_2 were seen in some of the samples fabricated at T = 570 °C. The Raman spectra was used to estimate the peaks of the monoclinic CTS structures. The grain sizes for the produced CATS thin films increased as the Ag/(Ag+Cu) molar ratio in the evaporation materials increased. In particular, large crystal grains were formed at T = 570 °C. The parameters for highest performance solar cell fabricated in this study at Ag/(Ag+Cu) = 0.05 in the evaporation material at T = 570 °C were measured to be V_{oc} = 244 mV, J_{sc} = 36.9 mA/cm^2, FF = 0.45, and η = 4.07 %. These results are for the most efficient CATS thin film solar cell yet reported. The band-gap energies of the CATS thin film solar cells fabricated in this study ranged from 0.928 eV to 0.934 eV, and the slight expansion of the band-gap energies and improvements in the cell performance was confirmed as the Ag/(Ag+Cu) molar ratio in the films increased.

REFERENCES

[1] W. Wang, M. T. Winkler, O. Gunawan, T. Gokmen, T. K. Todorov, Y. Zhu, D. Mitzi, Device Characteristics of CZTSSe Thin-Film Solar Cells with 12.6% Efficiency, Ext. Abstr. Adv. Energy Mater. **4**, 1301465 (2014).

[2] W. Shockley, H. J. Queisser, Detailed Balance Limit of Efficiency of p-n Junction Solar Cells, J. Appl. Phys. **32**, 510 (1961).

[3] M. Morihama, F. Gao, T. Maeda, T. Wada, Crystallographic and optical properties of $Cu_2Zn(Sn_{1-x}Ge_x)Se_4$ solid solution, Jpn. J. Appl. Phys. **53**, 04ER09 (2014).

[4] W. Gong, T. Tabata, K. Takei, M. Morihama, T. Maeda, T. Wada, Crystallographic and optical properties of $(Cu, Ag)_2ZnSnS_4$ and $(Cu, Ag)_2ZnSnSe_4$ solid solutions, Phys. Status Solidi C **12** 700, (2015).

[5] E.J. Bernard, A. Zunger, Optical bowing in zinc chalcogenide semiconductor alloys, Phys. Rev. B **34**, 5992 (1986).

[6] X. Liu, S.G. Bishop, J.N. Baillargeon, K.Y. Cheng, Band gap bowing in $GaP_{1-x}N_x$ alloys, Appl. Phys. Lett. **63**, 208 (1993).

[7] A. Silverman, A. Zunger, R. Kalish, J. Adler, Atomic-scale structure of disordered $Ga_{1-x}In_xP$ alloys, Phys. Rev. B **51**, 10795 (1995).

[8] T. Gershon, Y.S. Lee, P. Antunez, R. Mankad, S. Singh, D. Bishop, O. Gunawan, M. Hopstaken, R. Haight, Photovoltaic Materials and Devices Based on the Alloyed Kesterite Absorber $(Ag_xCu_{1-x})_2ZnSnSe_4$, Adv. Energy Mater. **6**, 1502468 (2016).

[9] M. Umehara, Y. Takeda, T. Motohiro, T. Sakai, H. Awano, R. Maekawa, $Cu_2Sn_{1-x}Ge_xS_3$ (x = 0.17) Thin-Film Solar Cells with High Conversion Efficiency of 6.0%, Appl. Phys. Express **6**, 045501 (2013).

[10] E. Belandria, B. J. Fernandez, Temperature Dependence of the Optical Absorption of the Ternary Compound Ag_2SnS_3, Jpn. J. Appl. Phys. **39**, 293 (2000).

[11] A. O. Fedorchuk, O. Ye, G. Lakshminarayana Zhbankov, I. V. Kityk, Y. Tokaichuk, G. L. Myronchuk, G. Ye, O. V. Yakymchuk Davydyuk, O. V. Parasyuk, Synthesis and spectral features of Ag_2SnS_3 crystals, Mater. Chem. Phys. **135**, 249 (2012).

[12] A. Kanai, K. Toyonaga, K. Chino, H. Katagiri, H. Araki, Fabrication of Cu_2SnS_3 thin-film solar cells with power conversion efficiency of over 4%, Jpn. J. Appl. Phys. **54**, 08KC06 (2015).

[13] N. Aihara, A. Kanai, K. Kimura, M. Yamada, K. Toyonaga, H. Araki, A. Takeuchi, H. Katagiri, Sulfurization temperature dependences of photovoltaic properties in Cu_2SnS_3-based thin-film solar cells, Jpn. J. Appl. Phys. **53**, 05FW13 (2014).

[14] K. Chino, J. Koike, S. Eguchi, H. Araki, R. Nakamura, K. Jimbo, H. Katagiri, Preparation of Cu_2SnS_3 Thin Films by Sulfurization of Cu/Sn Stacked Precursors, Jpn. J. Appl. Phys. **51**, 10NC35 (2012).

[15] D. M. Berg, R. Djemour, L. Gütay, S. Siebentritt, P. J. Dale, X. Fontane, V. Izquierdo-Roca, A. Pérez-Rodriguez, Raman analysis of monoclinic Cu_2SnS_3 thin films, Appl. Phys. Lett. **100**, 192103 (2012).

[16] H. D. Shelke, A. C. Lokhande, J. H. Kim, C. D. Lokhande, Photoelectrochemical (PEC) studies on Cu_2SnS_3 (CTS) thin films deposited by chemical bath deposition method, J. Colloid Interf. Sci. **506**, 144 (2017).

[17] G. Zoppi, I. Forbes, R. W. Miles, P. J. Dale, J. J. Scragg, L. M. Peter, $Cu_2ZnSnSe_4$ thin film solar cells produced by selenisation of magnetron sputtered precursors, Prog. Photovolt. Res. Appl. **17**, 315 (2009).

CHAPTER 7

Summary

7.1 Research summary

The photovoltaic power system including the solar cell is one of the promising technologies of the renewable energy in consideration of the global environment. In particular, CZTS-based and CTS are expected as the promising solar cell materials which have potential to obtain high conversion efficiency with no rare elements. However, the suitable fabrication method which obtain the high conversion efficiency of the practical use level is not established. Therefore, it is necessary to investigate the properties of the CZTS-based and CTS thin films and solar cells

fabricated using a new preparation process. This study has been performed from the above standpoint. The results revealed through this study are summarized as follows.

In **Chapter 2**, the CZTSe thin films and solar cells were fabricated by using the new single-step evaporation process, and used the CZTSe compound as the starting evaporation materials. Furthermore, influences by annealing of the characteristics of these thin films and solar cells were investigated. The Zn content was varied between 2.0 and 3.0 at a constant contents for the remaining evaporation materials equal to Zn : Sn : CZTSe : Na_2Se = x : 1.2 : 1.2 : 0.024 (x = 2.0 and 3.0), and the condition of annealing was 30 min at 500 °C under mixed Se and Sn atmosphere with a Sn/Se molar ratio of 0.2. The compositional, the structural, morphological, optical, and electrical characterization were carried out by electron probe microanalysis (EPMA), X-ray diffraction (XRD), Raman spectroscopy, scanning electron microscopy (SEM), quantum efficiencies (QE), and Current-voltage (J-V) characteristics measurements. The Sn content in the films decreased and the Zn content increased after annealing owing to Sn re-evaporation. The SnSe phase formed in the vicinity of the Mo layer in the thin films fabricated by proposed evaporation method, and it disappeared after subsequent annealing. The grain sizes increased with annealing; however, some voids were seen in the annealed samples. The best solar cell fabricated at x = 2.0 without the annealing was characterized by V_{oc} = 240 mV, J_{sc} = 27.6 mA/cm^2, FF = 0.41, and η = 2.76 %. The solar cell fabricated by proposed evaporation method had QE in the wavelength range between 350 nm and 1400 nm.

In **Chapter 3**, the CTS thin films and solar cells were fabricated by sulfurization process from the stacked Cu/Sn precursors deposited by sequential evaporation of Sn and Cu elements, and the optimum value of the Cu/Sn molar ratio of the CTS thin film solar cells was investigated. The Cu/Sn molar ratio of the evaporation materials was changed from 1.33 to 2.0 under keeping constant at Cu molar ratio of 2.0. The precursors which were deposited by evaporation of Sn and Cu were crystallized by annealing in sulfur/tin mixing atmosphere for 30 min at 570 °C.

From EPMA, the Cu/Sn molar ratios range in the thin films were from 1.43 to 1.87, and S/(Cu+Sn) molar ratios range were from 1.34 to 1.73. The thin films fabricated in this Chapter had a monoclinic CTS structure from Raman spectra. The grain sizes were largest in the CTS thin film which fabricated with Cu/Sn molar ratio of 1.67. The composition of inside of the thin films had gradation, and the S contents existed near the surface. The largest V_{oc} in this Chapter of 247.5 mV was obtained with Cu/Sn molar ratio of 1.67.

In **Chapter 4**, the CTS thin films and solar cells were fabricated by sulfurization from NaF/Cu/Sn stacked precursor deposited by the sequential evaporation of Sn, Cu and NaF, and the effects of NaF addition on the cell performances of CTS thin film solar cells were investigated. The NaF/Cu/Sn stacked precursors prepared with varied the NaF/Cu molar ratio from 0 to 0.12 while keeping constant the Cu and Sn molar ratios at 1.0 and 0.6, respectively, and the CTS thin films were fabricated by annealing of these precursors in a sulfur/tin mixing atmosphere for 30 min at 570 °C. The XRD patterns of thin films which fabricated in this Chapter showed several peaks corresponding to only the diffraction lines of the monoclinic structure with increasing NaF/Cu molar ratio. In addition, the XRD patterns showed unknown diffraction peaks which were observed in low NaF/Cu molar ratios. The grain sizes of CTS thin films decreased with increasing NaF/Cu molar ratio, and this phenomenon was same as CIGS. The cell performances of the CTS thin film solar cells in this Chapter had an upward trend with increasing NaF/Cu molar ratio, and the CTS solar cell which was fabricated with NaF/Cu = 0.075 molar ratio demonstrated V_{oc} = 283 mV, J_{sc} = 37.3 mA/cm^2, FF = 0.439, and η = 4.63 %, including the record conversion efficiency. From QE curve of this solar cell, two steps of the sharp optical absorptions around 1200 and 1300 nm were seen, and the band-gap energies of this solar cell were estimated to be 0.93 and 1.02 eV.

In **Chapter 5**, the CTS thin films and solar cells with KF addition were fabricated by sulfurization. Two kinds of KF addition methods, two-stage annealing and the use of four-layer

precursors, were carried out, and the effective method of KF addition of CTS thin film solar cells were investigated. In the first experiment using two-stage annealing method, the molar ratio of the evaporation materials of the NaF/Cu/Sn stacked precursors was Cu : Sn : NaF = 1:0 : 0:6 : 0:075, and these precursors were crystallized by annealing in sulfur/tin mixed atmosphere for 30 min at 570 °C. Next, KF was deposited on it (KF/Cu molar ratios were 0.02 and 0.05), and the KF/film-bilayer samples were annealed again in sulfur/tin mixed atmosphere for 30 min (second annealing temperature were 350 and 500 °C). In the second experiment using four-layer precursors, the molar ratio of the evaporation materials of the four-layer KF/NaF/Cu/Sn precursors was Cu : Sn : NaF : KF = 1:0 : 0:6 : 0:075 : x (x = 0.02 and 0.05) and Cu : Sn : NaF : KF = 1:0 : 0:6 : y : 0:02 (y = 0 to 0.075). These precursors were crystallized by annealing in sulfur/tin mixed atmosphere for 30 min at 570 °C. By EPMA analysis, the Cu/Sn molar ratios of the CTS thin films fabricated in this Chapter were range from 0.81 to 1.51, and it means the film compositions became Cu-poor by KF addition. Moreover, the Cu/Sn molar ratios of the samples fabricated by two-stage annealing were approximately stable, whereas the samples prepared using four-layer precursors had various Cu/Sn molar ratios. The XRD patterns and Raman spectra showed several peaks corresponding to the monoclinic CTS structure. The best solar cell in this Chapter showed V_{oc} of 293 mV, J_{sc} of 24.71 mA/cm^2, FF of 0.41, and η of 2.93 %; it was fabricated by two-stage annealing with NaF/Cu = 0.075 and KF/Cu = 0.02, and the improvement of V_{oc} was seen by KF addition. Furthermore, V_g ($E_g/q - V_{oc}$, E_g is the band-gap energy, q is the electron charge) of the CTS thin film solar cell, i.e., the difference between the band-gap energy and V_{oc}, was improved from 0.65 V to 0.64 V.

In **Chapter 6**, the CATS thin films and solar cells which were Ag doping of CTS were fabricated by sulfurization from NaF/Sn/(Ag+Cu) stacked precursors deposited by sequential evaporation of Ag, Cu and Sn elements and NaF, and the effects of Ag doping on the band-gap energy and V_{oc} of CATS thin film solar cells were investigated. The molar ratio of the

evaporation materials of the stacked NaF/Sn/(Ag+Cu) precursors was (Ag+Cu) : Sn : NaF = 1.0 : 0.6 : 0.075, and the Ag/(Ag+Cu) molar ratio of the evaporation materials was varied from 0 to 0.2. These precursors were crystallized by annealing in a mixed sulfur/tin atmosphere for 30 min at *T* °C (*T* =530 and 570 °C). The (Ag+Cu)/Sn molar ratio in the thin films fabricated at 530 °C and 570 °C were in the range from 1.38 to 1.73 and 1.26 to 2.03, respectively. In addition, the (Ag+Cu)/Sn molar ratio in the thin films decreased as Ag/(Ag+Cu) molar ratio in the evaporation materials increased. For all samples, the XRD patterns showed several peaks near the diffraction line of the monoclinic CTS structure. Moreover, foreign phases of Na_9Sn_4 and MoS_2 were seen in some of the samples fabricated at *T* = 570 °C, and these foreign phases existed even in the solar cell devices. From the lattice spacing calculated from Bragg's equation, the CATS was fabricated by gradual substitution of Cu for Ag until around Ag/(Ag+Cu) = 0.05, and that quantities of Ag higher than Ag/(Ag+Cu) = 0.1 did not contribute to the formation of the alloyed CATS crystals. The grain sizes in the thin films increased with increasing the Ag/(Ag+Cu) molar ratio and the sample of the Ag/(Ag+Cu) = 0.05 with *T* = 570 °C had a close-packed structure and large crystal grains in comparison to that of the other samples. The cell performances of the CATS thin film solar cells had upward trends until the Ag/(Ag+Cu) molar ratio in the evaporation materials reached 0.05, and the best solar cell in this Chapter fabricated with Ag/(Ag+Cu) = 0.05 and *T* = 570 °C showed V_{oc} of 244 mV, J_{sc} of 36.9 mA/cm^2, FF of 0.45, and η of 4.07 %. These cell performances are the first reports of CATS thin film solar cells. The band-gap energies of the CATS thin film solar cells ranged from 0.928 eV to 0.934 eV, and the expansion of the band-gap energy by Ag doping to the CTS was confirmed. Therefore, it is evident that the V_{oc} of the CATS thin film solar cells were improved by the expansion of the band-gap energy.

In this research work, the characteristics of the CZTSe, CTS and CATS thin films and solar cells fabricated by several fabrication methods were investigated as above. In particular, the

CATS which was fabricated by Ag doping of CTS used for solar cell materials for the first time, and showed its potential. However, the conversion efficiencies of these solar cells in this study are not the practical use level yet. For the further improvement of the conversion efficiency, it is necessary to improve the V_{oc} and J_{sc} of these solar cells. For the improvement of V_{oc}, increase of carrier concentration and expansion of the band-gap energy are effective. Furthermore, measurement and improvement of the defect levels in absorber layer are important. For the improvement of J_{sc}, increase of the diffusion length of minority carrier by improvement of thin film morphology such as formation of large crystal grain size is effective. Therefore, further investigations of the fabrication conditions in this study of CZTSe, CTS and CATS thin films are necessary. Furthermore, it is also important to investigate about each layer that configures the thin film solar cell such as back contact, CdS buffer layer, transparent conducting layer, and etc.

The fabrication methods of CZTSe, CTS and CATS thin film solar cells in this study can be extended to other solar cell materials.

7.2 Acknowledgement

I would like to express my sincerest gratitude to the supervisor of the present thesis, Prof. Dr. Masanobu Izaki (Toyohashi University of Technology), for the many helpful suggestions, ideas, discussions and comments.

I would like to express the deepest appreciation to the great teacher of my life, Prof. Dr. Toshiyuki Yamaguchi (National Institute of Technology, Wakayama College), for the many helpful suggestions, discussions and valuable guidance.

I would like to offer my special thanks to Dr. Junji Sasano (Toyohashi University of Technology) for his supports and comments.

I would like to show my greatest appreciation to Prof. Dr. Yoshikazu Todaka (Toyohashi University of Technology), Dr. Toshiaki Yasui (Toyohashi University of Technology) and Dr. Masakazu Kobayashi (Toyohashi University of Technology) for their valuable comments.

I would like to gratefully acknowledge Prof. Katagiri (National Institute of Technology, Nagaoka College) and Prof. Araki (National Institute of Technology, Nagaoka College) for the measurements of characteristics of solar cells.

I would like to thank Prof. Dr. Shigeyuki Nakamura (National Institute of Technology, Tsuyama College), Prof. Dr. Satoru Seto (National Institute of Technology, Ishikawa College) and Dr. Yoji Akaki (National Institute of Technology, Miyakonojo College) for their helpful suggestions and comments.

I owe a very important debt to the students of Yamaguchi laboratory in National Institute of Technology, Wakayama College for the technical assistances in the experiments.

I am deeply grateful to all members of Department of Electrical and Computer science Engineering of National Institute of Technology, Wakayama College for the continuing encouragement and support.

I wished to express my deep appreciation to my parents for their support and encouragement. Finally, special thanks to Mayumi, my wife, Riku and Saku, my sons, for their support, encouragement and love.

Wakayama, Japan

July 2018

Mitsuki Nakashima

7.3 Research achievements

7.3.1 List of publications

[1] Fabrication of $Cu_2ZnSnSe_4$ Thin Films by Selenization of Precursor using $Cu_2ZnSnSe_4$ Compound for Photovoltaic Applications, **Mitsuki Nakashima**, Toshiyuki Yamaguchi, Kengo Kusumoto, Shohei Yukawa, Junji Sasano, Masanobu Izaki, Physica Status Solidi C Vol.12, No.6, 729-732 (2015).

[2] Cu_2SnS_3 Thin Film Solar Cells Prepared by Thermal Crystallization of Evaporated Cu/Sn Precursors in Sulfur and Tin Atmosphere, **Mitsuki Nakashima**, Toshiyuki Yamaguchi, Hiroki Itani, Junji Sasano, Masanobu Izaki, Physica Status Solidi C Vol.12, No.6, 761-764 (2015).

[3] Cu_2SnS_3 thin-film solar cells fabricated by sulfurization from NaF/Cu/Sn stacked precursor, **Mitsuki Nakashima**, Junya Fujimoto, Toshiyuki Yamaguchi, Masanobu Izaki, Applied Physics Express 8, 042303(4 pages) (2015).

[4] Effect of annealing on the morphology and compositions of $Cu_2ZnSnSe_4$ thin films fabricated by thermal evaporation for solar cells, **Mitsuki Nakashima**, Toshiyuki Yamaguchi, Shohei Yukawa, Junji Sasano, Masanobu Izaki, Thin Solid Films 621, 47-51 (2017).

[5] KF addition to Cu_2SnS_3 thin films prepared by sulfurization process, **Mitsuki Nakashima**, Junya Fujimoto, Toshiyuki Yamaguchi, Junji Sasano, Masanobu Izaki, Japanese Journal of Applied Physics 56, 04CS02(4 pages) (2017).

[6] Fabrication of $(Cu,Ag)_2SnS_3$ thin films by sulfurization for solar cells, **Mitsuki Nakashima**, Toshiyuki Yamaguchi, Koichi Hatayama, Hideaki Araki, Sigeyuki Nakamura, Satoru Seto, Yoji Akaki, Junji Sasano, Masanobu Izaki, Thin Solid Films 642, 8-13 (2017)

7.3.2 List of conferences

[1] $Cu_2ZnSnSe_4$ thin films prepared by selenization of precursor evaporated from $Cu_2ZnSnSe_4$ and Na_2Se, Mitsuki Nakashima, Kohei Kawamoto, Toshiyuki Yamaguchi, Shigetoshi Niiyama, Toshito Imanishi, The 2013 Japan Society of Applied Physics Materials Research Society Joint Symposia (JSAP-MRS), September 16-20, 2013, Kyoto, Japan.

[2] Fabrication of $Cu_2ZnSnSe_4$ Thin Films by Selenization of Precursor using $Cu_2ZnSnSe_4$ Compound for Photovoltaic Applications, Mitsuki Nakashima, Toshiyuki Yamaguchi, Kengo Kusumoto, Shohei Yukawa, Junji Sasano, Masanobu Izaki, The 19th International Conference on Ternary and Multinary Compounds, September 1-5, 2014, Niigata, Japan.

[3] Cu_2SnS_3 Thin Film Solar Cells Prepared by Thermal Crystallization of Evaporated Cu/Sn Precursors in Sulfur and Tin Atmosphere, Mitsuki Nakashima, Toshiyuki Yamaguchi, Hiroki Itani, Junji Sasano, Masanobu Izaki, The 19th International Conference on Ternary and Multinary Compounds, September 1-5, 2014, Niigata, Japan.

[4] $Cu_2ZnSnSe_4$ Thin Films Prepared by Annealing from Precursor Using $Cu_2ZnSnSe_4$ Compound in Selenium and Tin Mixing Atmosphere, Mitsuki Nakashima, Toshiyuki Yamaguchi, Kengo Kusumoto, Shohei Yukawa, Junji Sasano, Masanobu Izaki, The 6th World Conference on Photovoltaic Energy Conversion (WCPEC6), November 23-27, 2014, Kyoto, Japan.

[5] $Cu_2ZnSn(S,Se)_4$ Thin Films Prepared by Annealing in Sulfur, Selenium and Tin Mixing Atmosphere for Photovoltaic Applications, Mitsuki Nakashima, Toshiyuki Yamaguchi, Yuichi Mizui, Junji Sasano, Masanobu Izaki, The 6th World Conference on Photovoltaic Energy Conversion (WCPEC6), November 23-27, 2014, Kyoto, Japan.

[6] Fabrication of Cu_2SnS_3 thin film solar cells by sulfurization process from NaF addition precursor, Mitsuki Nakashima, Toshiyuki Yamaguchi, Junya Fujimoto, Junji Sasano, Masanobu Izaki, The 25th International Photovoltaic Science and Engineering Conference (PVSEC25), November 15-20, 2015, Busan, Korea.

[7] $Cu_2ZnSnSe_4$ thin film solar cells prepared by evaporation of $Cu_2ZnSnSe_4$ compound and effect of annealing, Mitsuki Nakashima, Toshiyuki Yamaguchi, Shohei Yukawa, Junji Sasano, Masanobu Izaki, The 25th International Photovoltaic Science and Engineering Conference (PVSEC25), November 15-20, 2015, Busan, Korea.

[8] Fabrication of $Cu_2ZnSn(S,Se)_4$ thin film solar cells by thermal crystallization using $Cu_2ZnSnSe_4$ compound in S/Se atmosphere, Mitsuki Nakashima, Toshiyuki Yamaguchi, Yuichi Mizui, Junji Sasano, Masanobu Izaki, The 25th International Photovoltaic Science and Engineering Conference (PVSEC25), November 15-20, 2015, Busan, Korea.

[9] KF addition to Cu_2SnS_3 thin films prepared by sulfurization process, Mitsuki Nakashima, Junya Fujimoto, Toshiyuki Yamaguchi, Junji Sasano, Masanobu Izaki, The 2016 International Conference on Solid State Devices and Materials (SSDM2016), September 26-29, 2016, Tsukuba, Japan.

[10] Effect of KF addition to Cu_2SnS_3 thin film by two-stage annealing, Mitsuki Nakashima, Junya Ue, Toshiyuki Yamaguchi, Junji Sasano, Masanobu Izaki, The 27th International Photovoltaic Science and Engineering Conference (PVSEC27), November 12-17, 2017, Otsu, Japan.

[11] Fabrication of $(Cu,Ag)_2SnS_3$ thin film solar cells by sulfurization from stacked NaF/Sn/(Cu+Ag) precursors, Mitsuki Nakashima, Koichi Hatayama, Toshiyuki Yamaguchi, Hideaki Araki, Shigeyui Nakamura, Satoru Seto, Yoji Akaki, Junji Sasano, Masanobu Izaki, The 27th International Photovoltaic Science and Engineering Conference (PVSEC27), November 12-17, 2017, Otsu, Japan.